LEHIGH

University

SOME BASIC PROBLEMS ON THE MECHANICS OF FUNCTIONALLY GRADED MATERIALS

Final Progress Report

F. Erdogan

December 1998

U.S. ARMY RESEARCH OFFICE

GRANT NO. DAAH04-95-1-0232

Department of Mechanical Engineering & Mechanics
19 Memorial Drive West
Lehigh University, Bethlehem, PA 18015-3085

SF 298 MASTER COPY KEEP THIS COPY FOR REPRODUCTION PURPOSES

REPORT DOCUMENTATION PAGE

Form Approved
OMB NO. 0704-0188

1. AGENCY USE ONLY *(Leave blank)*	2. REPORT DATE	3. REPORT TYPE AND DATES COVERED
	January 1999	5/1/95-9/30/98

4. TITLE AND SUBTITLE
Some basic problems on the mechanics of functionally graded materials

5. FUNDING NUMBERS
DAAH04-95-1-0232

6. AUTHOR(S)
Fazil Erdogan

7. PERFORMING ORGANIZATION NAMES(S) AND ADDRESS(ES)
Lehigh University, ME-MECH Department
Bethlehem, PA 18015

8. PERFORMING ORGANIZATION REPORT NUMBER
533249

9. SPONSORING / MONITORING AGENCY NAME(S) AND ADDRESS(ES)
U.S. Army Research Office
P.O. Box 12211
Research Triangle Park, NC 27709-2211

10. SPONSORING / MONITORING AGENCY REPORT NUMBER
ARO 33534.9-EG

11. SUPPLEMENTARY NOTES
The views, opinions and/or findings contained in this report are those of the author(s) and should not be construed as an official Department of the Army position, policy or decision, unless so designated by other documentation.

12a. DISTRIBUTION / AVAILABILITY STATEMENT
Approved for public release; distribution unlimited.

12 b. DISTRIBUTION CODE

13. ABSTRACT *(Maximum 200 words)*

Grading thermomechanical properties of composites by continuously varying the volume fractions of their constituents is becoming a powerful tool in designing new materials for specific applications. The broad objective of this project has been to identify and study a series of basic mechanics problems relating to the failure of this new class of composites called *functionally graded materials*. The fields selected for investigation which also have important technological applications are fracture mechanics of thermal barrier coatings and thermoelectric cells, contact mechanics of graded materials, and wave propagation in inhomogeneous solids. In each case first the basic concepts are studied analytically. Then a series of benchmark problems are considered in order to demonstrate the distinguishing features of the mechanics of graded materials and to provide some results that could be used in practical applications. Because of its importance in life prediction and failure analysis of structural components, a greater part of the research effort in the project was devoted to the fracture mechanics of graded materials. In solving the benchmark problems the method used has been generally analytical, the exceptions being the layered thermal barrier coatings and the nonlinear post-buckling examination of spallation problems for which finite element methods were used.

14. SUBJECT TERMS	15. NUMBER IF PAGES
Functionally graded materials, fracture mechanics, contact mechanics, wave propagation, spallation surface cracking, interface cracking, material orthotropy	16. PRICE CODE

17. SECURITY CLASSIFICATION OR REPORT	18. SECURITY CLASSIFICATION OF THIS PAGE	19. SECURITY CLASSIFICATION OF ABSTRACT	20. LIMITATION OF ABSTRACT
UNCLASSIFIED	UNCLASSIFIED	UNCLASSIFIED	UL

TABLE OF CONTENTS

ABSTRACT

Grading thermomechanical properties of composites by continuously varying the volume fractions of their constituents is becoming a powerful tool in designing new materials for specific applications. The broad objective of this project has been to identify and study a series of basic mechanics problems relating to the failure of this new class of composites called *functionally graded materials*. The fields selected for investigation which also have important technological applications are fracture mechanics of thermal barrier coatings and thermoelectric cells, contact mechanics of graded materials, and wave propagation in inhomogeneous solids. In each case first the basic concepts are studied analytically. Then a series of benchmark problems are considered in order to demonstrate the distinguishing features of the mechanics of graded materials and to provide some results that could be used in practical applications. Because of its importance in life prediction and failure analysis of structural components, a greater part of the research effort in the project was devoted to the fracture mechanics of graded materials. In solving the benchmark problems the method used has been generally analytical, the exceptions being the layered thermal barrier coatings and the nonlinear post-buckling examination of spallation problems for which finite element methods were used.

In this report, after providing the necessary review and background information on the applications of graded materials, the objectives of the research program is briefly described and the main body of the technical work is presented. Typical benchmark problems discussed in the appendices include a nonlinear spallation model for graded coatings, the interface cracking of inhomogeneous coatings due to thermal loading, contact mechanics of graded materials and coatings in the presence of friction, an axisymmetric spallation problem in a graded medium, wave propagation in a graded elastic plate, and the influence of material orthotropy in an inhomogeneous medium under mixed-mode conditions. The area of multiple site cracking in graded materials is described in detail in a separate technical project report. The report also includes some results concerning the distortion of isochromatics due to material inhomogeneity and the effect of curvatures, and inhomogeneities of the contacting elastic solids and of friction on the distribution of contact stresses.

1. BACKGROUND INFORMATION ON FUNCTIONALLY GRADED MATERIALS

In order to meet the increasingly stringent demands of future technologies in power generation, aerospace, microelectronics and transportation, in current research a great deal of emphasis is being placed on material design, more specifically, on developing new materials or material systems tailored for specific applications. Generally, such materials tend to be composites and intermetallics that have homogeneous bulk properties. Most modern composites are fiber or filament reinforced, particulate or layered in structure. Many of the laminated materials, thin films and coatings fall into the latter category. A common feature of composites is that they consist of bonded dissimilar homogeneous materials with very complex microstructure. Consequently, in studying mechanics, particularly failure mechanics of such materials the nature of interfaces or interfacial regions would play an extremely important role. From a viewpoint of failure mechanics, material property discontinuities across the interfaces generally have two undesirable consequences, namely higher residual, thermal and mechanical stresses, and weaker bonding strength. To circumvent these difficulties, very often the interfacial regions are modified by introducing a third medium in the form of an interlayer or mechanically roughening the contacting surfaces or using suitable coupling agents.

A relatively new alternative concept which may also be used to overcome some of the shortcomings of bonded dissimilar homogeneous materials, particularly of layered materials, would be the introduction of interfacial regions or coatings with *graded* thermomechanical properties* [1-6]. Thus, by varying the volume fractions of the constituents between zero to one hundred percent, thereby obtaining a continuous through-thickness property variation, it is possible to obtain not only smoother stress distributions and lower stress concentrations [7], [8], but also higher bonding strength [9]. For example, in [7] it was shown that the points of intersection of free surfaces and interfaces between dissimilar materials are points of stress singularity and, consequently, potential locations of debonding fracture initiation. On the other hand, if the sharp interface is eliminated by introducing a graded layer, the singularity disappears and the stress distribution becomes considerably smoother [7], [10].

In many of the deposition and bonding processes used in ceramic coatings, it is difficult to obtain the desired strength for the interfacial zones. This is due largely to poor adhesion and partly to high stress concentrations. The adverse influence of both of these factors can be reduced significantly by introducing a graded interfacial zone between the two materials. The technique can be particularly useful for material pairs in which bonding is inherently difficult. For example, in [9] it was shown that for a diamond film synthesized over a 50/50 W/Mo alloy by using a DC plasma jet, the measured bonding strength is less than 10 kg/cm^2. On the other hand if a graded interfacial zone is introduced by first plasma-spraying the substrate with tungsten carbide and then gradually adding increasing amounts of methane and hydrogen before growing the diamond film, the adhesive strength is measured to be over 150 kg/cm^2.

* The numbers in bracket refer to the references listed in the Bibliography section of this report.

These mostly particulate composites with continuously varying volume fractions are called *functionally graded materials* (FGMs). By controlling not only the composition profile but also the microstructure, the concept of FGMs could provide a great deal of flexibility in material design. As the processing techniques improve, the potential for special application of FGMs appears to be nearly unlimited. However, in the immediate future the primary application of these new materials will most likely be limited to thermal barrier coatings, tribology (with wear and corrosion-resistant coatings), abradable seals, impact-resistant structures, and thermoelectric cells. In the remainder of this section these potential applications of FGMs will be briefly described. The primary objectives of the research program will be outlined in Section 2. The fundamental concepts relating to the failure mechanics of FGMs and underlying fracture and contact problems will be discussed in Section 3. The details of the specific technical material have been presented in the form of technical reports, manuscripts, reprints of journal articles and articles that appeared in proceedings.

1.1 Thermal Barrier Coatings

Within the past decade considerable progress has been made in using ceramic coatings to protect metallic components from high temperatures. These *thermal barrier coatings* (TBCs) are currently being used in conjunction with air cooling to prolong the life of hot section turbine components in aircraft engines. The application of ceramic TBCs also offers the possibility of increasing the thermodynamic efficiency of landbased turbines by increasing the inlet temperature of gases. TBC technology is thus considered to be a viable means for developing more efficient aircraft engines and stationary gas turbines. There are, however, several major technical issues involving the next generation of TBCs that need to be addressed: (a) improvement in processing techniques from both economic and performance standpoints, (b) understanding the failure mechanisms of TBCs in simulated and actual turbine environments and developing the appropriate techniques for their modeling and analysis, and (c) developing thermomechanical material characterization and test methodologies to measure the material properties necessary for the application of life prediction models.

The current approach for accommodating the material property mismatch between the ceramic coating and the metallic substrate is to make the ceramic layer to be more compliant or strain-tolerant by introducing a segmented columnar structure (or in some cases pores and microcracks). The difficulty with this solution is that the particular microstructural features that provide compliant coatings also provide rapid diffusion paths for oxygen. The experience seems to indicate that by far the most critical factor limiting the performance of the state-of-the-art TBCs is the spallation of ceramic layers which take place either along a plane parallel to the ceramic/oxide layer interface (as in plasma-spray coatings) or bond coat/oxide interface (as in coatings processed by using electron beam physical vapor deposition). Usually a micron-thick oxide layer (generally Al_2O_3) forms between the bond coat and the top coat during processing. It then gradually grows during operation as the system is subjected to sustained high temperature until most of the aluminum in the bond coat is depleted. Thus, the life of TBCs seems to be controlled by the number and exposure time of thermal cycles and the process of local initiation, growth and coalescence of microcracks.

Main desirable characteristics of an ideal TBC appear to be low conductivity for thermal insulation, high coefficient of thermal expansion to match that of the metallic substrate, and high resistance to oxygen diffusion. It is highly unlikely to find all these favorable properties in a single material. Many of the well-known ceramics have either high conductivity and low oxygen diffusivity or low conductivity and high oxygen diffusivity. To prevent oxygen diffusion at some point a layer of Al_2O_3 or mullite ($Al_2O_3 \bullet 2SiO_2$) may be needed. However, these materials have considerably higher thermal conductivity than that of, for example, YSZ (ytria-stabilized zerconia). Thus, the problem appears to be an optimal design of a multi-layered structure, including graded interfacial zones and coatings.

Typically, the current design of TBCs consists of a partially stabilized zirconia coating deposited on an intermediate metallic bond coat (e.g., NiCr A*l*Y) which is plasma sprayed on the (superalloy) substrate [6]. The main function of the bond coat is to protect the substrate against oxidation. It also helps to reduce thermal expansion mismatch between the ceramic coating and the metallic substrate, and provides the surface texture needed to improve bonding. At high temperatures an oxide (Al_2O_3) scale is formed along the PSZ-bond coat interface. Even though this Al_2O_3 layer forms an oxygen diffusion barrier, it also introduces a weak cleavage plane which, under thermal cycling, may lead to spallation. This difficulty may be overcome by introducing a graded (NiCrAl_2Y-PSZ) layer between the bond coat and the ceramic layer [6].

The basic premise behind using the FGM concept is that by replacing sharp interfaces with graded interfacial zones or by replacing homogeneous ceramic layers with graded metal/ceramic composites it is possible to improve the resistance of the coating to spallation as a result of reduced stress levels and improved bonding strength.

The fundamental fracture mechanics concepts relating to the failure of FGM coatings and interfacial zones will be described in Section 3 of this report and results summarizing some of the research carried out on the subject will be presented in Appendices A and B.

1.2 Applications in Tribology

An obvious application of ceramic coatings seems to be to provide the necessary hardness or wear resistance to the surfaces of structural components transmitting forces through contact, such as gears, bearings, cams and machine tools. Intuitively it is clear that the fatigue life of these components may be improved quite considerably by using graded rather than homogeneous ceramic coatings on the main load-bearing metallic substrate. In these load-transfer components FGM coatings would provide the necessary surface hardness without sacrificing toughness.

A wear-related application of FGM coatings or interfacial zones may be found in abradable seals used in some stationary gas turbines to help minimize the gas leakage through the gap between the tips of rotating blades and turbine shroud. Here the main components in the shroud are the metallic structure or the substrate, the bond coat, a layer of high density ceramic and a layer of very low density ceramic with a graded zone replacing every sharp interface [11]. The underlying mechanics problem is again a contact problem and the primary desirable material property requirements are toughness and abradability.

In the past wear and corrosion-resistant coatings have been used quite extensively in industrial machinery. Coating materials have been metals such as stainless steels, Mo based alloys and WC-Co as well as ceramics such as Al_2O_3/NiCr have been extensively used in aircraft industry to coat various turbine/compressor components and mid-span stiffeners for improved wear-resistance. Other applications of wear-resistant coatings have been in printing rolls, steel mills, petrochemical industry and transportation industry. Most of these coatings have been deposited by using a thermal spray technique. Since thermal spray processes are readily suitable for composition grading, service life improvements can be obtained in all applications of wear and corrosion-resistant coatings by using the FGM concept.

The basic mechanics of crack and contact problems associated with the failure of wear and corrosion-resistant coatings and abradable seals will be described in Sections 3 and 4 of this report. The results of some specific studies will be presented in Appendices A through D and F.

1.3 Elastodynamics of Graded Materials

A first step in studying the failure mechanics of structural components usually is a detailed stress analysis for identifying the likely sites of failure initiation and for determining the peak values of stresses. In some cases the loading of these inhomogeneous components may be dynamic in nature. Thus, an important area of interest in considering the applications of graded materials would be to study the dynamic response of the component to, for example, impact or blast loading. In elastodynamics of materials with continuously varying properties, usually the pulse shape is distorted in time, the wave propagation speed is not constant, and there are no sharp interfaces that would cause wave reflections. Consequently, even in the simple case of one-dimensional wave propagation the locations and magnitudes of peak stresses cannot be determined by inspection.

Because of its relevance in geophysics and soil mechanics, in the past there has been quite considerable interest in the elastodynamics of inhomogeneous media. In 1946 Friedlander [5] proposed a solution that consists of a series of terms the first of which describes the wave motion predicted by geometrical optics and the subsequent terms account for certain types of diffraction effects. Karal and Keller [6] extended this method to treat general wave propagation problems in inhomogeneous elastic media by formulating the problem in terms of displacements and displacement potentials. Pekeris [7] used an asymptotic method to solve the problem for a half-space with a variable speed of sound and reduced the solution to a Fourier-Bessel series. Since then geophysics-oriented contributions to the field have been quite voluminous.

Among many others, there are two important reasons for studying the problem of wave propagation and impact in FGMs. The first is the interpretation and analysis of possible nondestructive testing and evaluation results. The second is related to service life and reliability of FGM components, specifically, to the evaluation of peak stresses for the purpose of spallation studies. A one-dimensional benchmark problem was considered in [15]. A brief description and summary of the results are also presented in Appendix E.

1.4 Thermoelectric Cells

In many conductors generally the electrical current and the thermal flux are coupled. This coupling can be used, in principle, to construct refrigerators or electric power generators. A temperature difference ΔT across any conductor would generate a voltage ΔV. Generally $S=\Delta V/\Delta T$ is a measure of the efficiency of the device where S is the Seebeck coefficient. A commonly known such device is the thermocouple. The efficiency of the device is also dependent on thermal conductivity k and electrical resistivity ρ. Thus, it has been shown that the dimensionless constant defined by $Z=TS^2/k\rho$ is the measure of device efficiency at temperature T(K), where Z is known as the figure of merit. Most metallic materials have very small values Z and, consequently, are not suitable for thermoelectric cell applications. The group of materials most suitable for refrigeration as well as power generation appears to be certain doped semiconductors [16]. Some of the typical applications for thermoelectric devices are power for deep space probes, remote weather stations, underwater and remote navigational systems in power generation area and spot cooling of electronic devices, infrared and X-ray detectors, fiber optic laser packages, and computer central processing units in refrigeration area.

In semiconductors suitable for thermoelectric cell application, the figure of merit is highly temperature dependent. In a typical temperature range such as 300-1000 (K) the use of a single material would be very inefficient. Thus, to optimize the power efficiency a layered material is necessary. This result of increasing the overall device efficiency can best be accomplished by using bonded dissimilar materials containing many layers each operating near its optimum temperature. To a lesser extent, it can also be accomplished by using a single semi-conductor with graded dopant concentration. In either case, the underlying mechanics is one of bonded dissimilar materials with stress-free surfaces subjected to steep temperature gradients. Here, because of stress singularities, debonding is a common mode of failure. It is, therefore, clear that, from the viewpoint of failure mechanics as well as the device efficiency, the problem is highly suitable for the application of FGM concept [17].

2. OBJECTIVES OF THE RESEARCH PROGRAM

The primary objectives of this research program have been to identify and study a series of fundamental problems relating to the *mechanics of functionally graded materials*. A particular emphasis has been on the investigation of failure oriented problems. Thus, considering present and potential technological applications of FGMs, following three specific areas were selected for investigation:

- Fracture mechanics of FGMs
- Contact mechanics of FGMs
- Elastodynamics of FGMs

Because of the relative importance of the topic, a greater portion of the research effort was devoted to fracture mechanics. Particular research concentration in this area has been on the following:

- The examination of the singular behavior of the solutions of crack problems in FGMs; specifically the investigation of the singularity problems in FGMs that are the counterpart of such anomalous behavior as oscillating and non-square-root power singularities in piecewise homogeneous materials.
- The development of analytical and effective numerical methods for solving the related crack and the nonlinear crack/contact problems.
- The identification and solution of some useful benchmark problems.

In studying the contact problems in load transfer components with FGM coatings, the main emphasis has been on the effect of material inhomogeneity parameters and the coefficient of friction on the contact stresses, specifically on their peak values, the nature of singularity if any, and fretting stresses. Also considered was the influence of the relative (positive or negative) curvatures of the contacting surfaces.

In elastodynamics of FGMs the primary objective was to provide the solution of a typical pulse propagation problem in a medium with finite thickness and fixed or free boundaries, to examine the distortion of the pulse and to determine the peak stresses.

In general, the results of the research program are intended to provide technical support for material scientists and engineers who are trying to develop methods for processing FGMs and for design engineers who are interested in applications. Also, the crack tip singularities found and benchmark solutions provided would be quite useful in the development and testing of finite element models for solving more complex problems involving FGMs.

3. FRACTURE MECAHNICS OF GRADED MATERIALS

In this section, after describing some elementary concepts of fracture mechanics of inhomogeneous materials, the FGM counterparts of the anomalous stress singularities arising from the study of crack problems in piecewise homogeneous materials will be examined and some recent results obtained from various benchmark solutions will be discussed.

3.1 Fracture Mechanics of FGMs - Basic Concepts

In a broad sense "fracture" is creation of new surfaces in solids. The fundamental criterion of fracture initiation and propagation is based on the energy balance concept. Let the solid contain a dominant flaw which is usually considered to be a planar crack of surface area A. Under given external loads if the crack grows by an amount dA in time dt, the thermodynamic equilibrium of the solid requires that

$$\frac{dU}{dt} = \frac{dV}{dt} + \frac{dT}{dt} + \frac{dD}{dt}, \qquad (1)$$

where U, V, T and D respectively are the work of the external loads, the recoverable internal energy, the kinetic energy, and the sum of all dissipated energies such as surface tension, plastic work, viscous dissipation, etc. If the energy dissipation takes place only around the advancing periphery of the crack, in a quasi-static case T is negligible and defining dD/dA=G_c (1) may be expressed as

$$\frac{d}{dA}(U-V)=G_c \quad . \tag{2}$$

In the fracture criterion given by (2) the left hand side is the energy available and G_c is the energy required to create a unit area of new fracture surface. They are also known as the *crack driving force* and the *fracture toughness*, respectively. By using the concept of crack closure it can then be shown that the increment d(U-V) of the energy available for fracture may be evaluated from the asymptotic stresses and the crack opening displacements near the crack tip which, in homogeneous solids, may be obtained from the three-dimensional elasticity solution as follows:

$$\sigma_{ij}(r,\theta)\cong\frac{k_1}{\sqrt{2r}}f_{1ij}(\theta)+\frac{k_2}{\sqrt{2r}}f_{2ij}(\theta)\ ,\ (i,j=x,y)\ , \tag{3}$$

$$\sigma_{iz}(r,\theta)\cong\frac{k_3}{\sqrt{2r}}f_{3i}(\theta),\ (i=x,y)\ , \tag{4}$$

$$v^+-v^-\cong\frac{2(1-\nu^2)}{E}k_1\sqrt{2r}\ ,u^+-u^-\cong\frac{2(1-\nu^2)}{E}k_2\sqrt{2r}\ , \tag{5}$$

$$w^+-w^-\cong\frac{k_3}{\mu}\sqrt{2r} \tag{6}$$

where k_1, k_2 and k_3 are the modes I, II, and III stress intensity factors, f_{1ij}, f_{2ij} and f_{3i} are known functions and E, ν and μ are the elastic constants, $E=2\mu(1+\nu)$. From the crack closure energy it may then be shown that

$$G_1=\frac{\pi(1-\nu^2)}{E}k_1^2\ ,G_2=\frac{\pi(1-\nu^2)}{E}k_1^2\ ,G_3=\frac{\pi}{2\mu}k_3^2\ , \tag{7}$$

$$G=\frac{d}{dA}(\text{U-V})=G_1+G_2+G_3 \tag{8}$$

where G is the total energy available for fracture.

Equation (7) indicates that one may also use k_i in place of G_i as the measure of the crack driving force. For mode I loading conditions, for example, defining

$$K_I = k_1\sqrt{\pi}\ ,\ G_{1c} = G_{IC}\ ,\ K_{IC} = \sqrt{G_{IC}E/(1-\nu^2)}\ \ , \tag{9}$$

the fracture criterion (2) may be expressed as

$$K_I \leq K_{IC}\ . \tag{10}$$

Equation (10) has proved to be very useful in considering the fracture stability. However, perhaps the most useful application of the stress intensity factors may be found in analyzing the subcritical crack growth processes.

In studying the fracture mechanics of FGMs one may have to deal with a number of distinct singularity problems. The first is the investigation of the nature of stress singularities near the tip of a crack embedded in an inhomogeneous medium. The second is the general problem of debonding and the effect of a possible "kink" in material property distributions on the behavior of stress singularities. And the third is the basic surface cracking problems and the nature of the stress singularities for cracks intersecting the interfaces.

To examine the influence of the material inhomogeneity on the asymptotic stress state near the crack tips, we first consider the plane elasticity problem for an infinite medium containing a line crack. For simplicity we will assume that the Poisson's ratio ν of the medium is constant and the shear modulus is approximated by

$$\mu(x,y) = \mu_o \exp(\beta x + \gamma y)\ , \tag{11}$$

where μ_o, β and γ are known constants. This problem was solved for a crack along y=0, -a<x<a under arbitrary loading conditions [18], [19]. It was shown that near the crack tip x=a the stresses have the following asymptotic behavior:

$$\sigma_{ij}(x,y) = \exp[r(\beta\cos\theta + \gamma\sin\theta)]\left[\frac{k_1}{\sqrt{2r}} f_{1ij}(\theta) + \frac{k_2}{\sqrt{2r}} f_{2ij}(\theta)\right], (i,j = x,y)\ , \tag{12}$$

where the stress intensity factors k_1 and k_2 are defined by

$$k_1(a) = \lim_{x\to a}\sqrt{2(x-a)}\sigma_{yy}(x,0)\ ,\quad k_2(a) = \lim_{x\to a}\sqrt{2(x-a)}\sigma_{xy}(x,0)\ , \tag{13}$$

and the functions f_{1ij} and f_{2ij} are *identical* to those found for the *homogeneous* materials given in (3). Note that the asymptotic stress states for homogeneous materials (3) and FGMs (12) are identical only at r=0. However, since the crack opening displacement is also influenced in a way similar to stresses, the crack driving force (or, for "fixed grip" conditions, the strain energy release rate) was found to be identical to that calculated for the homogeneous materials, namely

$$G = \frac{\pi(1+\kappa)}{8\mu(a,0)}(k_1^2 + k_2^2) \tag{14}$$

where $\kappa=3-4\nu$ for plane strain and $\kappa=(3-\nu)/(1+\nu)$ for plane stress conditions.

Some sample results for an embedded crack of length 2a in an infinite medium under plane strain conditions are given in Table 1 [18,19]. Referring to (11) we first define

$$x' = x\cos\theta + y\sin\theta\ ,\ \beta = \omega\cos\theta\ ,\ \gamma = \omega\sin\theta\ ,\ \omega^2 = \beta^2 + \gamma^2\ , \quad (15)$$

$$\mu(x,y) = \mu(x') = \mu_o \exp(\omega x')\ . \quad (16)$$

The medium is assumed to be loaded by fixed grips away from the crack region with $\varepsilon_{y'y'}(x',\mp\infty) = \varepsilon_o$. Thus, the normalizing stress intensity factor for the results given in the table is

$$k_o = 2(1+\nu)\mu_o\varepsilon_o\sqrt{a}\ . \quad (17)$$

Note that the crack orientation angle $\theta=0$ corresponds to a mode I problem for which $k_2(\mp a) = 0$, whereas for $\theta=\pi/2$ the loading is parallel to the crack and, consequently, all stress intensity factors are zero.

Table 1. The effect of material nonhomogeneity parameter $a\omega$ and the crack orientation angle θ on the stress intensity factors; $\nu=0.3$; loading: uniform strain away from the crack region, $\varepsilon_{y'y'}(x',\mp\infty) = \varepsilon_0$.

aω	θ/π	$k_1(a)/k_0$	$k_1(-a)/k_0$	$k_2(a)/k_0$	$k_2(-a)/k_0$
	0	1.196	0.825	0	0
	0.1	1.081	0.750	-0.321	-0.254
	0.2	0.781	0.548	-0.514	-0.422
0.25	0.3	0.414	0.290	-0.504	-0.437
	0.4	0.121	0.075	-0.304	-0.282
	0.5	0	0	0	0
	0	1.424	0.674	0	0
	0.1	1.285	0.617	-0.344	-0.213
	0.2	0.925	0.460	-0.548	-0.365
0.5	0.3	0.490	0.247	-0.532	-0.397
	0.4	0.146	0.059	-0.314	-0.269
	0.5	0	0	0	0
	0	6.317	0.115	0	0
	0.1	5.376	0.117	-0.867	-0.037
	0.2	3.315	0.115	-1.155	-0.090
2.5	0.3	1.441	0.082	-0.900	-0.158
	0.4	0.369	0.004	-0.429	-0.179
	0.5	0	0	0	0

Table 2. Stress intensity factors for a plane strain and a penny-shaped crack in a graded medium under tension σ_0 perpendicular to the plane of the crack; ν=0.3.

ωa	0	0.1	0.25	0.5	1.0	2.5	5.0
Plane Strain Crack							
$k_1/\sigma_0\sqrt{a}$	1	1.008	0.036	1.101	1.258	1.808	2.869
$k_2/\sigma_0\sqrt{a}$	0	0.026	0.065	0.129	0.263	0.697	1.567
Penny-Shaped Crack							
$k_1/\left(\frac{2}{\pi}\sigma_0\sqrt{a}\right)$	1	1.002	1.012	1.038	1.118	1.442	2.083
$k_2/\left(\frac{2}{\pi}\sigma_0\sqrt{a}\right)$	0	0.017	0.041	0.083	0.168	0.440	0.960

Table 2 shows some limited results comparing plane strain and penny-shaped crack solutions for a graded material under uniform tension σ_0 perpendicular to the plane of the crack where ω=0 corresponds to the results for a homogeneous medium. The table shows that the stress intensity factors in FGMs are higher than that in homogeneous materials and that the influence of the material inhomogeneity on the stress intensity factors is more severe for a plane strain than for a penny-shaped crack. For further results see [18-25]. Also, for the solution of embedded crack problems in an FGM layer under mechanical or thermal loading see [26] and [27].

3.2 The Debonding Problems in FGMs

Consider the crack problems shown in Figs. 1a and 1b. Figure 1a describes the debonding problem in piecewise homogeneous materials, whereas Fig. 1b refers to a FGM bonded to a homogeneous substrate. In both cases h=0 refers to an "interface crack". In terms of the unknown functions

$$f_1(x)=\frac{\partial}{\partial x}(v^+-v^-)\ ,\quad f_2(x)=\frac{\partial}{\partial x}(u^+-u^-)\ , \tag{18}$$

in each case the formulation of the problem may be reduced to a system of integral equations of the form

$$\frac{1}{\pi}\int_{-a}^{a}\sum_{1}^{2}\left[\frac{\delta_{ij}}{t-x}+k_{ij}^{s}(x,t)+k_{ij}^{f}(x,t)\right]f_j(t)dt=\frac{1+\kappa}{2\mu_1(0)}p_i(x)$$

$$(i=1,2),\ -a<x<a \tag{19}$$

where the kernels k_{ij} are known functions which depend on h and the material parameters, k_{ij}^s is associated with the infinite medium, k_{ij}^f represents the geometry of the medium, and

$$p_1(x)=\sigma_{yy}(x,0)\ ,\ p_2(x)=\sigma_{xy}(x,0) \tag{20}$$

are the crack surface tractions which may be expressed in terms of the external load. The kernels k_{ij}^f are bounded for all values of h. For h>0 the functions k_{ij}^s are also bounded. Thus, for h>0 the crack is an embedded crack and (19) would lead to the asymptotic stresses given by (3) and (12) for problems described by Figs. 1a and 1b, respectively. On the other hand, for h=0 in problem 1a the kernels k_{11}^s and k_{22}^s would become a Cauchy kernel $(t-x)^{-1}$ and k_{12}^s and k_{21}^s would degenerate to a delta function $\delta(t-x)$ [28], [29]. Consequently, in this interface crack problem the integral equations become one of the second kind leading to the well-known anomalous stress oscillation behavior very near the crack tips.

For h=0 in problem 1b, however, the leading terms of the kernels k_{ij}^s become

$$k_{11}^s = k_{22}^s = -\frac{\pi\gamma}{8}\frac{|t-x|}{t-x}\ ,$$

$$k_{12}^s = -k_{21}^s = = +\frac{\gamma}{4}\log|t-x|\ ,\ \gamma=\tan\phi_0\ , \tag{21}$$

which would indicate that (19) would remain to be an ordinary system of singular integral equations of the first kind and would have the asymptotic solution given by (12). It is, therefore, seen that the anomalous behavior of the crack tip stress oscillations may be eliminated by "smoothing" the material property distribution (or by removing the property discontinuity). A qualitative description of the interface crack geometries and the singular kernels k_{ij}^s may be seen in Fig. 2.

3.3 Cracking Perpendicular to Interfaces and Surfaces

In ceramic and ceramic/metal FGM components generally a common mode of failure is surface cracking which could penetrate to the interface and cause debonding. The main problem here is assessing the influence of the material inhomogeneity on the fracture mechanics parameters (such as G and k_1) for surface cracks and cracks terminating at an interface. Figures 1c and 1d show the crack geometry for the latter problem in piecewise homogeneous and in inhomogeneous materials. Because of symmetry, generally these are all mode I problems. Thus, if we define the unknown function and the crack surface traction by

$$g(x)=\frac{\partial}{\partial x}[v(x,+0)-v(x,-0)]\ ,\ p(x)=\sigma_{yy}(x,0)\ ,\ a<x<b\ , \tag{22}$$

the integral equation for the general problem may be expressed as

$$\frac{1}{\pi}\int_a^b\left[\frac{1}{t-x}+k_s(x,t)+k_f(x,t)\right]g(t)dt=\frac{1+\kappa_2}{2\mu_2}p(x)\ ,\ a<x<b\ , \tag{23}$$

where, again, k_s is associated with two bonded semi-infinite media, k_f represents the geometry of the composite medium, and k_f is always bounded. For an embedded crack, a>0 and k_s is also bounded. However, for a=0, k_s could be singular. In fact, for a=0 in piecewise homogeneous materials (Fig. 1c) it is known that

$$k_s(x,t)=\frac{c_1}{t+x}+\frac{c_2x}{(t+x)^2}+\frac{c_3x^2}{(t+x)^3}\ ,\ (0<(t,x)<b)\ , \tag{24}$$

where c_1, c_2, and c_3 are bimaterial constants [30]. Note that as t and x approach the end point x=0, k_s tends to infinity and, hence, would contribute to the singular behavior of the solution giving

$$\sigma_{ij}(r,\theta)=\frac{k_1}{r^\alpha}g_{ij}(\theta)\ ,\ 0\le\theta\le\pi\ ,\ (i,j=x,y)\ ,\ 0<\alpha<1 \tag{25}$$

where g_{ij} are known functions, k_1 is a "stress intensity factor" and the power of stress singularity $\alpha>1/2$ for $\mu_2>\mu_1$ and $\alpha<1/2$ for $\mu_2<\mu_1$, $\alpha=1/2$ being the value for $\mu_2=\mu_1$. From the viewpoint of fracture mechanics, the consequence of having $\alpha\neq1/2$ is that as the crack intersects the interface, the stress and deformation states would not remain self-similar and, hence, it would not be possible to use the fracture theories based on the energy balance concept to calculate a strain energy release rate or to use the stress intensity factors as the crack driving force. This, then, is the second anomalous behavior regarding the stress state near the crack tip in bonded dissimilar homogeneous materials.

If we now "smooth" the material property distribution and assume that medium 1 is a FGM (Fig. 1d), it can be shown that for a=0 the leading terms of k_s become [31]

$$k_s(x,t)\cong\frac{d_1t}{t+x}+\frac{d_2x}{t+x}+\frac{d_3tx}{(t+x)^2}+d_4\log(t+x) \tag{26}$$

where $d_1\ldots d_4$ are bimaterial constants. Note that the kernel given by (26) is square integrable and, therefore, would have no contribution to the stress singularity at x=0. Consequently, the stresses would have the standard square-root singularity and, by smoothing the material property distribution through the introduction of FGM, the anomalous behavior of the stress state would again be eliminated.

Figure 3 shows the mode I stress intensity factor for a=0 and $p(x)=-\sigma_0$ in Fig. 1d. The normalized stress intensity factors shown in the figure are defined by

$$k(a)=k_1(0)/\sigma_0\sqrt{b/2}\ ,\ k(b)=k_1(b)/\sigma_0\sqrt{b/2}\ , \tag{27}$$

$$k_1(0) = \lim_{x\to 0}\sqrt{-2x}\sigma_{1yy}(x,0) \ , \quad k_1(b) = \lim_{x\to b}\sqrt{2(x-b)}\sigma_{2yy}(x,0) \ . \tag{28}$$

The shear modulus of FGM in Fig. 1d is assumed to be

$$\mu_1(x) = \mu_2 \exp(\beta x) \tag{29}$$

where μ_2 is constant. It is thus seen that for $\beta\to\infty$ $\mu_1\to 0$ and the problem becomes an ordinary edge crack problem in a homogeneous half space for which

$$k_1(0) \to \infty \ , \ k_1(b) \to 1.5861\sigma_0\sqrt{b/2} \ . \tag{30}$$

For $\beta=0$ the medium is homogeneous and

$$k_1(0) = k_1(b) = \sigma_0\sqrt{b/2} \ . \tag{31}$$

In the other limiting case of $\beta= -\infty$, μ_1 becomes infinite and for the resulting problem of a crack terminating at the interface we have

$$k_1(0) \to 0 \ , \ k_1(b) \to 0.8710\sigma_0\sqrt{b/2} \ . \tag{32}$$

The analytical details and further results for this problem may be found in [31].

3.4 The End Effects

Generally the stress-free ends in bonded materials are locations of high stress concentrations and potential debonding fracture. In bonded dissimilar homogeneous materials the point at which the interface intersects the free boundary (or the apex of two 90 degree bonded wedges) is, in fact, a point of singularity near which the stress state is given by [32]

$$\sigma_{ij}(r,\theta) = \frac{K}{r^{\beta}} F_{ij}(\theta) \ , \ (i,j = x,y) \ , \ 0 < \beta < 1/2 \ , \tag{33}$$

when (r,θ) are the polar coordinates, β and F_{ij} depend on the bimaterial constants and K is a measure of the load amplitude or stress intensity. For β to be positive the material properties need to be discontinuous across the interface. In FGM coatings, since the material properties are made continuous through composition grading, it can be shown that the singularity β becomes zero and, consequently, the stresses become finite.

The effect of stress-free ends is analytically studied in [10] as a part of the general problem of a crack in a layered medium perpendicular to the boundary. The geometry of the problem may be described in Fig. 1d in which the materials 1 and 2 have finite thicknesses and contain collinear cracks along y=0, $-h_1<a_1<x<b_1<0<a_2<b_2<h_2$. For $a_1=-h_1$

or $b_2=h_2$ we have surface cracks whereas for $b_1=0=a_2$ crack crosses the interface. From a viewpoint of stress singularity the latter case corresponds to a stress-free end. It was shown in [10] that in this case the power of singularity is indeed zero, meaning that the stresses are bounded. For all possible crack combinations detailed results are given in [10]. Reference [10] also gives the solution of some crack/contact problems which may arise under thermal or residual stresses or under certain bending/membrane load combinations where the medium may be under compression on the surface and tension in the interior region.

Figure 4 describes the geometry of a specimen considered as an example. The composite medium is assumed to undergo a homogeneous temperature change ΔT. The problem is one of plane strain. The substrate is a nickel-based superalloy (Rene 41) and the coating is either a piecewise homogeneous or a functionally graded metal/ceramic layer, the ceramic component being partially stabilized zirconia (PSZ). The thermomechanical constants of the two materials are

$$E_s=219.7 \text{ GPa}, \nu_s=0.3, \alpha_s=1.67\text{x}10^{-5}\text{°K}^{-1},$$

$$E_c=151 \text{ GPa}, \nu_s=0.3, \alpha_c=10^{-5}\text{°K}$$

where the subscripts s and c refer to the substrate and the ceramic, respectively. The stepwise variation of the material properties in piecewise homogeneous coatings is shown in Fig. 5. Some calculated results are shown in Figures 6-10. For the FGM coating used in the example, the modulus variation is given by

$$E(y) = \begin{cases} E_s, & 0<y<0.0125 \text{ m.} \\ E_c+(E_s-E_c)\left(\dfrac{0.0145-y}{0.002}\right)^p, & 0.0125<0.0145 \text{ m.} \end{cases}$$

The same expression is used for the thermal expansion coefficient, α. Figure 11 shows the thickness variation of the stiffness E(y) (or the thermal expansion coefficient $\alpha(y)$) for the three FGMs considered, namely the metal-rich, linear and ceramic rich compositions.

Figures 6 and 7 show the interface stresses $\sigma_{yy}(x,h_2)$ and $\sigma_{xy}(x,h_2)$ for the piecewise homogeneous coating. Note that since the material properties are discontinuous for $y=h_2$, the interface stresses become unbounded for $y=h_2$, $x\rightarrow l$. The corresponding results for the FGM coatings are shown in Figures 8 and 9. It may be observed that as a result of material property smoothing (or eliminating the property discontinuities), the stress singularities are eliminated and at the point $y=h_2$, $x\rightarrow l$ $\sigma_{yy}(x,h_2)$ becomes bounded and $\sigma_{xy}(x,h_2)$ becomes zero. One may also observe that, except for values of x near the end ($x=l$), the behavior of interface stresses for piecewise homogeneous and FGM coatings are quite similar. Figure 10 shows the variation of the tensile stress $\sigma_{yy}(l,y)$ at the ends of the specimen for $0<y<h_1+h_2$. Note that at the interface $y=h_2$ there is a stress concentration and the stress concentration factor σ_{yy}/σ_0 decreases with increasing metal content of the coating. Further results on this problem may be found in [7].

3.5 The Effect of Material Orthotropy

Due to the nature of processing techniques used, FGM coatings are seldom isotropic. For example, of the two most commonly used techniques, invariably the thermal spray gives a lamellar and electron beam physical vapor deposition technique gives a columnar structure. These structures could clearly be modeled as material orthotropy. From a standpoint of failure mechanics, the main problem is the investigation of the effect of material orthotropy as well as that of material inhomogeneity on, for example, fracture mechanics parameters. The problem is intractable if the elastic parameters are assumed to be independent functions of the space variables. However, (in the case of plane elasticity problems) by replacing the four engineering parameters E_{11}, E_{22}, G_{12} and ν_{12} by a stiffness parameter $E=\sqrt{E_{11}E_{22}}$, a stiffness ratio $\delta=(E_{11}/E_{22})^{1/4}$, an averaged Poisson's ratio $\nu=\sqrt{\nu_{12}\nu_{21}}$, and a shear parameter $\kappa_o=(E/2G_{12})-\nu$, assuming that ν is constant and E_{11}, E_{22} and G_{12} vary proportionately, and by using δ as a scaling constant for the coordinates, displacements and stresses, it was shown that the problem becomes tractable. The solution of mode I crack problem is given in [22] and [24]. The results show that in the mode I problem the stress intensity factors and the strain energy release rate depend on material inhomogeneity and on the elastic parameters ν and κ_o but not on E and δ. The mixed mode crack problem for an orthotropic inhomogeneous medium is studied in [23]. In this case the results depend on δ as well as on ν and κ_o.

3.6 Crack Tip Stress Fields - Isochromatics

Photomechanics in general and photoelasticity in particular has been used very extensively in fracture mechanics primarily to evaluate the stress intensity factors. This is usually done by comparing the quantitative information given by experimentally determined isochromatic fringes with the maximum shear stress calculated in terms of stress intensity factors from the asymptotic expressions for small values of r near the crack tip. In homogeneous materials the technique seems to have been very successful, especially in three-dimensional problems with relatively complex crack geometries. Recent interests in the so-called functionally graded materials, specifically in metal/ceramic composites with smoothly graded thermo-mechanical properties, raise the question of the influence of the material inhomogeneity on the asymptotic behavior of stress state near the crack tips and on the interpretation of the experimental results obtained from photomechanics in terms of such fracture mechanics parameters as stress intensity factors and the strain energy release rate. Some of these concerns are addressed in this project.

It has been shown that the asymptotic behavior of stresses and displacements near the crack tip in inhomogeneous materials is identical to that in homogeneous materials provided the crack is planar, the crack front is a smooth curve and there are no discontinuities in the elastic properties at the crack front (see Section 3.1). However, this identity is valid only for the leading term and only in limit as r tends to zero (see equations 3 and 12). Consequently, for $r > 0$ in graded materials isochromatics could be distorted. Theoretically in inhomogeneous materials, even for small values of r, the

isochromatics corresponding to a given maximum shear stress obtained from the full field solution and that determined by using the asymptotic expressions may not be the same. Since no analytical closed form solution exists for any plane elasticity problem in an inhomogeneous medium containing a crack, to investigate some of these questions one needs to consider a problem which can be solved quite accurately with a minimal computational effort. Such a problem is the mode I collinear plane crack problem for a graded medium with elastic properties varying in the direction parallel to the cracks and subjected to fixed grip loading perpendicular to the cracks [24]. The problem is reduced to an integral equation the kernel of which is evaluated in closed form; and hence the full field solution can be obtained to any desired degree of accuracy. After giving some results regarding the dependence of the stress intensity factors on the material inhomogeneity parameter, material orthotropy and relative dimensions, full field and asymptotic isochromatics are separately calculated at the leading and trailing crack tips and various comparisons are made with the results obtained from the corresponding homogeneous, isotropic elastic medium. The details of the collinear crack solution is given in [24] (see the ARO Technical Report P. 19).

The full-field results for isochromatics obtained from

$$\tau_{\max} = \sqrt{\left(\frac{\sigma_{xx} - \sigma_{yy}}{2}\right)^2 + \sigma_{xy}^2} \tag{34}$$

are given in Figures 12-19 and the comparison of full field and asymptotic results is shown in Figures 20-25. In this problem it is assumed the an isotropic inhomogeneous elastic medium contains a crack along -a<x<a, y=0 and is loaded through fixed grip perpendicular to the plane of the crack. The material inhomogeneity is defined by

$$E(x, y) = E_o e^{\alpha x} \tag{35}$$

where αa is the dimensionless inhomogeneity parameter. Thus, the load amplitude is $\varepsilon_{yy}(x, \mp\infty) = \varepsilon_o$ and the stresses are normalized with respect to $\varepsilon_o E_o$. For reference, Figure 12 shows the isochromatics obtained from the closed form plane strain full-field solution of a cracked homogeneous plane. The curves show the lines of constant maximum shear stress τ_{max} around the crack region. Note that the magnitudes of τ_{max} become greater as the crack tips are approached. The corresponding results for $\tau_{max}/\varepsilon_o E_o$=0.25, 0.35, 0.5 and 1 in an inhomogeneous plate with αa=0.25, 0.5 and 1.0 are given in Figures 13, 14 and 15, respectively. In these figures $\tau_{max}/\varepsilon_o E_o$=0.25 is shown by a dashed line for clarity. For relatively small values of $\tau_{max}/\varepsilon_o E_o$ these figures show clearly the distortion of the isochromatics. Figures 16-19 show the effect of the material inhomogeneity parameter αa on isochromatics for fixed values of $\tau_{max}/\varepsilon_o E_o$=0.25, 0.35, 0.5 and 1.0 where αa=0 given by the dashed line corresponds to a homogeneous medium and is depicted in Figure 12. Note that the isochromatics take the shape of familiar loops only for higher values of τ_{max}.

For relatively high values of τ_{max} the comparison of full-field and asymptotic results is shown in Figures 20-25. Figures show the effect of material inhomogeneity

constant (αa=0, 0.25, 0.5,1.0) on isochromatics near the right and left crack tips (i.e. near y=0, x=a and x=-a) for fixed values of $\tau_{max}/\varepsilon_o E_o$=1, 2, 4, 6 and 10. In these figures the asymptotic results are the first term approximations and, except for the stress intensity factor, are identical to homogeneous results (shown by αa=0). Note that the material inhomogeneity intensifies the stress state at the right crack tip (x/a=1) and diminishes it at the left (x/a=-1). Also note that the discrepancy between asymptotic and full-field results at the right tip is greater than at the left tip and decreases as τ_{max} increases (or as the crack tip is approached). Finally, for a fixed value of αa=0.5 Figure 25 shows the comparison of isochromatics obtained from the full-field (full lines) and asymptotic solutions (dashed lines).

The figures show that even for relatively large τ_{max}'s, in FGMs the distortion in full-field isochromatics from the symmetric loops corresponding to homogeneous materials and given by the asymptotic solutions could be quite significant.

3.7 Benchmark Solutions/Fracture Mechanics

Topics studied in this project may generally be classified in two main groups. The first is the development of fundamental concepts and that of the related analytical or numerical methods of solution. The second deals with the identification and solution of a series of benchmark problems that may have relevance in applications. Sections 3.1 through 3.6 of this report deals with the fundamentals of fracture mechanics of FGMs. In this section some specific benchmark problems studied in the program will be very briefly described. The detailed results have been presented in ARO Technical Project Reports, Journal articles and articles in proceedings listed in Section 8 of this report.

3.7.1 Fracture under thermal stresses

In FGM layers or FGM coatings on homogeneous layers very often the fracture process begins with the formation of microcracks at corrosion pits, surface flaws, or severe stress concentrations. Generally a number of microcracks coalesce and form a dominant surface crack, which would then propagate subcritically under cyclic or sustained loading. In many high temperature applications the loads are thermally induced. Since the medium is inhomogeneous, even a constant change in temperature would cause thermal stresses leading to fatigue, corrosion, or creep crack growth. In the process of subcritical crack propagation, the stress intensity factor at the crack tip is the primary crack driving force. In Reference [P1]* the basic surface crack problem in a metal/ceramic FGM layer under a homogeneous temperature change or a steady-state heat conduction is considered. It is assumed that the thermomechanical properties of the medium vary in thickness direction only. In this problem the main results are the mode-I stress intensity factor calculated as a function of the dimensionless length parameters, material inhomogeneity constants and the temperature amplitudes. The results are given for subsurface as well as surface cracks (see the reprint enclosed for details). In this problem, since the stresses are statically self-equilibrating, the thermal stresses in the

* References [P1] through [P19] refer to the articles and Technical Reports listed in Section 8, "List of Publications"

interior and that near the surfaces would have opposite signs. Thus, a peculiarity of the problem is that, depending on the crack tip location, the crack may propagate under heating or cooling cycle. This generally requires the solution of a nonlinear crack/contact problem to calculate the crack driving force. The solution of this problem is also described in [P1] and some examples are given. The technique used in [P1] is analytical and the results are intended to provide a benchmark for the numerical solution of more complicated crack problems.

The second thermal stress problem studied is concerned with the debonding of a FGM coating from a homogeneous substrate. The substrate is metal (generally a superalloy) and coating is a metal/ceramic composite with graded volume fractions (in the examples considered Rene 41/partially stabilized zirconia). In piecewise homogeneous layered materials with free edges the points of intersection of the interfaces with the boundaries are known to be points of stress singularity, and hence, natural locations of debonding crack initiation [7]. These singularities can be eliminated by removing the material property discontinuities through composition grading. However, even in FGM coatings under thermal loading these points still remain to be locations of relatively high stress concentrations and, consequently, likely sites of interface crack initiation. This problem of interface cracking in a coated medium with free ends under a uniform temperature change was considered previously [P6]. In the current study described in [P2], to simulate the practical applications somewhat more closely and particularly to investigate the effect of partial thermal insulation along the crack surfaces, the coated medium with stress-free ends under steady-state heat flow is considered. It is assumed that the medium contains two symmetrically located edge cracks along the interface and is under plane strain conditions. The surface of the coating on top is exposed to a high temperature convective environment, the surface of the substrate on the bottom is forced-cooled and the ends are under natural convection. To model the partial insulation on the crack surfaces a "heat conductivity index" k^* is introduced ($0 \le k^* \le 1$). The limiting values $k^*=0$ and $k^*=1$ represent, respectively, the perfect insulation and perfect conduction along the crack surfaces.

It was previously shown analytically that in bonded materials by removing the material property discontinuities through composition grading, the anomalous behavior of stress and displacement oscillations near the interface crack tip is also removed and the asymptotic behavior of the stress state at the crack tip becomes identical to that of a crack in a homogeneous medium. Thus, asymptotically the interface crack problem under consideration may be treated as a conventional plane strain crack problem with modes I and II stress intensity factors and the strain energy release rate as the primary fracture mechanics parameters. The main variables in this problem are the material inhomogeneity constants and the crack length. The calculated quantities include the temperature distribution, the total heat flow, the stress intensity factors, the strain energy release rate and the crack opening displacement. The relative crack opening is needed to verify the fact that there is no material interference along the crack surfaces (for details see the technical report enclosed).

The axisymmetric debonding problem of graded thermal barrier coatings under a uniform temperature change is considered in [P8] (see also Appendix B). It is assumed that the disk-shaped specimen consists of a nickel-based superalloy substrate, a NiCrA*l*Y bond coat and a graded PSZ/NiCrA*l*Y thermal barrier coating (TBC). The fracture starts

from the stress concentration at the cylindrical surface along TBC-Bond coat interface and propagates in a plane perpendicular to the axis. The main variables in the problem are the material inhomogeneity parameters, size and location of the crack and the relative dimensions of the specimen. The method of solution and the results are described in [P8] and Appendix B.

3.7.2 The influence of material orthotropy

Generally, in FGM coatings the subcritical crack propagation and spallation-related failures involve two types of cracks, namely a surface crack growing perpendicular to the boundary and a debond crack parallel to the interface. This is partly due to the fact that, because of the techniques used in processing, the graded medium is seldom isotropic and the two crack planes mentioned usually correspond to the principal planes of material orthotropy and, consequently, to relatively weak fracture planes. For example, the materials processed by using plasma spray technique have generally a lamellar structure. Flattened splats and relatively weak splat boundaries provide an oriented material that has a higher stiffness and weaker cleavage planes parallel to the surface. On the other hand, graded materials processed by using an electron beam vapor deposition technique would invariably have a columnar structure, resulting in a higher stiffness in thickness direction and weaker fracture planes perpendicular to the boundary. Clearly, in studying the fracture mechanics of these materials assuming the medium to be isotropic would be rather unrealistic. A closer approximation would be to assume that the inhomogeneous medium is orthotropic with the principal directions parallel and perpendicular to the boundary.

In FGM coatings since the material property grading is usually in the thickness direction and dominant components of the residual and thermal stresses are generally parallel to the boundary, in the first crack problem of interest, namely in the surface crack problem the plane of the crack is a plane of symmetry in material properties as well as in loading. Consequently, the resulting problem is a mode I crack problem for an orthotropic inhomogeneous medium. Such a problem is considered in [P3] which is solved for fixed grip loading away from the crack region and for polynomial crack surface tractions in order to accommodate more general loading conditions. It is assumed that x_1 and x_2 are the principal axes of orthotropy, the crack is located along $x_2=0$, $|x_1|<a$ and material properties vary in x_1 direction only. In the crack problems for orthotropic inhomogeneous materials analytically the problem is intractable if all material parameters are assumed to be variable. However, by replacing the four engineering parameters E_{11}, E_{22}, G_{12}, and ν_{12} by a stiffness parameter $E=\sqrt{E_{11}E_{22}}$, a stiffness ratio $\delta=(E_{11}/E_{22})^{1/4}$, a Poisson's ratio $\nu=\sqrt{\nu_{12}\nu_{21}}$ and a shear parameter $\kappa_o=(E/2G_{12})-\nu$, assuming that ν is constant and the moduli E_{11}, E_{22}, G_{12} vary proportionately, and by using δ as a scaling constant for the coordinates, stresses and displacements, it is shown that the problem becomes tractable and one can study the influence of the material orthotropy on the stress intensity factors and the crack opening displacement. The solution of mode I problem is given in [3]. Some of the main conclusions drawn from this study is that the results depend on the inhomogeneity parameter α and the elastic constants ν and κ_o but not on E_o and δ, where

$E(x_1)=E_o\exp(\alpha x_1)$, and the stress component $\sigma_{22}(x_1,0)$ and the mode I stress intensity factors at the crack tips $x_1=\mp a$ are invariant with respect to a 90° material rotation (see [P3] for details). It is further shown that the results are relatively insensitive to the change in ν.

The mixed mode crack problem that provides a benchmark for debonding problems is considered in [P4]. In this problem again the crack is located along $x_2=0$, $|x_1|<a$ and the same assumptions as in the mode I crack problem are made with regard to the material parameters and scaling. However, here it is assumed that the material properties vary in a direction perpendicular to the plane of the crack. Hence, the plane of the crack is no longer a plane of symmetry and, consequently, the problem is one of mixed mode. The solution is obtained for polynomial crack surface tractions $\sigma_{22}(x_1,0)=\sigma_o(x_1)$ and $\sigma_{12}(x_1,0)=\tau_o(x_1)$, $|x|<a$. The main calculated results are the modes I and II stress intensity factors, the strain energy release rate and the crack opening displacement. Other than the load amplitude, the primary variables are the material inhomogeneity parameter α, the shear parameter κ_o and the stiffness ratio δ. Again, the results are shown to be relatively insensitive to the variation in Poisson's ratio ν. It is found that generally the stress intensity factors increase with increasing α and κ_o and with decreasing δ. The main results are described in [P4]. Extensive numerical results are presented in the technical reports [P14] and [P15].

3.7.3 Spallation of FGM coatings

The basic benchmark problem considered in [P10] consists of a penny-shaped crack parallel to the surface of a semi-infinite graded medium. The problem is an axisymmetric mixed mode problem in which the crack surfaces may be subjected to shear as well as normal tractions. The main objective of the study is to determine the influence of material inhomogeneity constants and the dimensionless length parameter h/a on the stress intensity factors, where h is the distance of the crack from the surface and a is the radius of the crack. The problem is solved analytically by reducing it to a system of singular integral equations. The results are obtained for polynomial normal and shear tractions acting on the crack surfaces. As expected, generally the stress intensity factors increase with decreasing h/a and increasing material inhomogeneity. In addition to extensive results regarding the stress intensity factors, [P10] also includes the corresponding crack opening displacements (see, also, Appendix D).

A nonlinear spallation model is considered in [P7] (see, also, Appendix A). It is assumed that the medium consists of a substrate and an FGM coating, contains an interface crack and the coating is subjected to mechanically or thermally-induced compressive loading parallel to the interface. First by using a nonlinear continuum theory the problem is reduced to an eigenvalue problem and the instability load is evaluated analytically. A finite element technique is then developed to solve the elastic post-buckling problem. The strain energy release rate and stress intensity factors are directly calculated from special crack tip enriched elements.

4. CONTACT MECHANICS OF FGMS

4.1 Basic Concepts

The contact mechanics for a graded elastic medium acted upon by a rigid stamp of arbitrary profile is described in Appendix C. In the most general case of two elastic inhomogeneous solids in contact in the presence of friction, the integral equation of the problem may be expressed as follows:

$$Ap(x)+\frac{B}{\pi}\int_{-a}^{b}\frac{p(t)}{t-x}dt+\int_{-a}^{b}k(x,t)p(t)dt=f(x)\ ,\ a<x<b\ , \tag{36}$$

$$\int_{-a}^{b}p(t)dt=P\ , \tag{37}$$

$$A=\xi\left(\frac{\kappa^{+}(0)-1}{4\mu^{+}(0)}-\frac{\kappa^{-}(0)-1}{4\mu^{-}(0)}\right),\quad B=\frac{\kappa^{+}(0)+1}{4\mu^{+}(0)}+\frac{\kappa^{-}(0)+1}{4\mu^{-}(0)} \tag{38}$$

where P is the resultant compressive force, $p(x)=-\sigma_{yy}(x,0)$, and $q(x)=\eta p(x)=-\sigma_{xy}(x,0)$ are the contact stresses, η is the coefficient of friction, $\mu^{+}(y)$, $\kappa^{+}(y)$, $\mu^{-}(y)$, $\kappa^{-}(y)$ are the elastic parameters of the contacting solids and $-a<x<b$, $y=0$ is the contact area (see the insert in Fig. 30). It is assumed that the curvatures of the contacting solids near the contact zone are smooth $a+b=\ell<<R_I$, where R_1 and R_2 are the radii of curvature (Fig. 26), and both curvatures may be positive or one may be negative. Defining now the sectionally holomorphic function

$$F(z)=\frac{1}{\pi}\int_{-a}^{b}\frac{p(t)}{t-z}dt \tag{39}$$

and by using the Plemelj formulas

$$F^{+}(x)-F^{-}(x)=\begin{cases}2ip(x)\ ,\ -a<x<b\\ 0,\ -\infty<x<-a,\ b<x<\infty\end{cases} \tag{40}$$

$$F^{+}(x)+F^{-}(x)=\begin{cases}\frac{2}{\pi}\int_{-a}^{b}\frac{p(t)}{t-x}dt\ ,\ -a<x<b\\ 4iF(x)\ ,\ -\infty<x<-a\ ,\ b<x<\infty\end{cases} \tag{41}$$

the fundamental solution and the fundamental function of (36) may be obtained as follows:

$$X(z)=(z-b)^{\alpha}(z+a)^{\beta}\ , \tag{42}$$

$$w(x)=(b-x)^{\alpha}(x+a)^{\beta}\ , \tag{43}$$

$$\alpha=\frac{1}{2\pi i}\log\left(\frac{A-iB}{A+iB}\right)+N\ ,\ -1<\mathrm{Re}(\alpha)<1\ , \tag{44}$$

$$\beta=-\frac{1}{2\pi i}\log\left(\frac{A-iB}{A+iB}\right)+M\ ,\ -1<\mathrm{Re}(\beta)<1\ . \tag{45}$$

In (44) and (45) N and M are arbitrary positive or negative integers or zero. The index of the problem is defined by

$$\kappa_o=-(\alpha+\beta)=-(N+M)\ . \tag{46}$$

In the problem under consideration the index is +1, 0 or -1 and is determined from physical considerations. From (44) and (45) it may be seen that

$$\alpha=-\frac{\theta}{\pi}+N\ ,\ \beta=\frac{\theta}{\pi}+M\ ,\ \theta=\arctan\frac{B}{A}\ . \tag{47}$$

After determining the fundamental function w(x), the solution of (36) may be expressed as

$$p(x)=g(x)w(x)\ ,\ -a<x<b \tag{48}$$

where g(x) is an unknown bounded function and is dependent on the geometry and material properties of the contacting media. The arbitrary constants N and M are determined in such a way that, for example, at the end point x=b, Re(α)>0 if the contact is smooth and Re(α)<0 if one of the contacting solids has a sharp corner (implying stress singularity).

4.2 Benchmark Solutions

The detailed solution of the contact problem for a rigid punch acting on a semi-infinite inhomogeneous elastic medium is given in [P16]. The contact problem for a rigid punch and a homogeneous medium coated by a graded layer is considered in [P9] (see also Appendix C). In this section some limited results for two contacting elastic solids are described.

Figure 26 shows the pressure distribution between two homogeneous dissimilar elastic cylinders under frictionless contact obtained by assuming plane strain conditions. Here the main variables are the stiffness ratio $\Gamma = \mu_o^+ / \mu_o^-$ and the curvature ratio $\chi=R_1/R_2$. In this frictionless problem a=b which is unknown and is determined from (37). Similar results for two graded elastic cylinders are given by Figures 27. In this example it is assumed that

$$\mu^+(y) = \mu_o^+ \exp(\gamma^+ x) \ , \ \mu^-(y) = \mu_o^- \exp(\gamma^- x) \tag{49}$$

and, again, ℓ=b+a.

Figures 28-30 show the effect of friction on the contact stress distribution in two contacting inhomogeneous elastic cylinders where it is assumed that $\gamma^-=-\gamma^+$ and $R_1=R_2$. For a constant coefficient of friction $\eta=0.3$ and $R_1=R_2$, Figures 31 and 32 show the effect of the material inhomogeneities γ^+ and γ^- and stiffness ratio Γ on the pressure distribution.

The effect of negative curvature on the contact stresses is shown in Figures 33-36. Figure 33 shows $p(x)=-\sigma_{yy}(x,0)$ for homogeneous cylinders. For a constant curvature ratio the effect of stiffness ratio Γ and coefficient of friction η is shown in Fig. 34. Some results for inhomogeneous cylinders for constant curvature ratio χ and constant coefficient of friction η are shown in Figures 35 and 36.

5. ELASTODYNAMICS OF GRADED MATERIALS

A benchmark problem concerning the elastodynamics in graded materials was considered in [P17] (see, also [P5], [P7] and Appendix E). The problem is a one-dimensional elastodynamic problem for a FGM plate having free-free or fixed/free boundary conditions. The former may approximate the impact problem in an unconstrained layer and the latter may simulate a FGM layer bonded to a very stiff substrate. The impact loading is approximated by a rectangular compressive pulse of a very short duration (0.2 μ sec.). Numerical results are obtained for a 5 mm. Thick Nickel-Zirconia FGM layer, two hypothetical FGMs with $(E_1/E_2)=(1/2)$, $(\rho_1/\rho_2)=1/3$ and $(E_1/E_2)=2$, $(\rho_1/\rho_2)=3$ and, for comparison, a homogeneous Ni plate, where E and ρ are the Young's modulus and mass density, respectively.

For the general variations in density $\rho(x)$ and stiffness E'(x), (E'=E(1-ν)/(1+ν)(1-2ν), the closed form solution is not possible. However, one can obtain an asymptotic solution which appears to be highly accurate.

The problem is first solved by assuming $E'(x)=E_o\exp(\alpha x)$,$\rho(x)=\rho_o\exp(\alpha x)$ giving a constant propagation velocity $c = \sqrt{E_o / \rho_o}$. In this case the solution can be obtained in closed form as well as asymptotically. The comparison of the two results shows that the error in a simple one term asymptotic approximation is less than 2% and a six digit accuracy is obtained by retaining the first six terms in the expansion. Next, a more general material property distribution is considered by assuming $E'(x)=E_o(ax+1)^m$ and $\rho(x)=\rho_o(ax+1)^n$ where $E_o=E'(0)$, $\rho_o=\rho(0)$ and a, m and n are arbitrary constants. It was shown that an estimate of maximum (spallation) stress may be obtained without solving the detailed wave propagation problem. This estimate is $[\sigma_{xx}(x)]_{max}=\sigma_o\varphi_o(x)$ for the

free/free case and $[\sigma_{xx}(x)]_{max}=2\sigma_o\varphi_o(x)$ for the fixed/free case, where σ_o is the amplitude of the input pulse and $\varphi_o(x)=[(ax+1)/a\ell+1)]^{(m+n)/4}$, ℓ being the thickness of the layer $(0<x<\ell)$.

In the general problem for which no closed form solution is feasible, it is shown that one may use the total energy balance as the criterion for the accuracy of the results (or for the convergence of extended asymptotic solutions). In the nondissipative system under consideration the conservation of energy requires that at any given time the total work done by the external loads be equal to the sum of kinetic and strain energies. The calculated results show that the error in this comparison is less than three percent which is within the acceptable range.

6. CONCLUDING REMARKS

From the viewpoint of failure mechanics the *functionally graded materials* seem to offer certain advantages among which one may mention the following:

- By eliminating the discontinuity in material property distributions, the mathematical anomalies regarding the crack tip stress oscillations for the interface cracks and the non-square-root singularities for the cracks intersecting the interfaces are also eliminated. In practice the importance of this result lies in the fact that in FGMs one can now use the crack tip finite element modeling developed for the ordinary square-root singularity and apply the methods of the energy balance-based theories of the conventional fracture mechanics.
- Use of FGMs as coatings and interfacial zones would reduce the magnitude of the residual and thermal stresses.
- Use of FGM coatings and interfaces would eliminate the stress singularities at the points of intersection of interfaces and stres-free ends in bonded materials.
- Replacing homogeneous coatings by FGM layers would both enhance the bonding strength and reduce the crack driving force.

7. BIBLIOGRAPHY

1. T. Hirano, T. Yamada, J. Teraki, M. Niino and A. Kumakawa, Proc. 16th Int. Symp. on Space Technology and Science, Sapporo, Japan, May 1988.

2. M. Yamanouchi, M. Koizumi, T. Hirai and I. Shiota, eds. FGM-90, Proc. of the First Int. Symp. on Functionally Gradient Materials, FGM Forum, Sendai, Japan, 1990.

3. J.B. Holt, M. Koizumi, T. Hirai and Z.A. Munir, eds., Proc. of the Second Int. Symp. on Functionally Gradient Materials, Ceramic Transactions, Vol. 34, American Ceramic Society, Westerville, OH , 1993.

4. B. Ilschner and N. Cherradi, eds., Proc. of the Third Int. Symp. on Structural and Functional Gradient Materials, Presses Polytechniques et Universitaires Romandes, Lausanne, Switzerland, 1995.

5. I. Shiota and Y. Miyamoto, eds., FGM'96 Functionally Graded Materials, Elsevier, 1997.

6. S. Sampath, H. Herman, N. Shimoda and T. Saito, MRS Bulletin, p. 27, January 1995.

7. Y.-D. Lee and F. Erdogan, "Residual/Thermal Stresses in FGM and Laminated Thermal Barrier Coatings," AFOSR Project Report, 1994. (Also published in *Int. J. of Fracture*, Vol. 69, pp. 145-165, 1995).

8. B.H. Rabin and I. Shiota, MRS Bulletin, p. 14, January 1995.

9. K. Kurihara, K. Sasaki and M. Kawarada, FGM-90, p. 65, FGM Forum, Sendai, Japan, 1990.

10. M. Kasmalkar, "The Surface Crack Problem for a Functionally Graded Coating Bonded to a Homogeneous Layer," Ph.D. Dissertation, Lehigh University, Bethlehem, PA 1997.

11. W. Y. Lee, D. P. Stinton, C. C. Berndt, F. Erdogan, Y.-D. Lee and Z. Mutasim, *J. Amer. Ceram. Soc.*, Vol. 79, pp. 3003-3012, 1996.

12. F. G. Friedlander 1946 *Proceedings of the Cambridge Philosophical Society, Mathematical and Physical Sciences* **43**, 360-373

13. F. C. Karal and J. B. Keller 1959 *The Journal of the Acoustical Society of America* **31**, 694-705

14. C. L. Pekeris 1946 *The Journal of the Acoustic Society of America* **18**, 295-315.

15. T. C. Chiu and F. Erdogan, "One-Dimensional Wave Propagation in a Functionally Graded Elastic Medium," *Journal of Sound and Vibration* (in press) 1999.

16. D. M. Rowe, ed., CRC Handbook of Thermoelectrics, Chemical Rubber, Roca Baton, FL 1995.

17. T. Hirai, Functional Gradient Materials, in Materials Science and Technology, R.W. Cahn, P. Haasen & E.J. Kramer, eds. VCH Verlagsgesellschaft mbH, Germany, 1996.

18. F. Erdogan, "Crack Problems in Nonhomogeneous Materials", *Fracture - A Topical Encyclopedia of Current Knowledge*, G.P. Cherepanov, ed., pp. 72-98, Krieger Publishing Company, Malabar, Florida, 1998.

19. N. Konda and F. Erdogan, *Engineering Fracture Mechanics*, Vol. 47, pp. 533-545, 1994.

20. F. Delale and F. Erdogan, *ASME Journal of Applied Mechanics*, Vol. 50, pp. 609-614, 1983.

21. M. Ozturk and F. Erdogan, *ASME Journal of Applied Mechanics*, Vol. 60, pp. 406-413, 1993.

22. M. Ozturk and F. Erdogan, Int. J. Engng. Sci., Vol. 35, pp. 869-883, 1997.

23. M. Ozturk and F. Erdogan, "Mixed-Mode Crack Problem in an Inhomogeneous Orthotropic Medium", *International Journal of Fracture* (in press), 1999.

24. M. Ozturk and F. Erdogan, "The Collinear Crack Problem in an Inhomogeneous Orthotropic Medium", ARO Technical Report, Grant No. DAAH04-95-1-0232, 1998.

25. A. Sahin and F. Erdogan, "Axisymmetric Crack Problem in a Functionally Graded Semi-Infinite Medium," Proc. 8th Japan-U.S. Conference on Composite Materials, G. Newaz and R.F. Gibson, eds., pp. 189-198, 1998.

26. F. Erdogan and B-H. Wu, *ASME J. Appl. Mech.*, Vol. 64, pp. 449-456, 1997.

27. F. Erdogan and B.H. Wu, "Crack Problems in FGM Layers Under Thermal Stresses", *Journal of Thermal Stresses*, Vol. 19, pp. 237-265, 1996.

28. F. Erdogan and G.D. Gupta, *Int. J. Solids Structures*, Vol. 7, pp. 39-61, 1971.

29. F. Erdogan and G.D. Gupta, *Int. J. Solids Structures*, Vol. 7, pp. 1089-1107, 1971.

30. T.S. Cook and F. Erdogan, *Int. J. Engng. Sci.*, Vol. 10, pp. 667-696, 1972.

31. F. Erdogan, A.C. Kaya and P.F. Joseph, *ASME Journal of Applied Mechanics*, Vol. 58, pp. 40-418, 1991.

32. F. Erdogan and V. Biricikoglu, *Int. J. Engng. Sci.*, Vol. 11, pp. 645-766, 1973.

8. LIST OF PUBLICATIONS

8.1 Journal Articles

P.1 F. Erdogan and B.H. Wu, "Crack Problems in FGM Layers Under Thermal Stresses", *Journal of Thermal Stresses*, Vol. 19, pp. 237-265, 1996.

P.2 Y.D. Lee and F. Erdogan, "Interface Cracking of FGM Coatings Under Steady-State Heat Flow", *Engineering Fracture Mechanics*, Vol. 59, pp. 361-380, 1998.

P.3 M. Ozturk and F. Erdogan, "Mode I Crack Problem in an Inhomogeneous Orthotropic Medium, *Int. J. Engng. Sci.*, Vol. 35, pp. 869-883, 1997.

P.4 M. Ozturk, F. Erdogan, "Mixed-Mode Crack Problem in an Inhomogeneous Orthotropic Medium", *International Journal of Fracture*, 1999 (in press).

P.5 T.C. Chiu and F. Erdogan, "One-Dimensional Wave Propagation in a Functionally Graded Elastic Medium", *Journal of Sound and Vibration*, 1999 (in press).

P.6 Y.D. Lee and F. Erdogan, "Interface Cracking of Graded Coatings", *International Journal of Fracture*, 1999 (in press).

8.2 Articles in Proceedings

P.7 T.C. Chiu and F. Erdogan, "Spallation of FGM Coatings - A Nonlinear Model", *Proc. 8th Japan-U.S. Conf. On Composite Materials*, G.M. Newaz and R.F. Gibson, eds., pp. 365-373, 1998.

P.8 B. Yildirim and F. Erdogan, "Interface Cracking of FGM Coatings Under Uniform Thermal Loading", *Proc. 8th Japan-U.S. Conf. On Composite Materials*, G.M. Newaz and R.F. Gibson, eds., pp. 388-396, 1998.

P.9 M.A. Guler and F. Erdogan, "Contact Mechanics of FGM Coatings", *Proc. 8th Japan-U.S. Conf. On Composite Materials*," G.M. Newaz and R.F. Gibson, eds. pp. 397-408, 1998.

P.10 A. Sahin and F. Erdogan, "Axisymmetric Crack Problem in a Functionally Graded Semi-Infinite Medium", *Proc. 8th Japan-U.S. Conference on Composite Materials*, G. M. Newaz and R.F. Gibson, eds., pp. 189-198, 1998.

P.11 T.C. Chiu and F. Erdogan, "Wave Propagation in a Functionally Graded Elastic Medium", *Proc. 8th Japan-U.S. Conference on Composite Materials*, G.M. Newaz and R.F. Gibson, eds., pp. 374-382, 1998.

P.12 F. Erdogan and M. Ozturk, "The Mixed-Mode Crack Problem in an Orthotropic Graded Medium," *Proc. 14th U.S. Army Symposium on Solid Mechanics*, K.R. Iyer and S.-C. Chou, eds., pp. 336-343, 1996.

8.3 Technical Project Reports

P.13 Y.D. Lee and F. Erdogan, "Interface Cracking of FGM Coatings Under Steady-State Heat Flow," 1996.

P.14 M. Ozturk and F. Erdogan, "Mode I Crack Problem in an Inhomogeneous Orthotropic Medium," 1996.

P.15 M. Ozturk and F. Erdogan, "Mixed-Mode Crack Problem in an Inhomogeneous Orthotropic Medium," 1996.

P.16 M.A. Guler and F. Erdogan, "The Problem of a Rigid Punch with Friction on a Graded Elastic Medium", 1997.

P.17 T.C. Chiu and F. Erdogan, "One-Dimensional Wave Propagation in a Functionally Graded Medium," 1997.

P.18 A. Sahin and F. Erdogan, "The Axisymmetric Crack Problem in a Semi-Infinite Nonhomogeneous Medium," 1997.

P.19 M. Ozturk and F. Erdogan, "The Collinear Crack Problem in an Inhomogeneous Orthotropic Medium," 1998.

9. SCIENTIFIC PERSONNEL

F. Erdogan, P.I., Professor of Mechanics, Lehigh University
Dr. Y.D. Lee, Post-Doctoral Associate (part-time)
Dr. M. Ozturk, Post-Doctoral Associate/Research Engineer (part-time)
M. Kasmalkar, Research Assistant (Ph.D. Candidate, part-time)
M.A. Guler, Research Assistant (M.S. and Ph.D. Candidate, part-time)
T.C. Chiu, Research Assistant (M.S. and Ph.D. Candidate, part-time)
A. Sahin, Research Assistant (M.S. and Ph.D. Candidate, part-time)
B. B. Yildirim, Research Assistant (M.S. and Ph.D. Candidate, part-time)

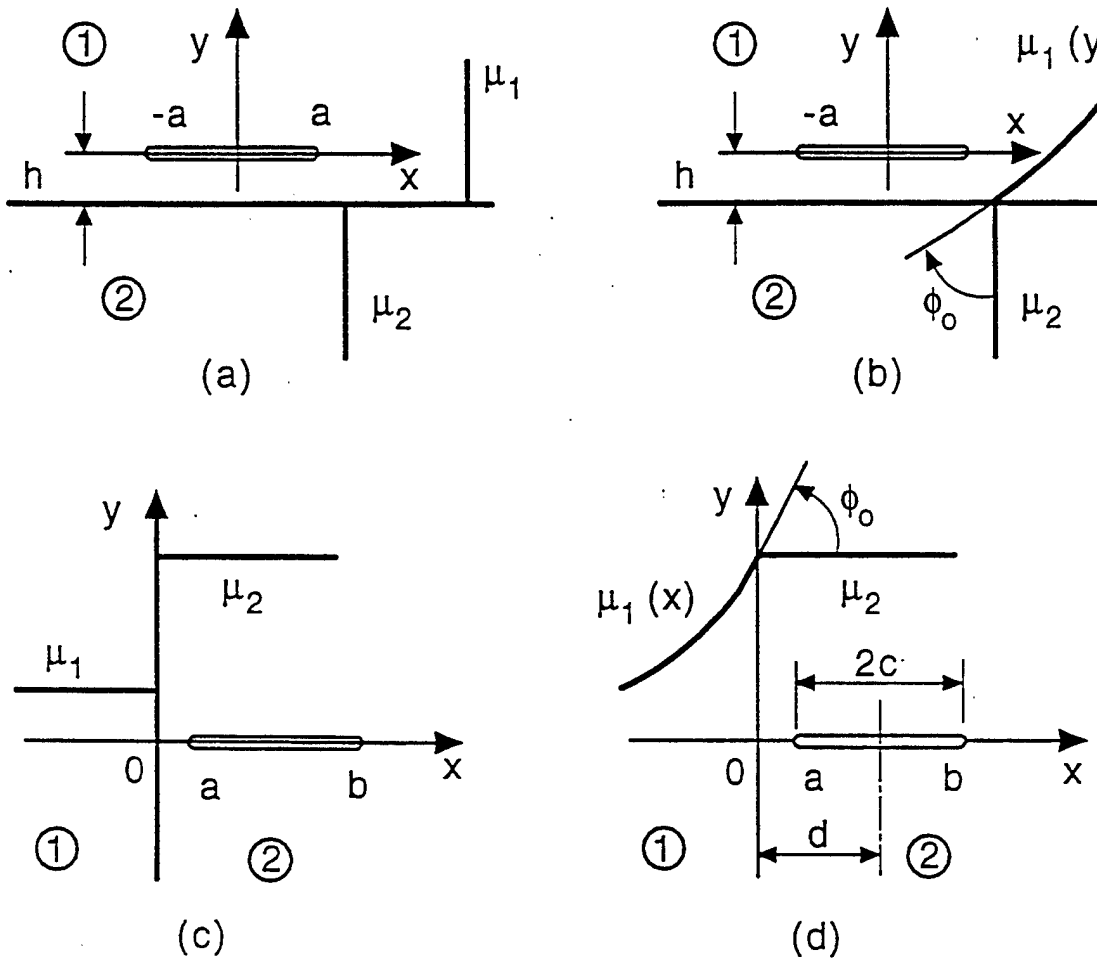

Figure 1 Geometry and notation for a plane crack in bonded homogeneous and nonhomogeneous materials

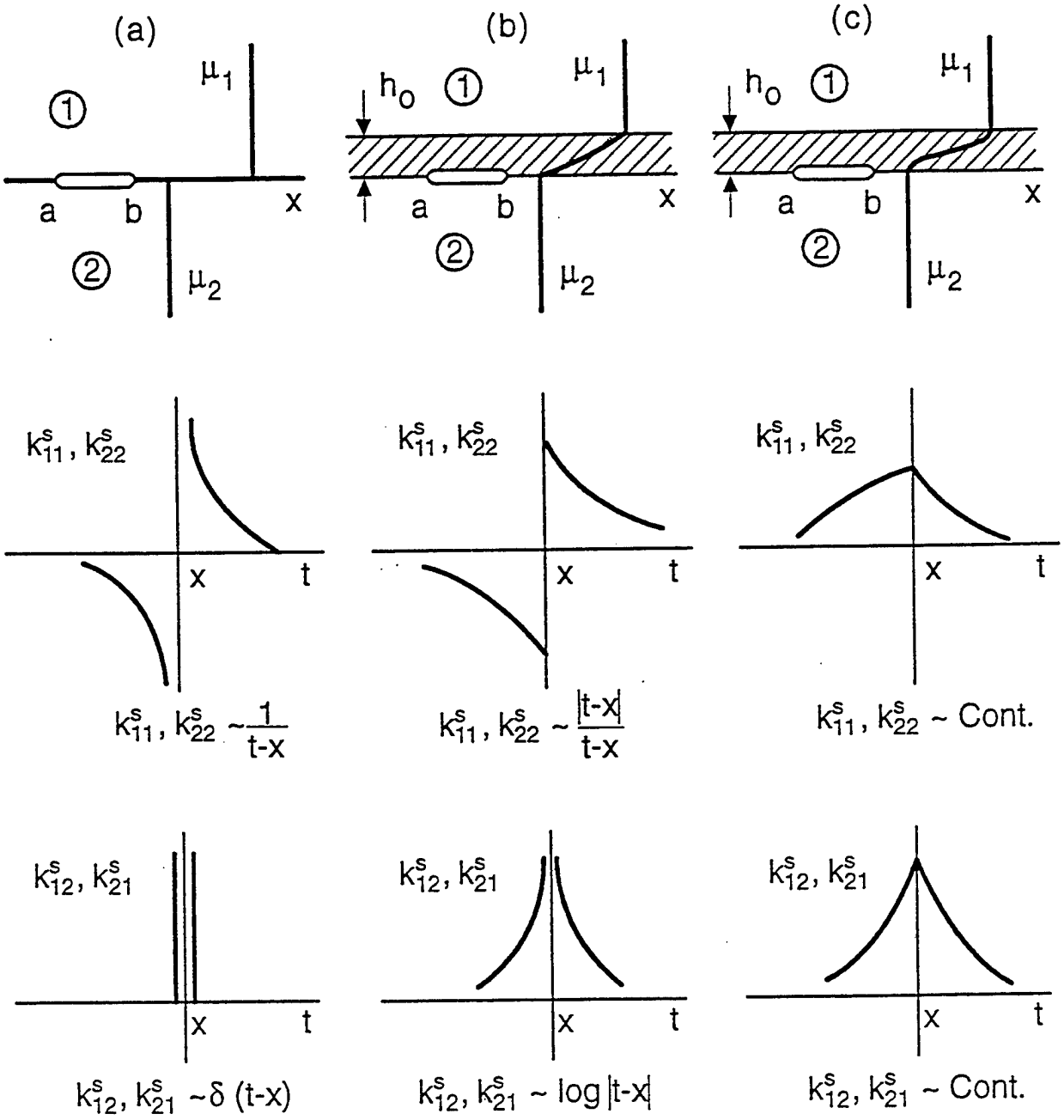

Figure 2 Singular behavior of the irregular kernels for an interface crack in bonded dissimilar materials.

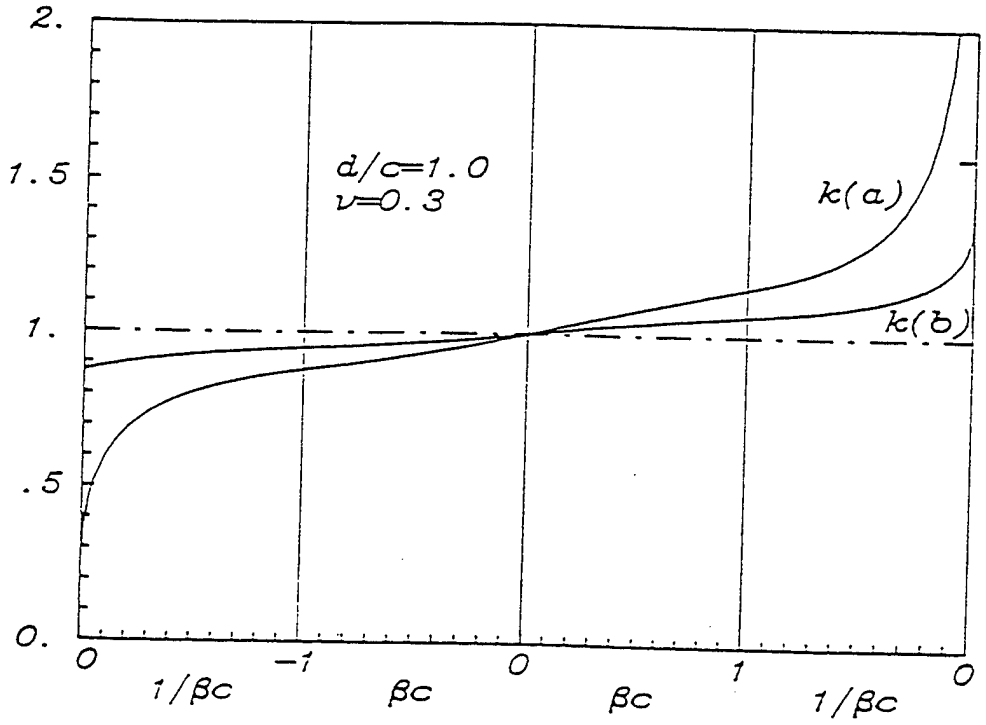

Figure 3 Normalized stress intensity factors for a plane crack terminating at the interface between a homogeneous medium and a FGM half space.

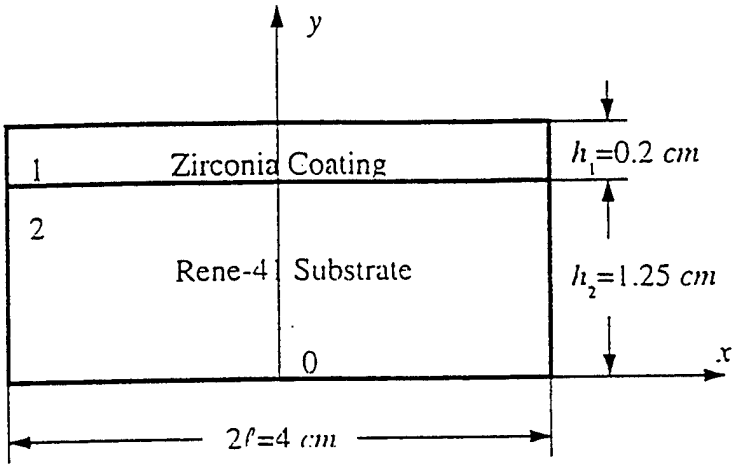

Figure 4 The geometry of the coating/substrate considered as an example.

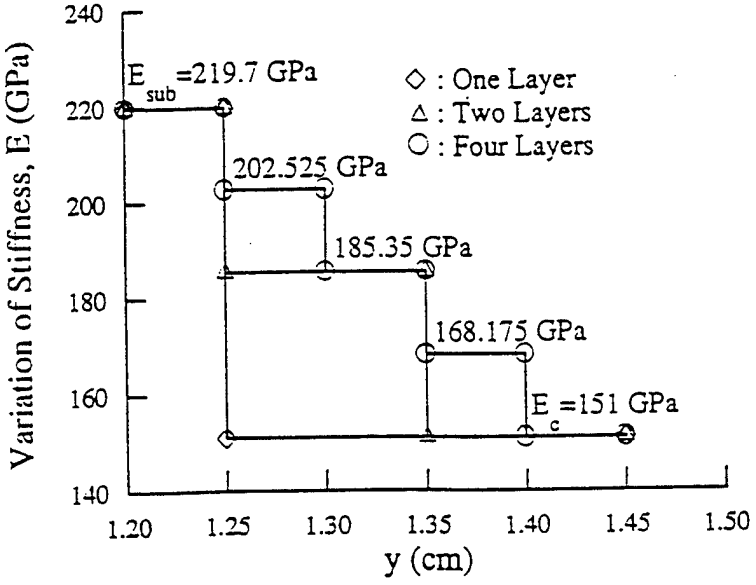

Figure 5 Stepwise distribution of the elastic modulus for a single, two and four layer homogeneous coatings.

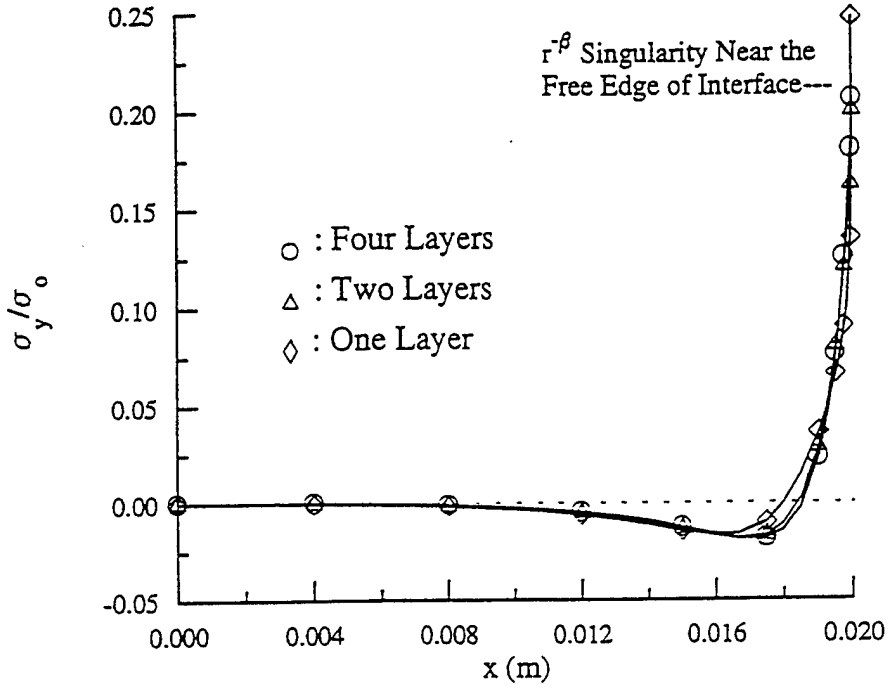

Figure 6 Variation of normalized σ_y along the 1st interface of laminated homogeneous coatings; $\sigma_0 = E_s\alpha_s\Delta T$.

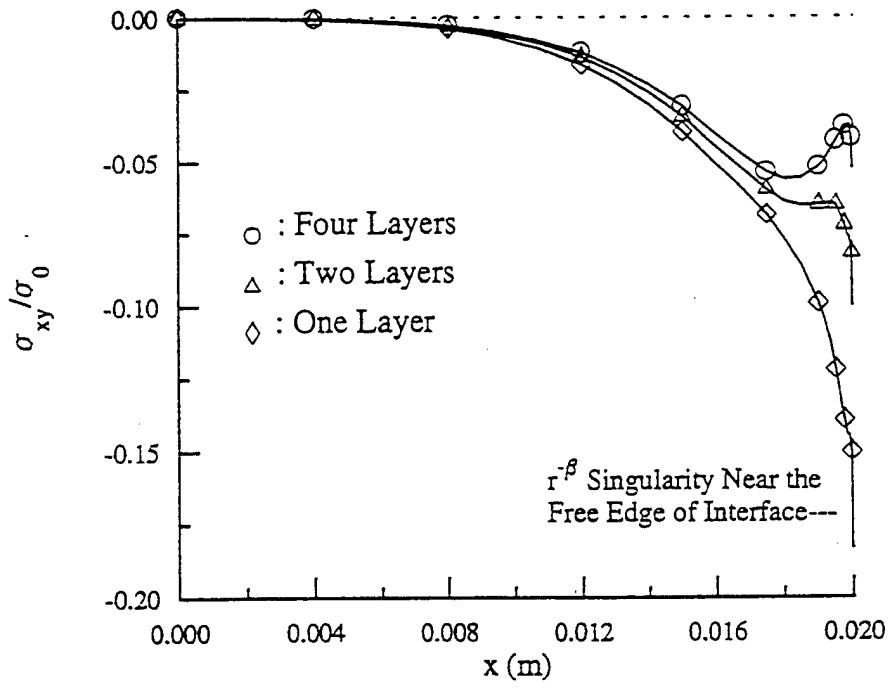

Figure 7 Variation of normalized σ_{xy} along the 1st interface of laminated homogeneous coatings; $\sigma_0 = E_s\alpha_s\Delta T$.

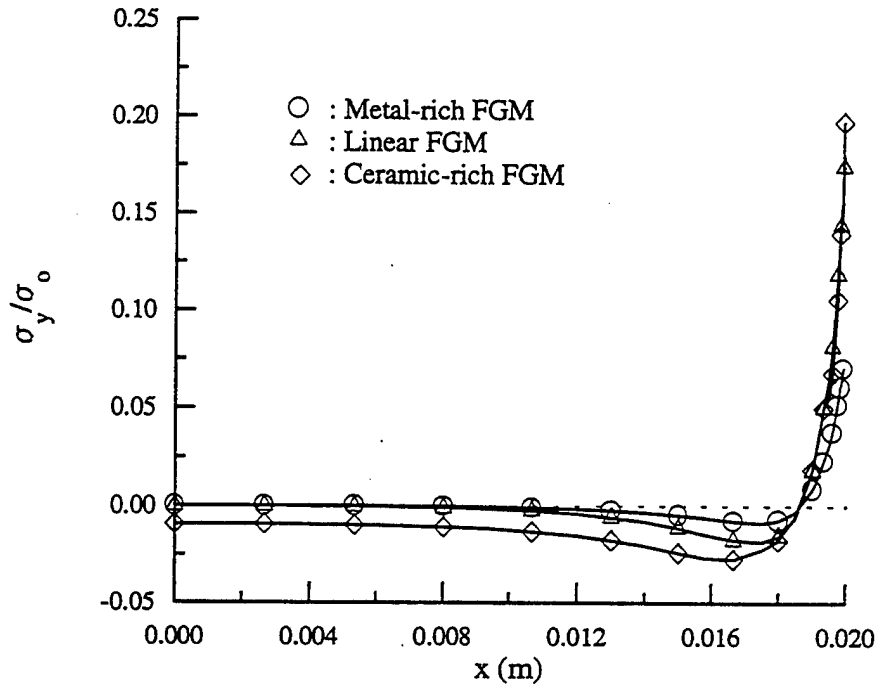

Figure 8 Variation of normalized σ_y along the interface $y = 0.0125$m for FGM coatings; $\sigma_0 = E_s\alpha_s\Delta T$.

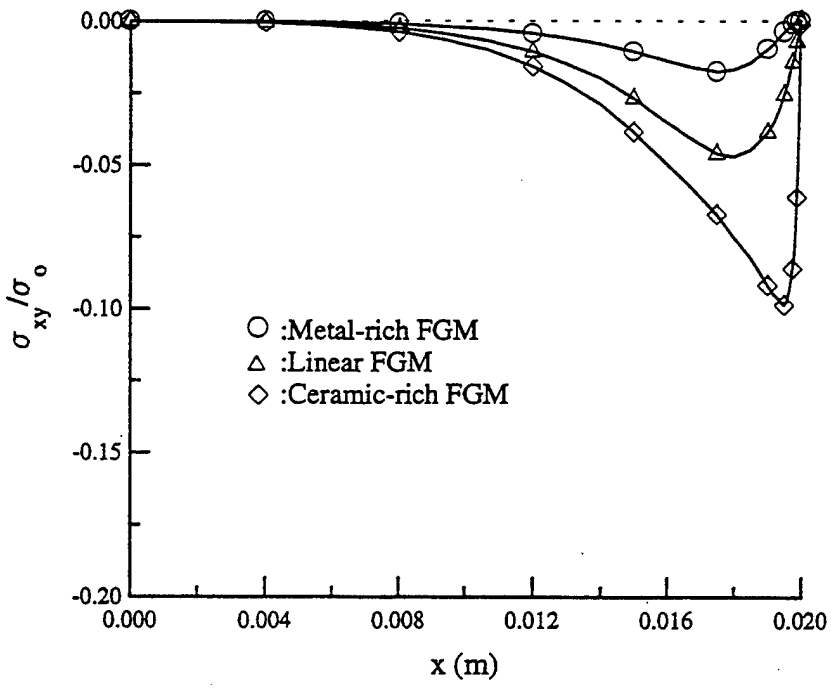

Figure 9 Variation of normalized σ_{xy} along the interface $y = 0.0125$m for FGM coatings; $\sigma_0 = E_s\alpha_s\Delta T$.

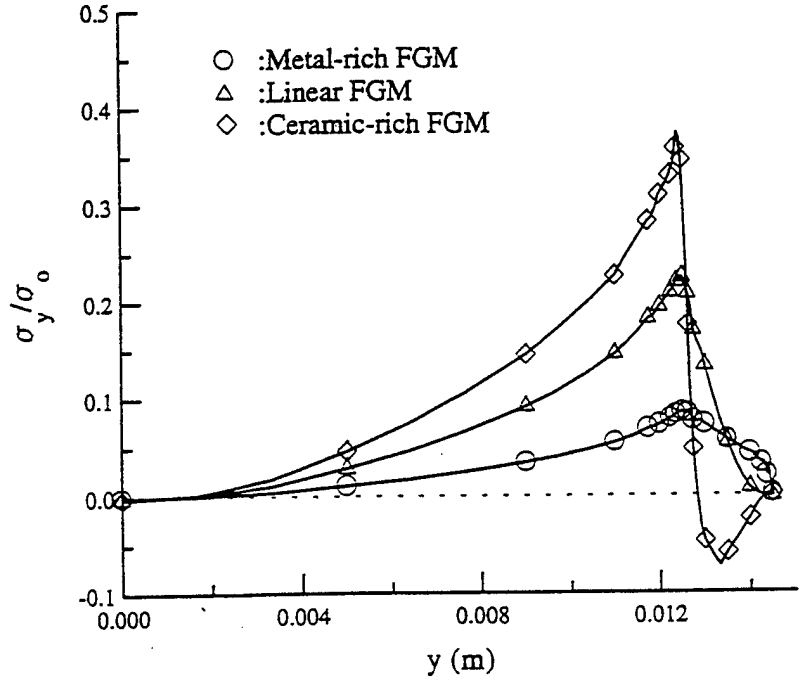

Figure 10 Variation of normalized σ_y along the end $x = \ell = 0.02$m for FGM coatings; $\sigma_0 = E_s\alpha_s\Delta T$.

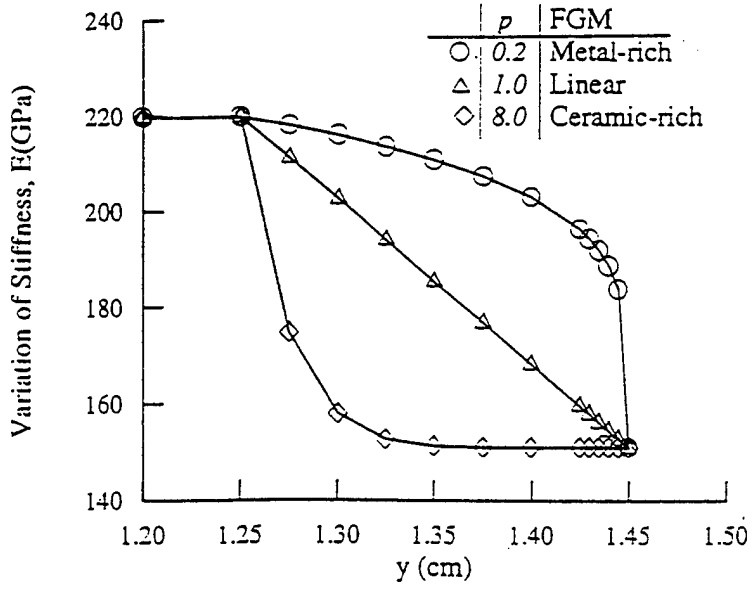

Figure 11 Distribution of the elastic modulus $E(y)$ for the FGM coatings.

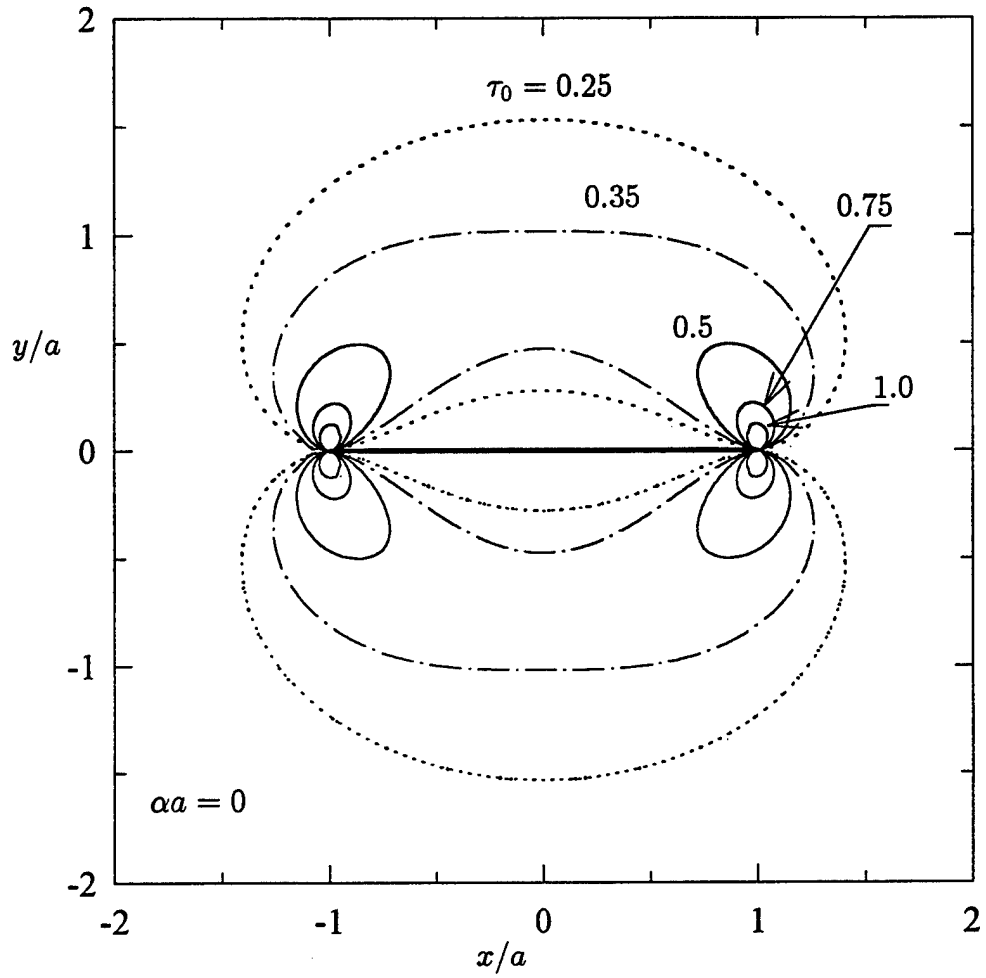

Figure 12 Isochromatics in a cracked homogeneous medium under uniform tension, $\sigma_{yy}(x,0) = -\sigma_0$, $\tau_0 = \dfrac{\tau_{\max}}{\sigma_0}$.

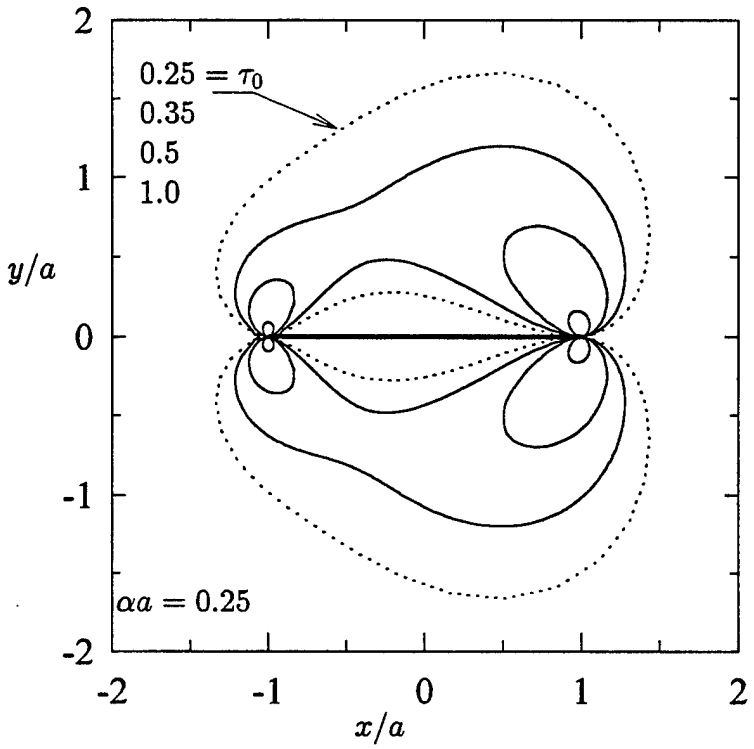

Figure 13 Isochromatics in an inhomogeneous medium under mode I fixed grip loading away from the crack region, $\tau_0 = \frac{\tau_{\max}}{\sigma_0}$, $\nu = 0.3$, $E(x) = \dot{E}_0 \exp(\alpha x)$.

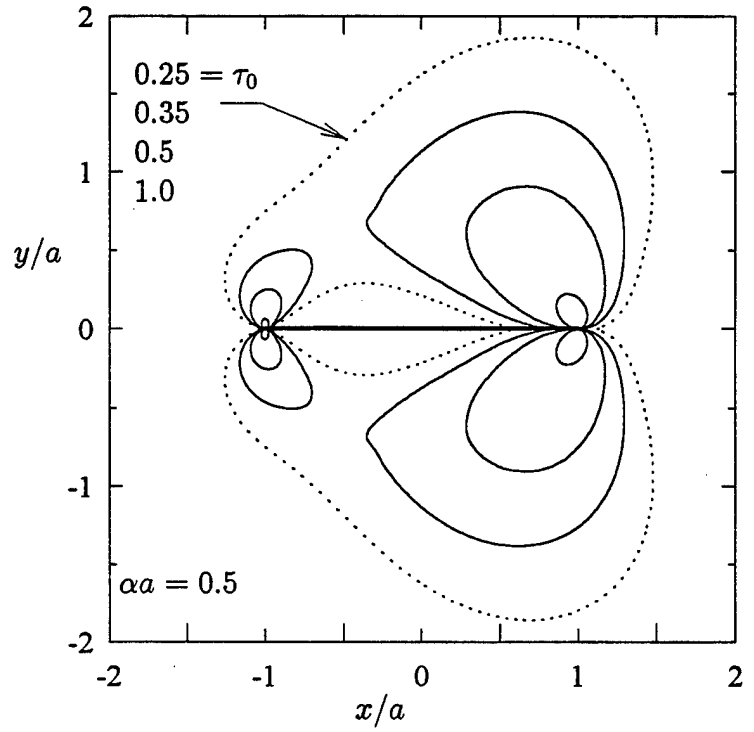

Figure 14 Same as Figure 13

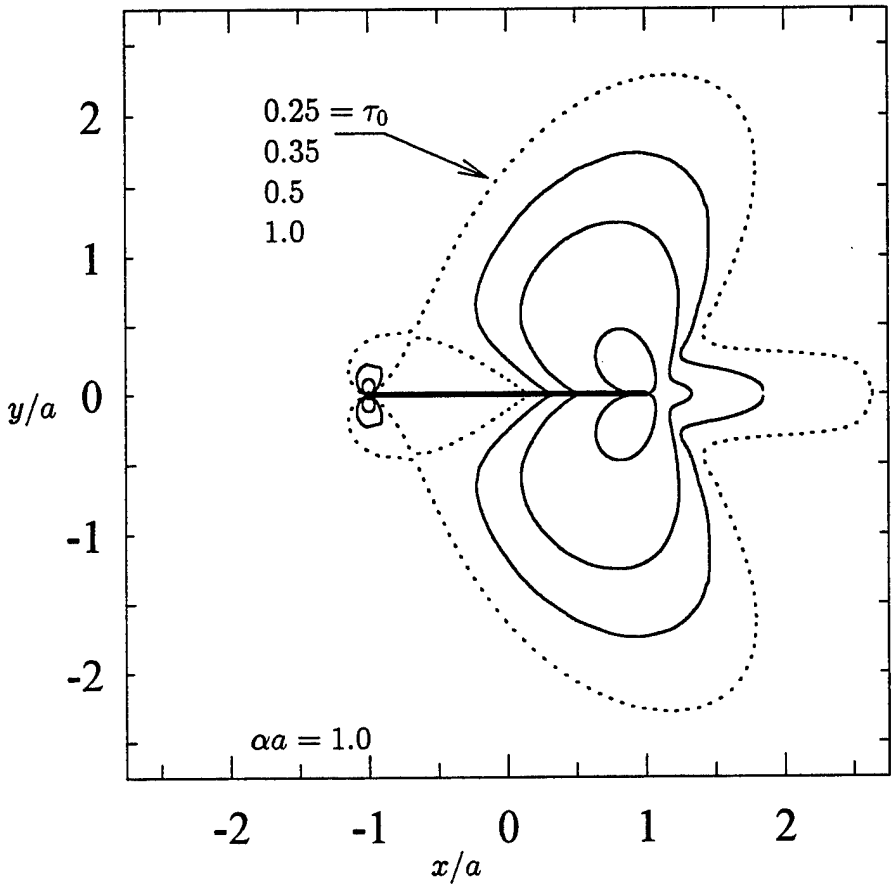

Figure 15 Same as Figure 13

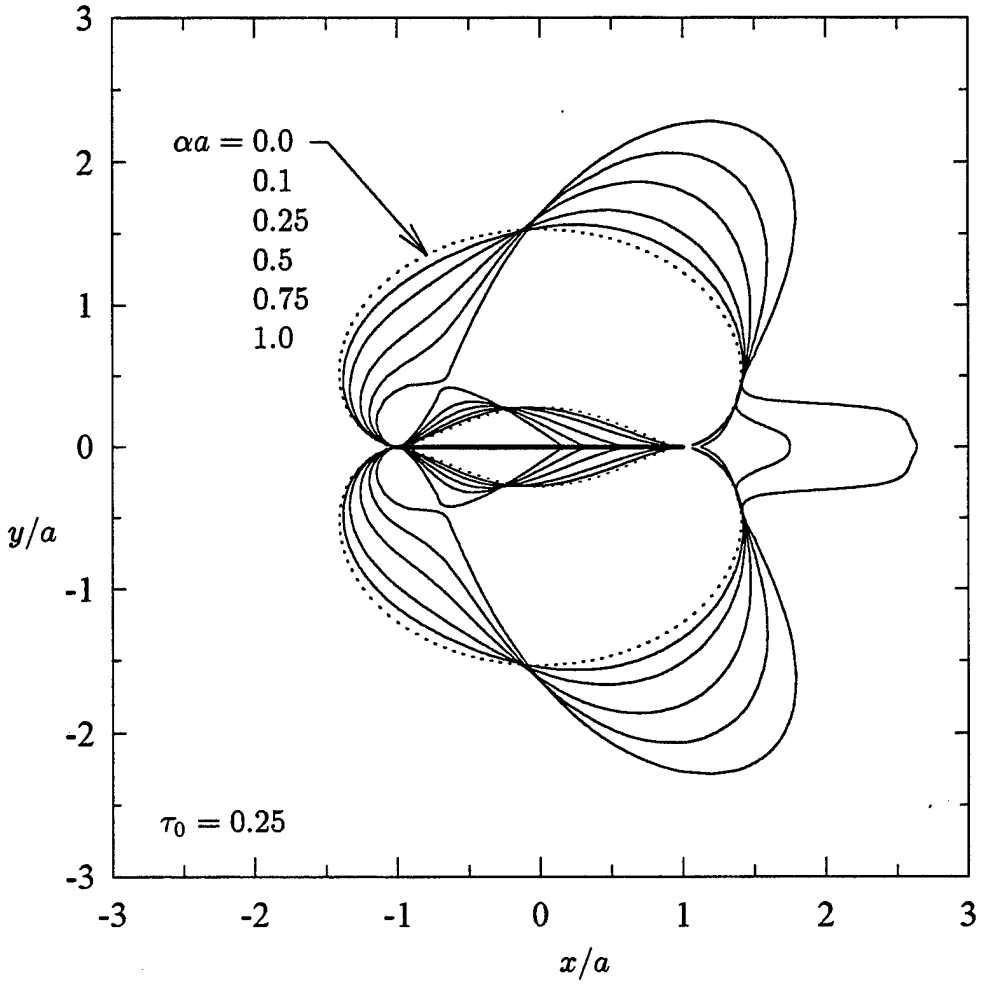

Figure 16 The effect of the inhomogeneity parameter αa on the isochromatics in an inhomogeneous medium under mode I fixed grip loading, $\tau_0 = \frac{\tau_{\max}}{\varepsilon_0 E_0}$, $\nu = 0.3$,

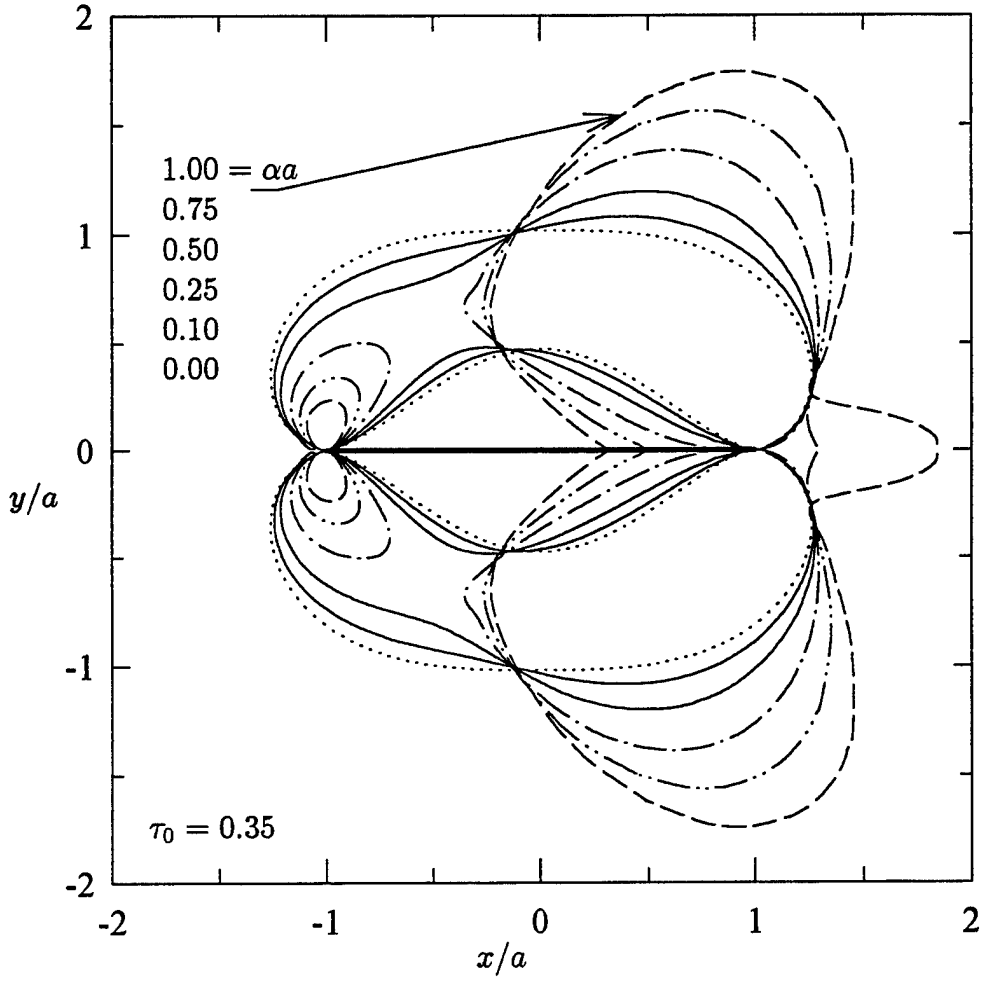

Figure 17 Same as Figure 16

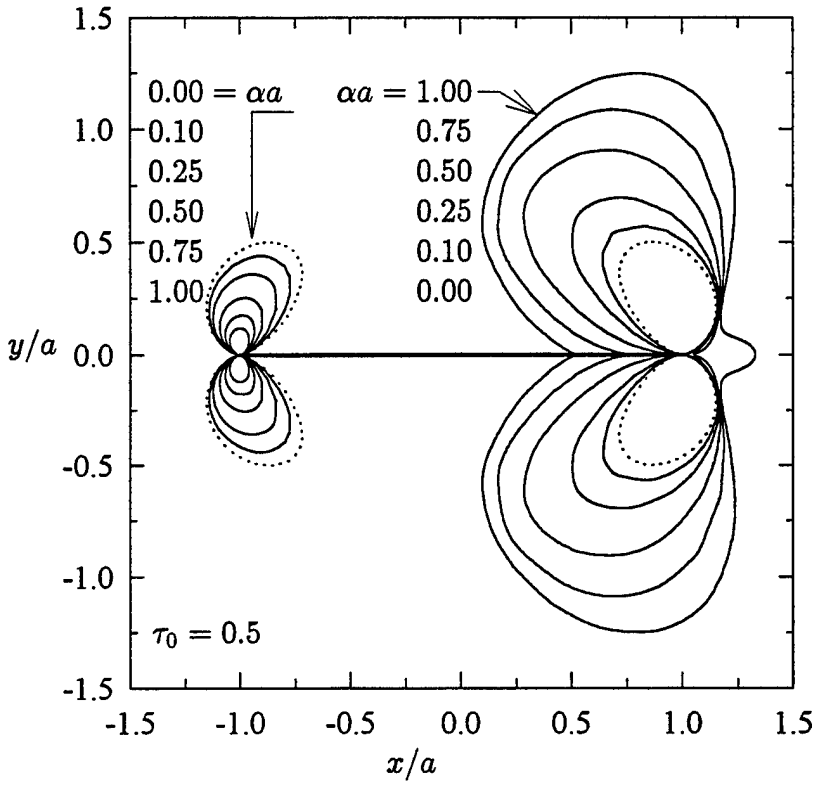

Figure 18 Same as Figure 16

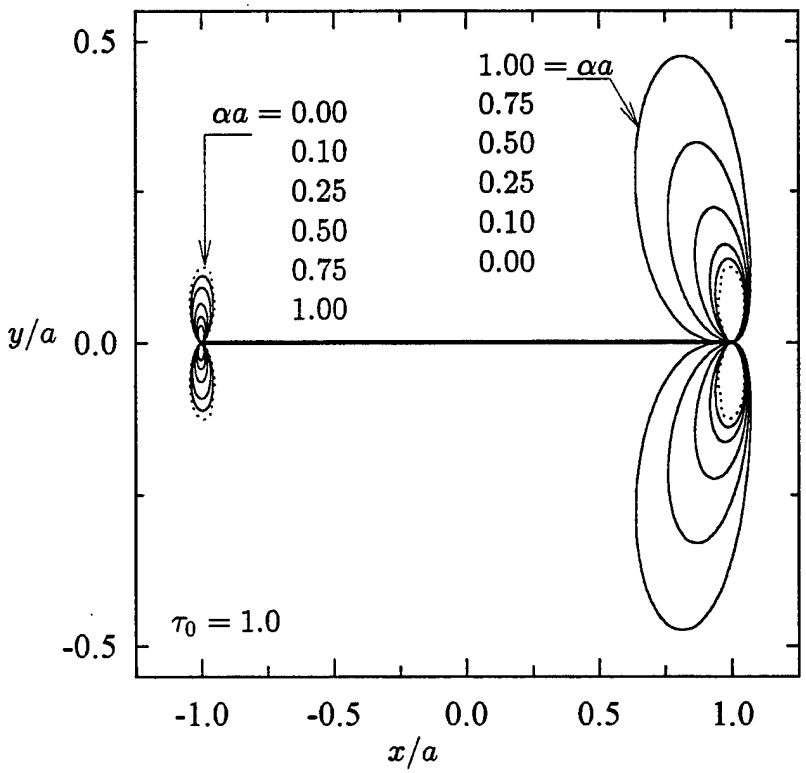

Figure 19 Same as Figure 16

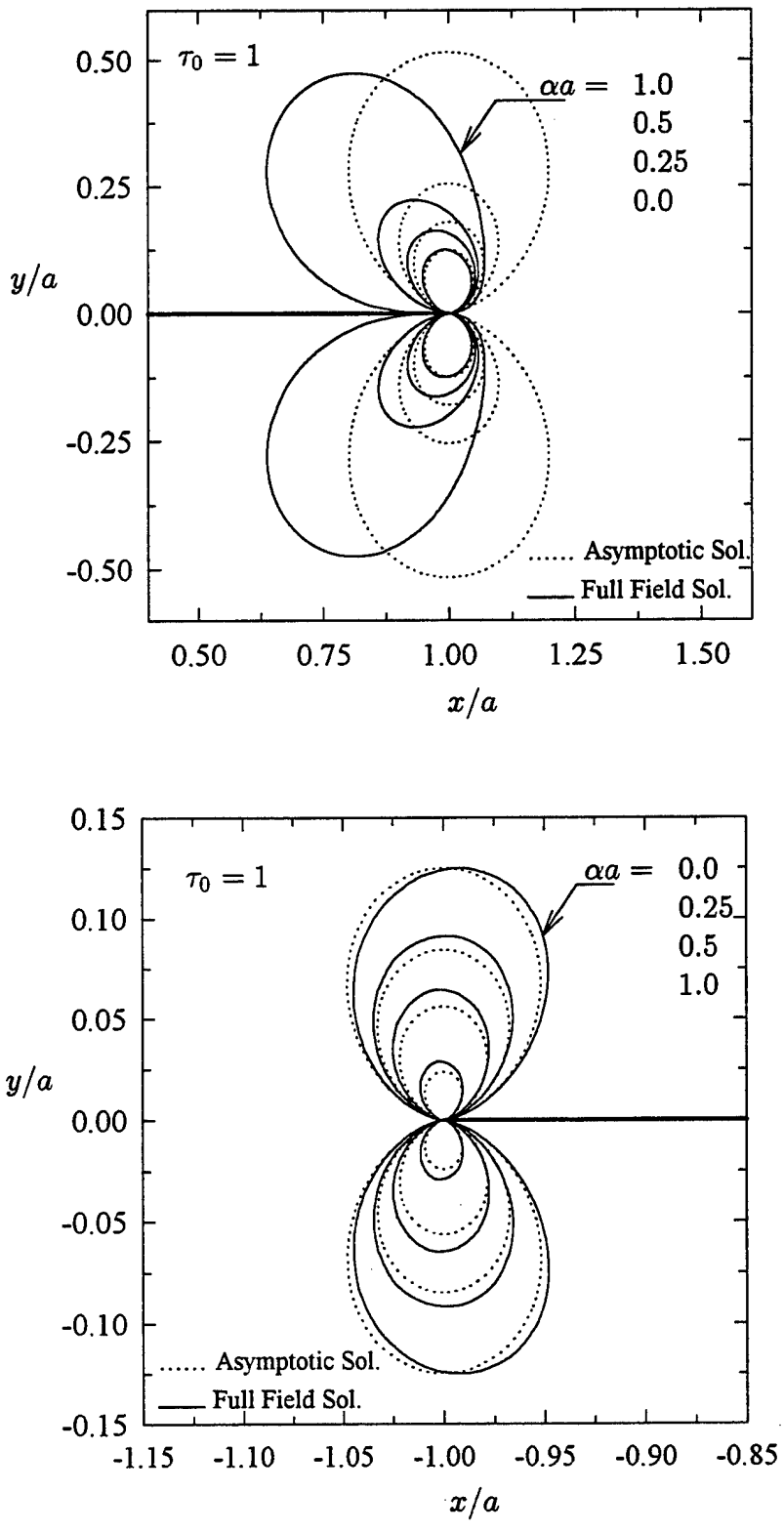

Figure 20 Same as Figure 19 with different scales for the right and left crack tip regions.

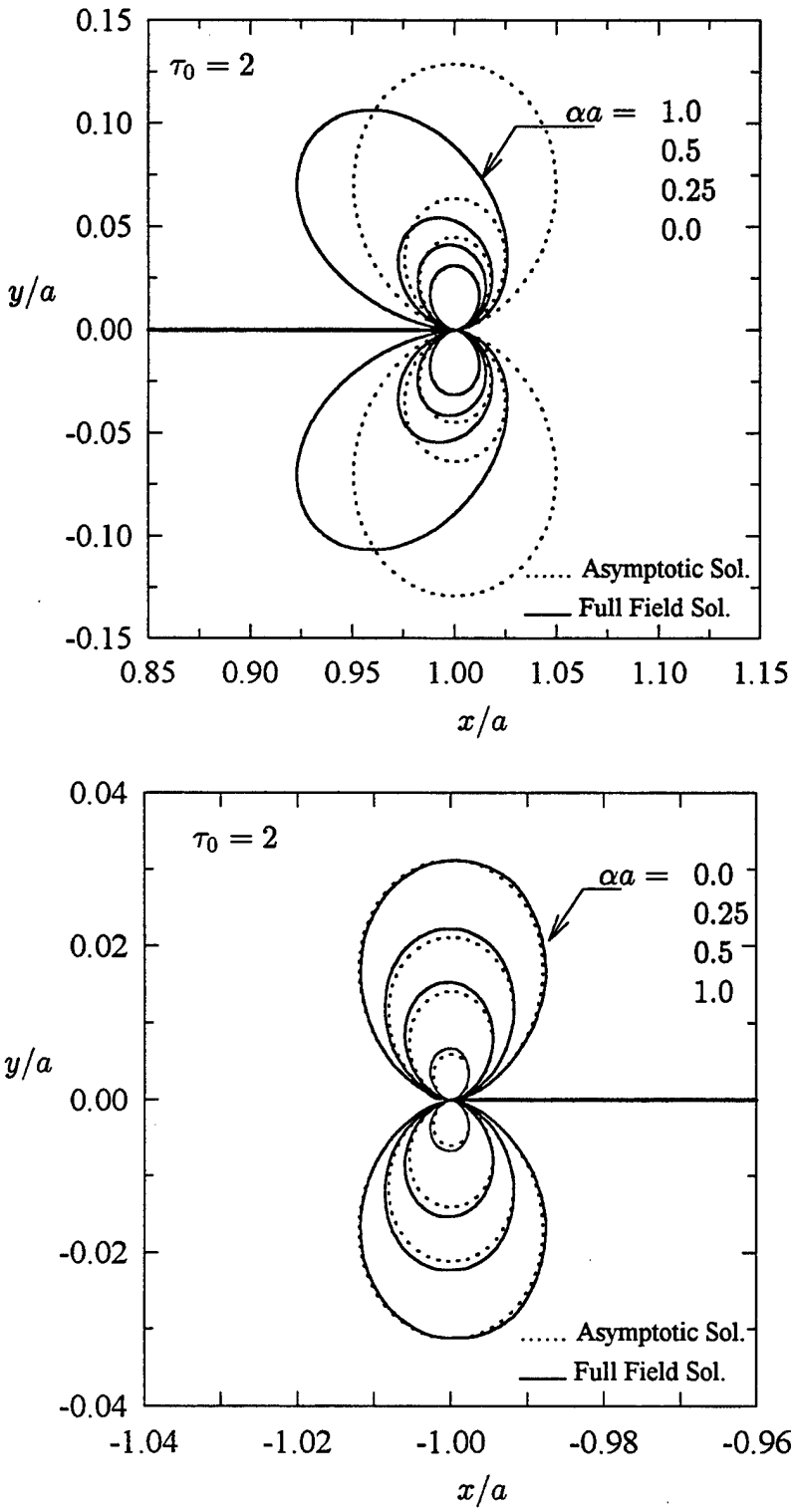

Figure 21 Same as Figure 20

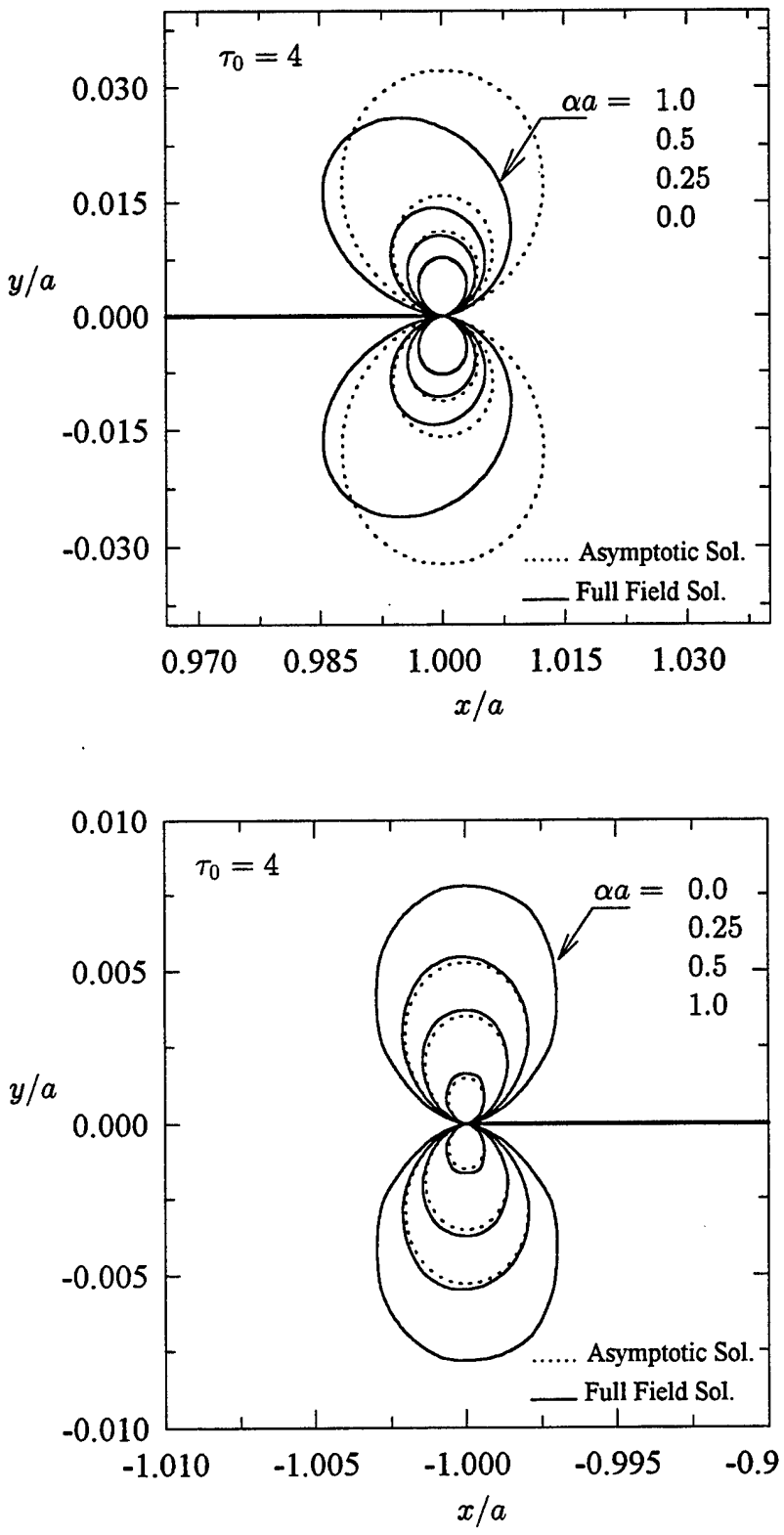

Figure 22 Same as Figure 20

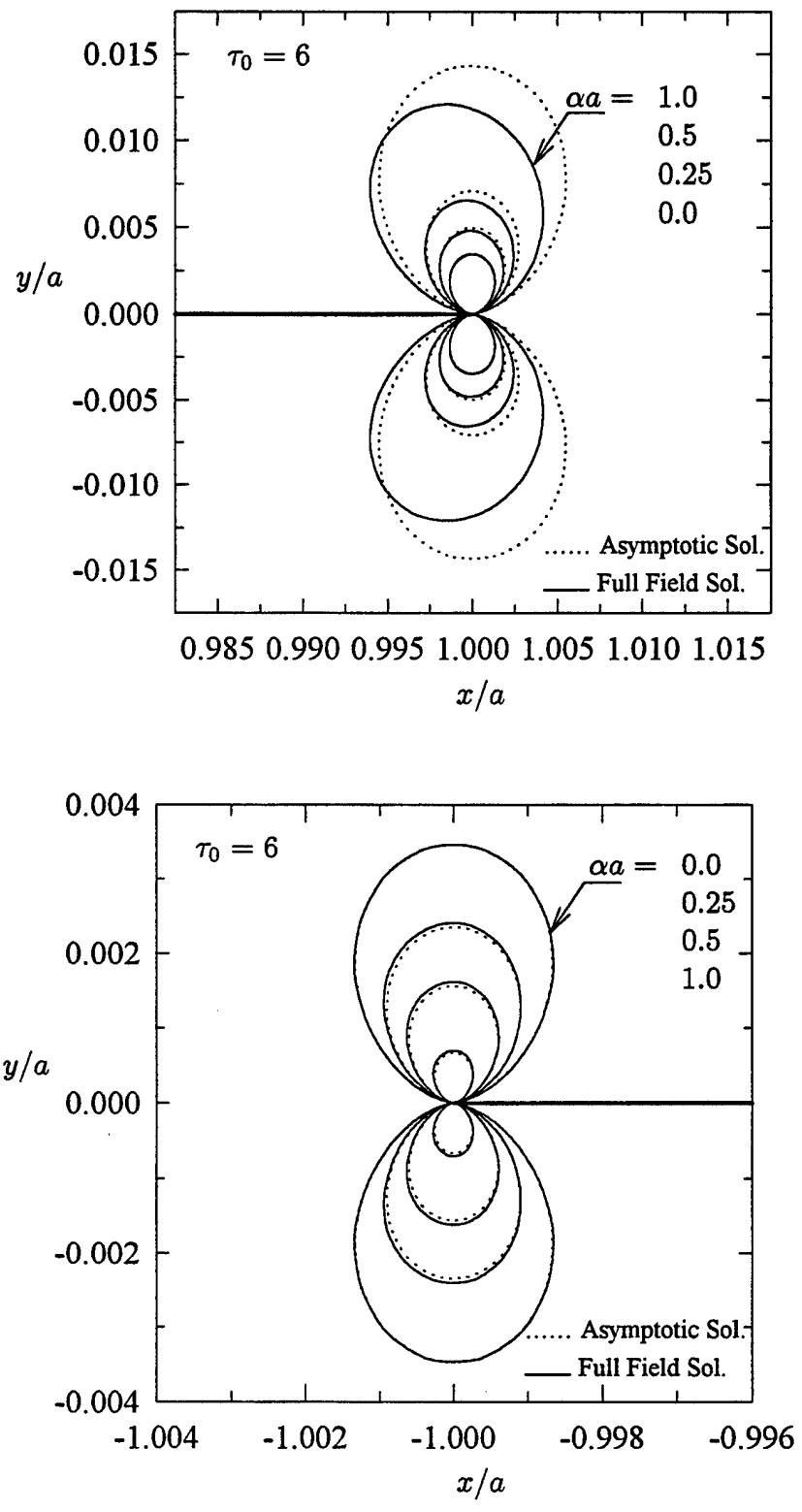

Figure 23 Same as Figure 20

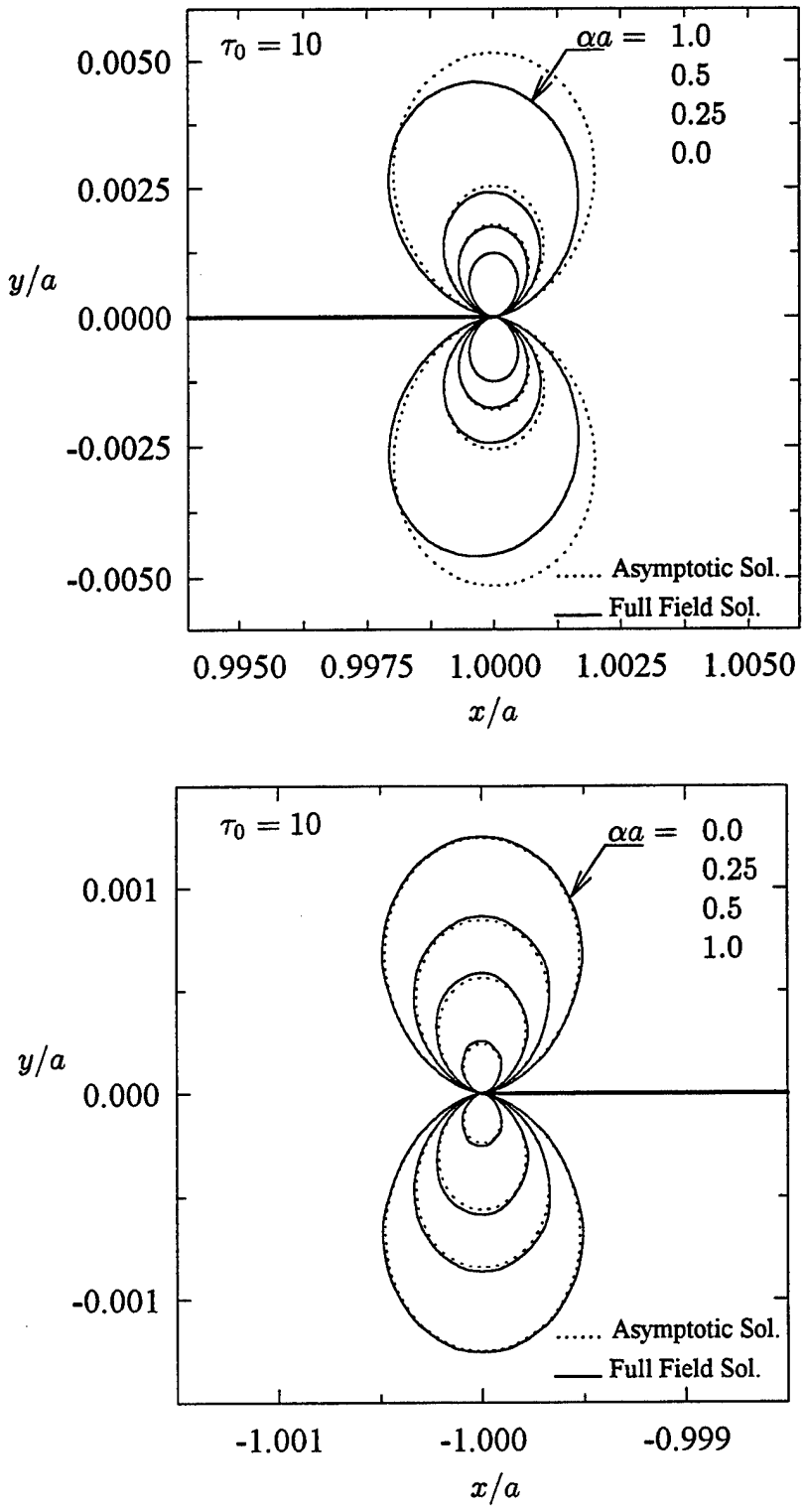

Figure 24 Same as Figure 20

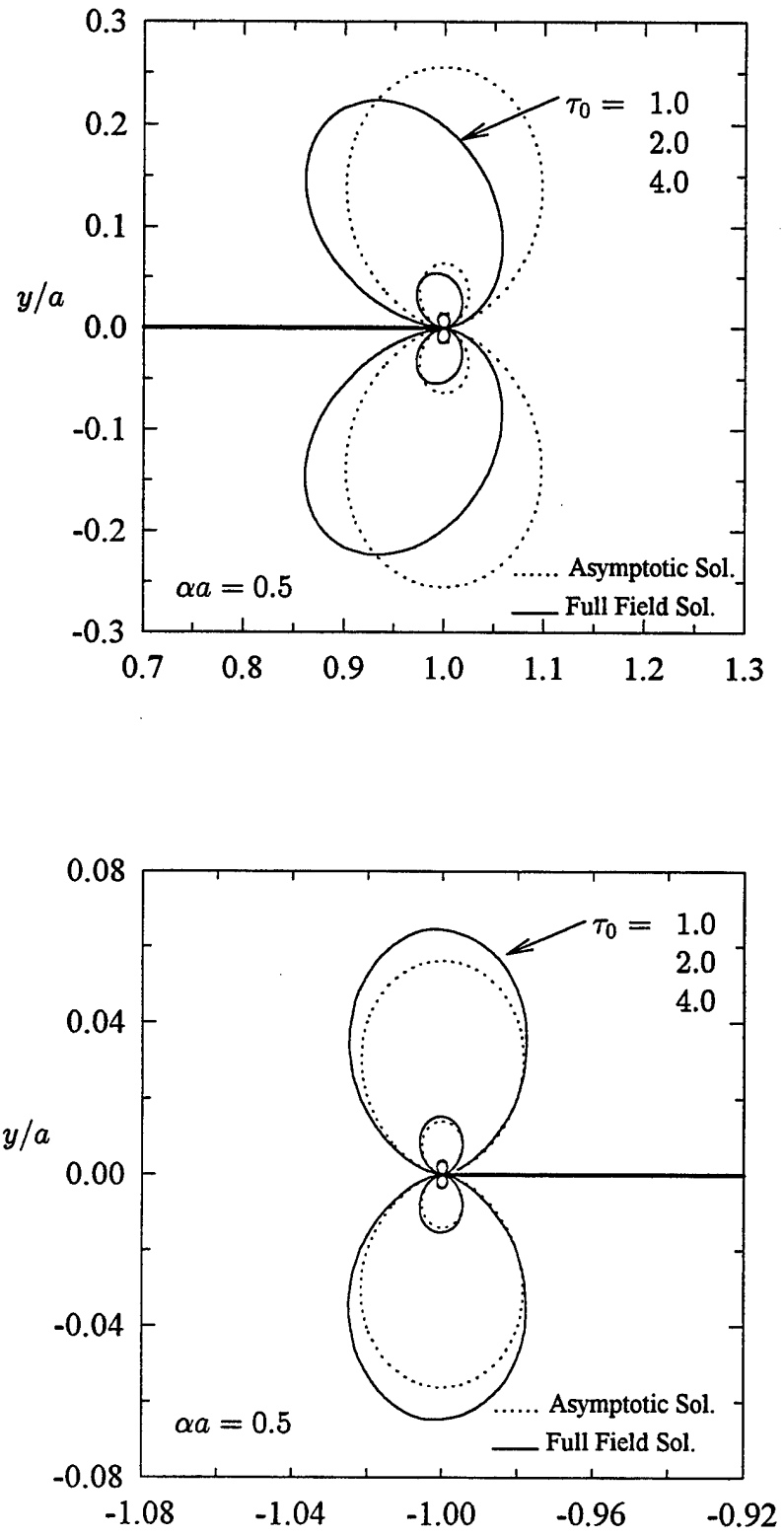

Figure 25 Isochromatics near right and left crack tips in an inhomogeneous medium under mode I fixed grip loading, $\tau_0 = \frac{\tau_{max}}{\varepsilon_0 E_0}$, $\nu = 0.3$, $E(x) = E_0 \exp(\alpha x)$

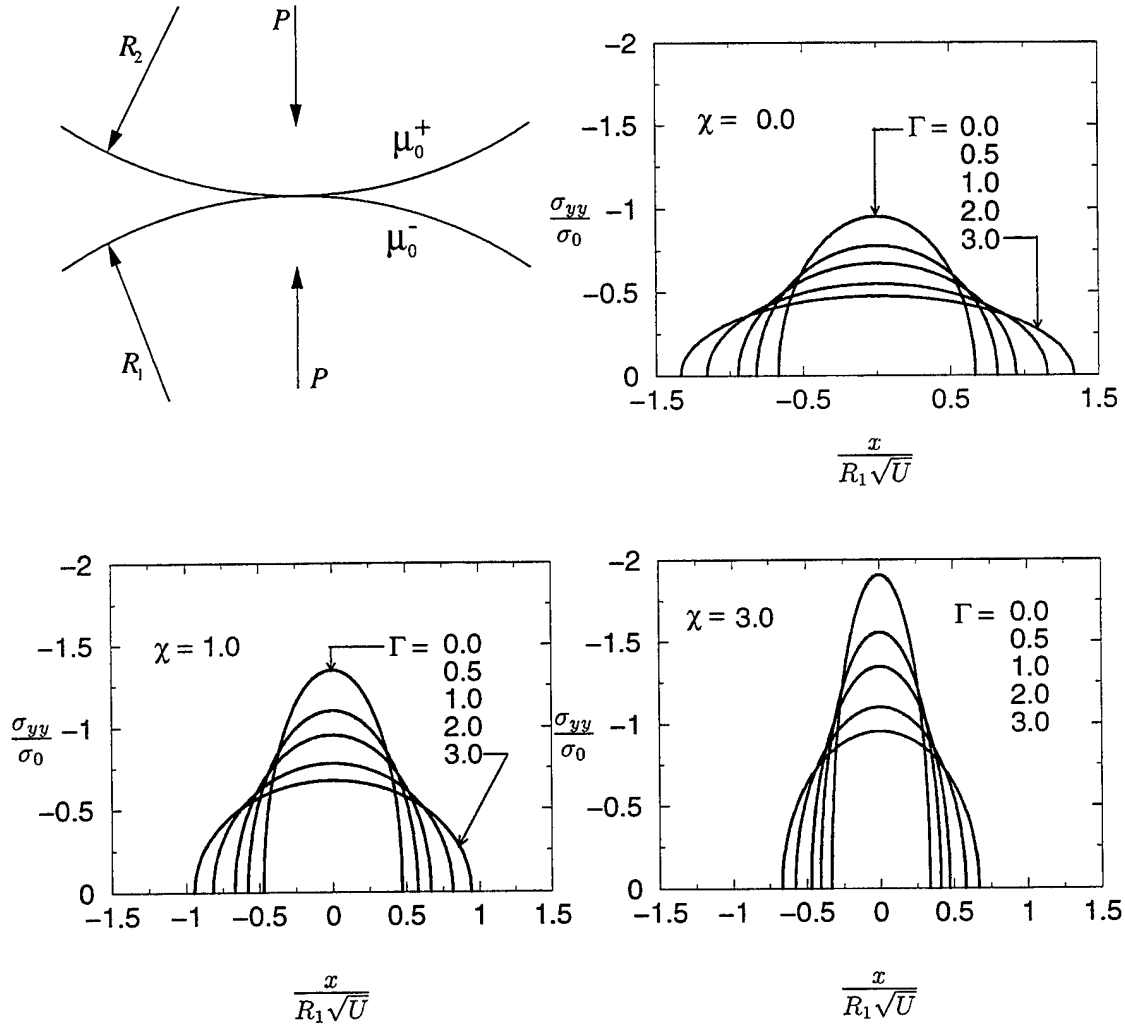

Figure 26: Stress distribution under hertzian contact where $\sigma_0 = \mu_0^+\sqrt{U}$, $U = \frac{P}{\mu_0^+ R_1}$, $\Gamma = \frac{\mu_0^+}{\mu_0^-}$, $\chi = \frac{R_1}{R_2}$ for homogeneous cylinders.

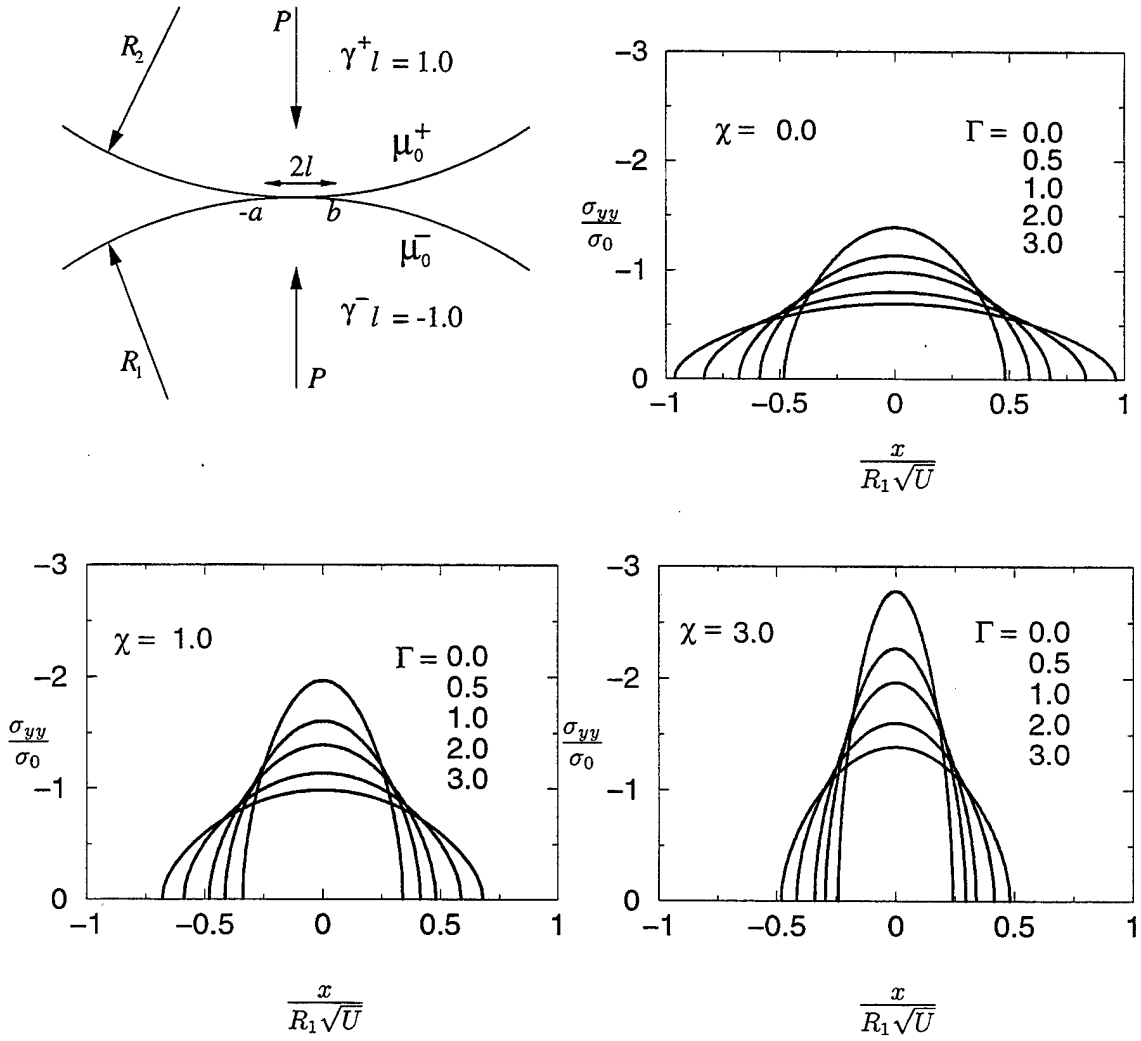

Figure 27: Stress distribution under hertzian contact where $\sigma_0 = \mu_0^+\sqrt{U}$, $U = \frac{P}{\mu_0^+ R_1}$, $\Gamma = \frac{\mu_0^+}{\mu_0^-}$, $\chi = \frac{R_1}{R_2}$ for inhomogeneous cylinders.

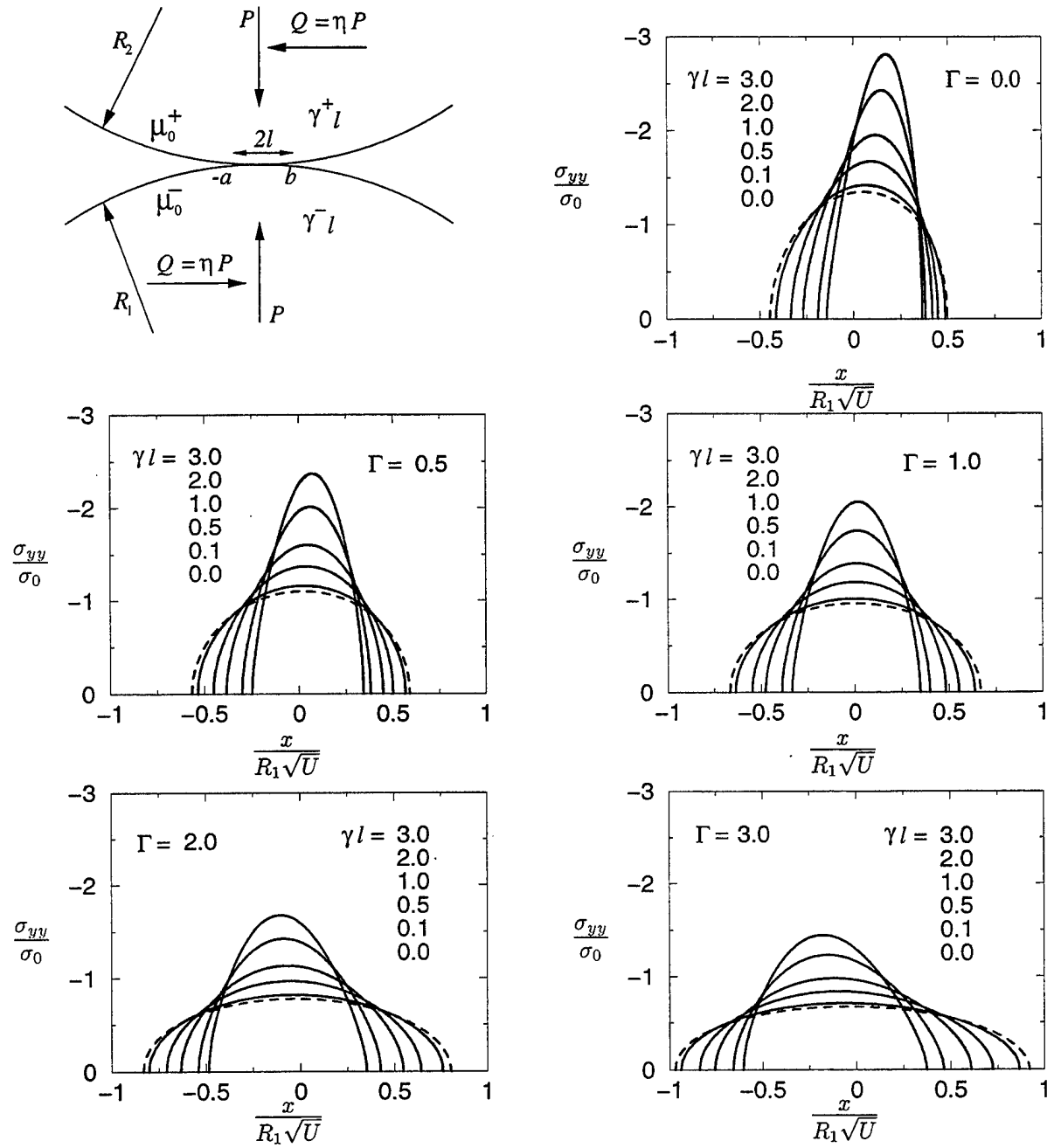

Figure 28: Stress distribution under hertzian contact where $\eta = 0.3$, $\chi = 1.0$, $\sigma_0 = \mu_0^+\sqrt{U}$, $U = \frac{P}{\mu_0^+ R_1}$, $\Gamma = \frac{\mu_0^+}{\mu_0^-}$, $\chi = \frac{R_1}{R_2}$, dashed lines homogeneous and full lines inhomogeneous cylinders, $\gamma^- = -\gamma^+ = -\gamma$.

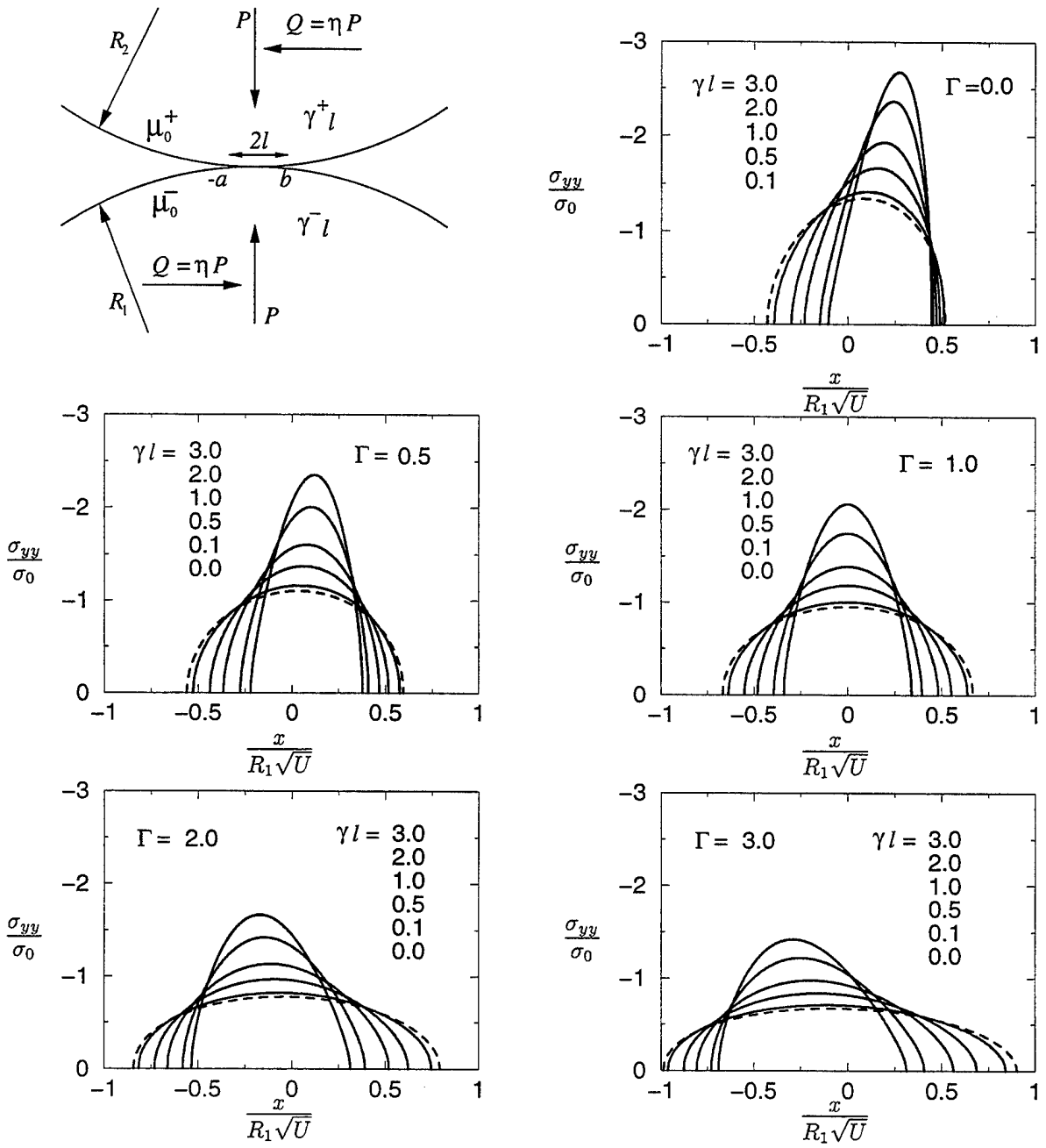

Figure 29: Stress distribution under frictional contact where $\eta = 0.5$, $\chi = 1.0$, $\sigma_0 = \mu_0^+\sqrt{U}$, $U = \frac{P}{\mu_0^+ R_1}$, $\Gamma = \frac{\mu_0^+}{\mu_0^-}$, $\chi = \frac{R_1}{R_2}$, dashed lines homogeneous and full lines inhomogeneous cylinders, $\gamma^- = -\gamma^+ = -\gamma$.

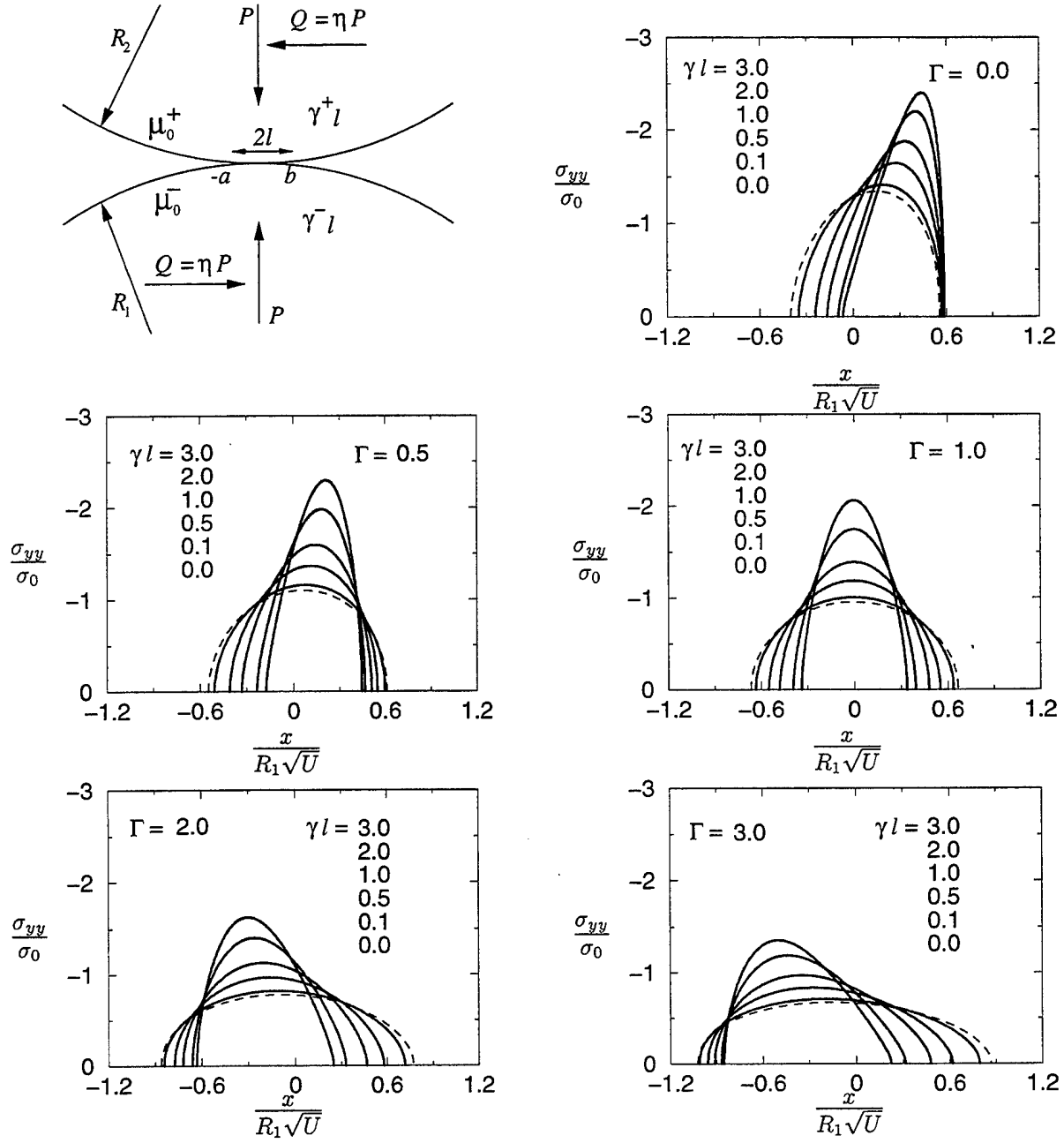

Figure 30: Stress distribution under frictional contact where $\eta = 0.9$, $\chi = 1.0$, $\sigma_0 = \mu_0^+\sqrt{U}$, $U = \frac{P}{\mu_0^+ R_1}$, $\Gamma = \frac{\mu_0^+}{\mu_0^-}$, $\chi = \frac{R_1}{R_2}$, dashed lines homogeneous and full lines inhomogeneous cylinders, $\gamma^- = -\gamma^+ = -\gamma$.

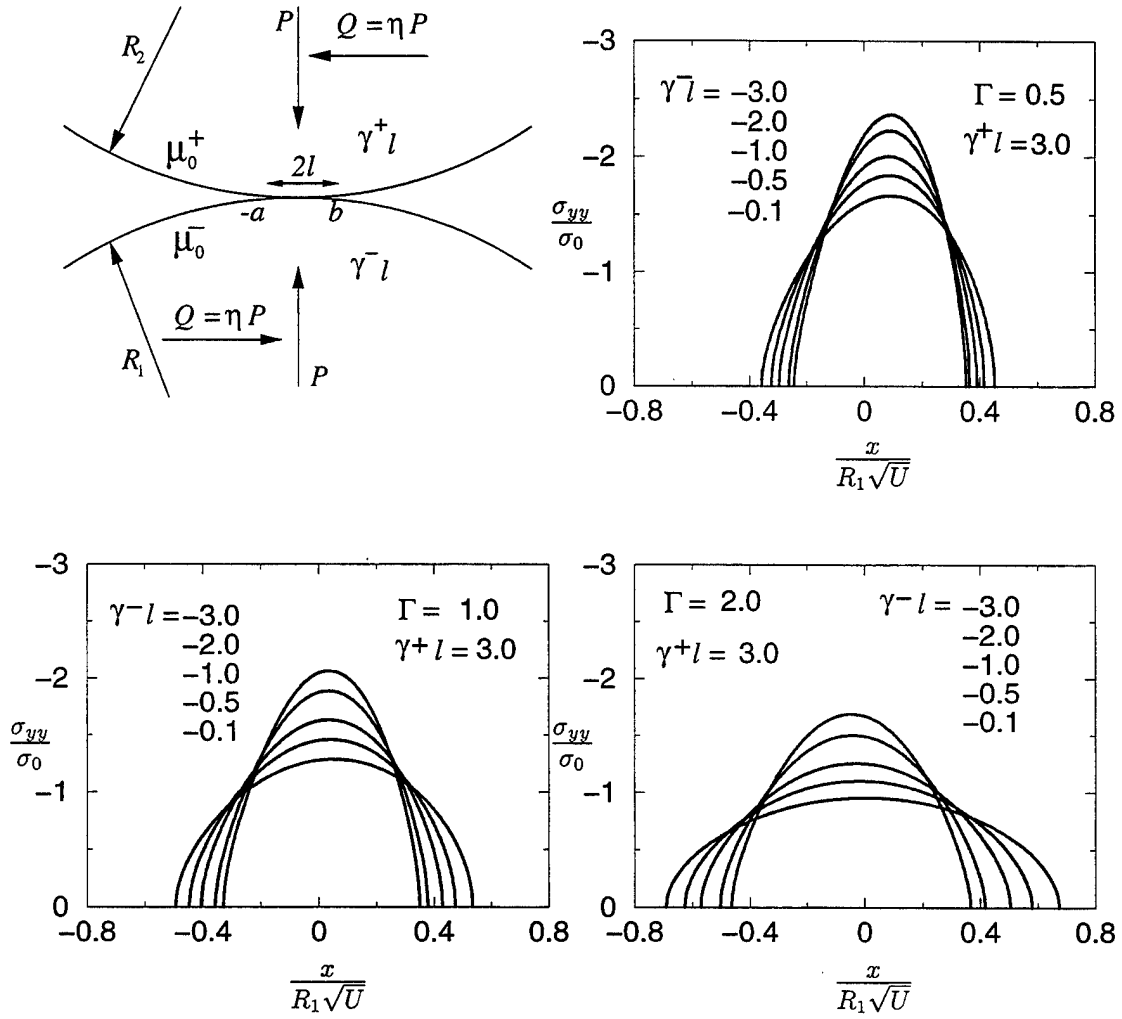

Figure 31: Stress distribution under frictional contact where $\eta = 0.3$, $\chi = 1$, $\sigma_0 = \mu_0^+\sqrt{U}$, $U = \frac{P}{\mu_0^+ R_1}$, $\Gamma = \frac{\mu_0^+}{\mu_0^-}$, $\chi = \frac{R_1}{R_2}$ for inhomogeneous cylinders.

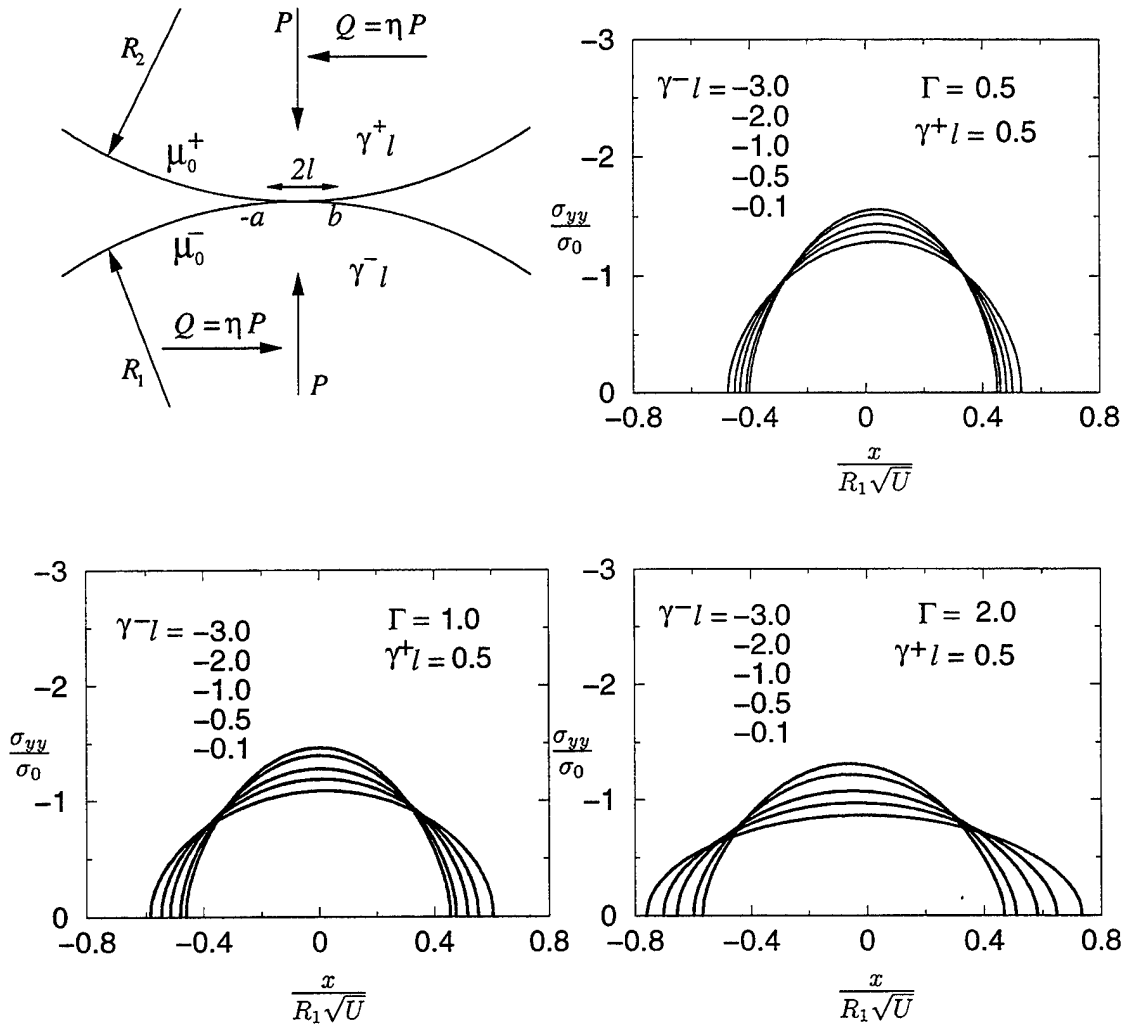

Figure 32: Stress distribution under frictional contact where $\eta = 0.3$, $\chi = 1$, $\sigma_0 = \mu_0^+\sqrt{U}$, $U = \frac{P}{\mu_0^+ R_1}$, $\Gamma = \frac{\mu_0^+}{\mu_0^-}$, $\chi = \frac{R_1}{R_2}$ for inhomogeneous cylinders.

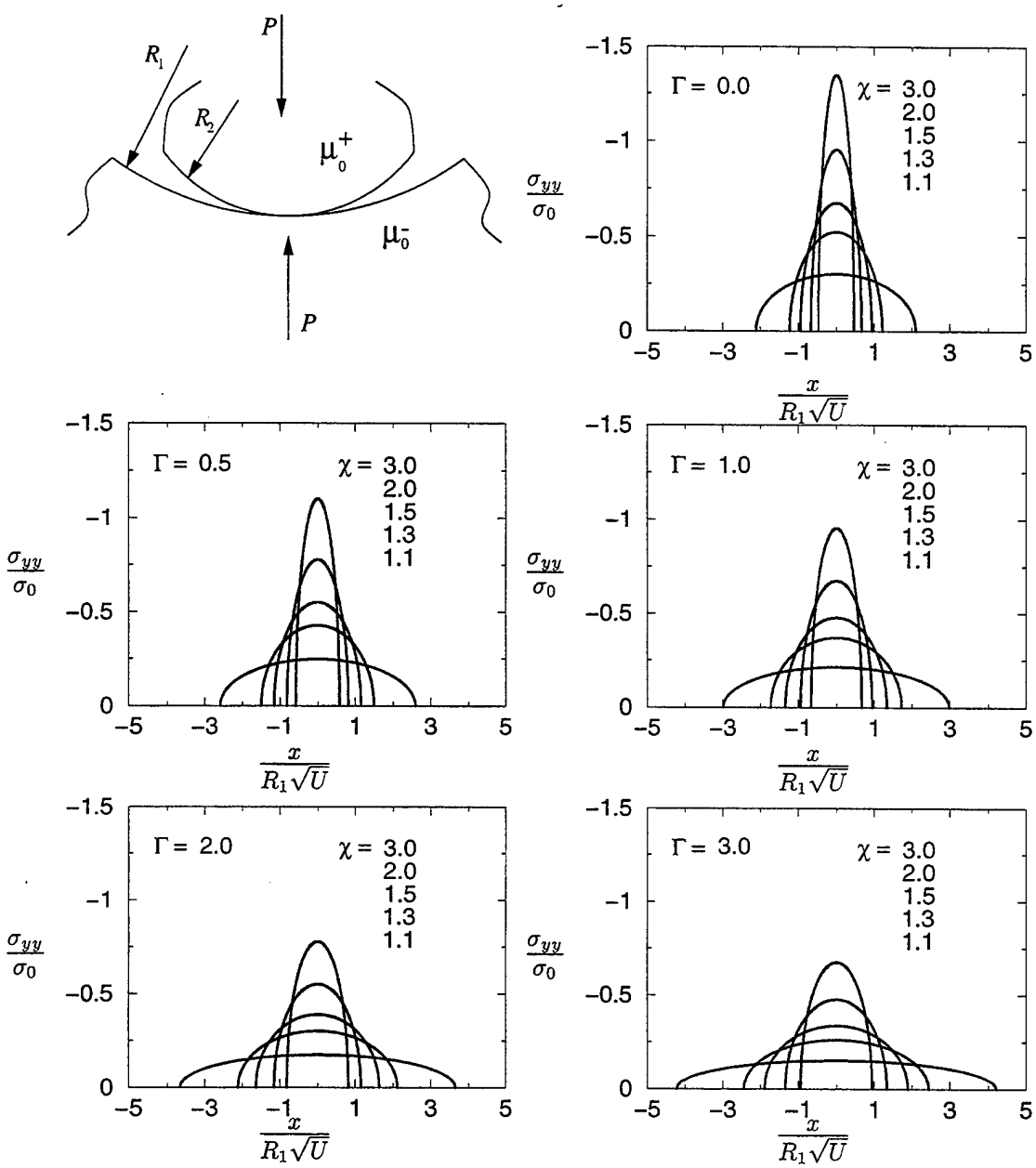

Figure 33: Stress distribution under hertzian contact where $\sigma_0 = \mu_0^+\sqrt{U}$, $U = \frac{P}{\mu_0^+ R_1}$, $\Gamma = \frac{\mu_0^+}{\mu_0^-}$, $\chi = \frac{R_1}{R_2}$, for homogeneous cylinders.

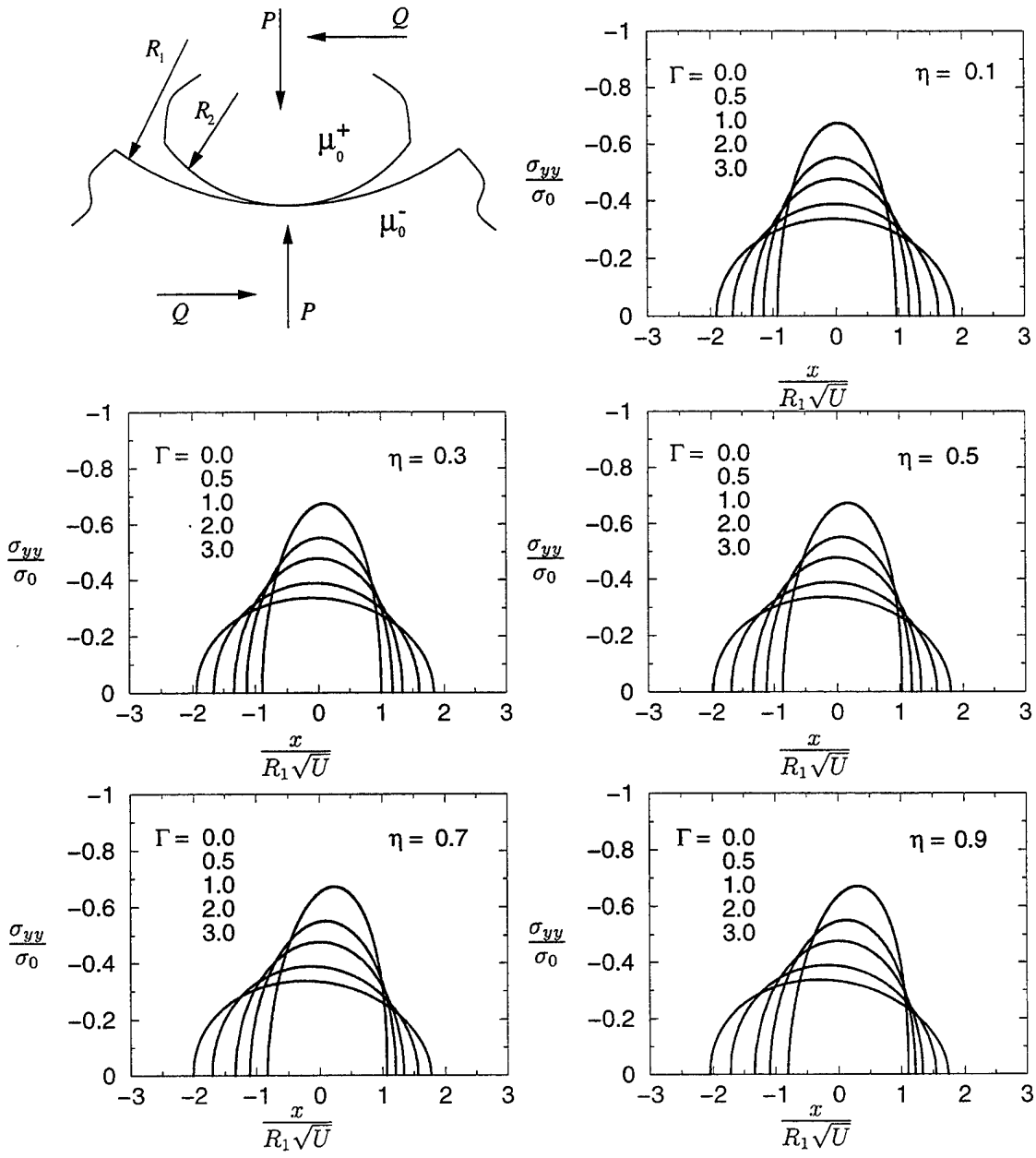

Figure 34: Stress distribution in homogeneous cylinders under frictional contact where $\sigma_0 = \mu_0^+\sqrt{U}$, $U = \frac{P}{\mu_0^+ R_1}$, $\Gamma = \frac{\mu_0^+}{\mu_0^-}$, $\chi = \frac{R_1}{R_2} = 1.5$

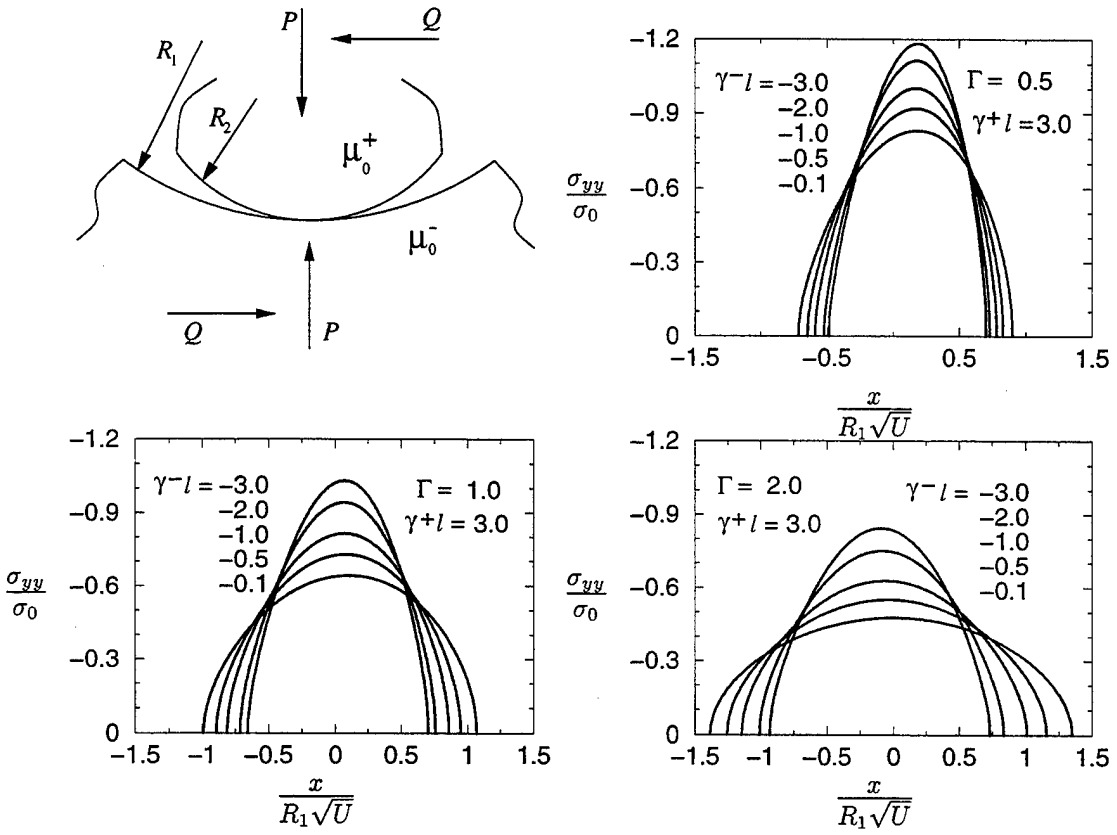

Figure 35: Stress distribution in inhomogeneous cylinders under hertzian contact where $\eta = 0.3$, $\chi = 1.5$, $\sigma_0 = \mu_0^+\sqrt{U}$, $U = \frac{P}{\mu_0^+ R_1}$, $\Gamma = \frac{\mu_0^+}{\mu_0^-}$, $\chi = \frac{R_1}{R_2}$

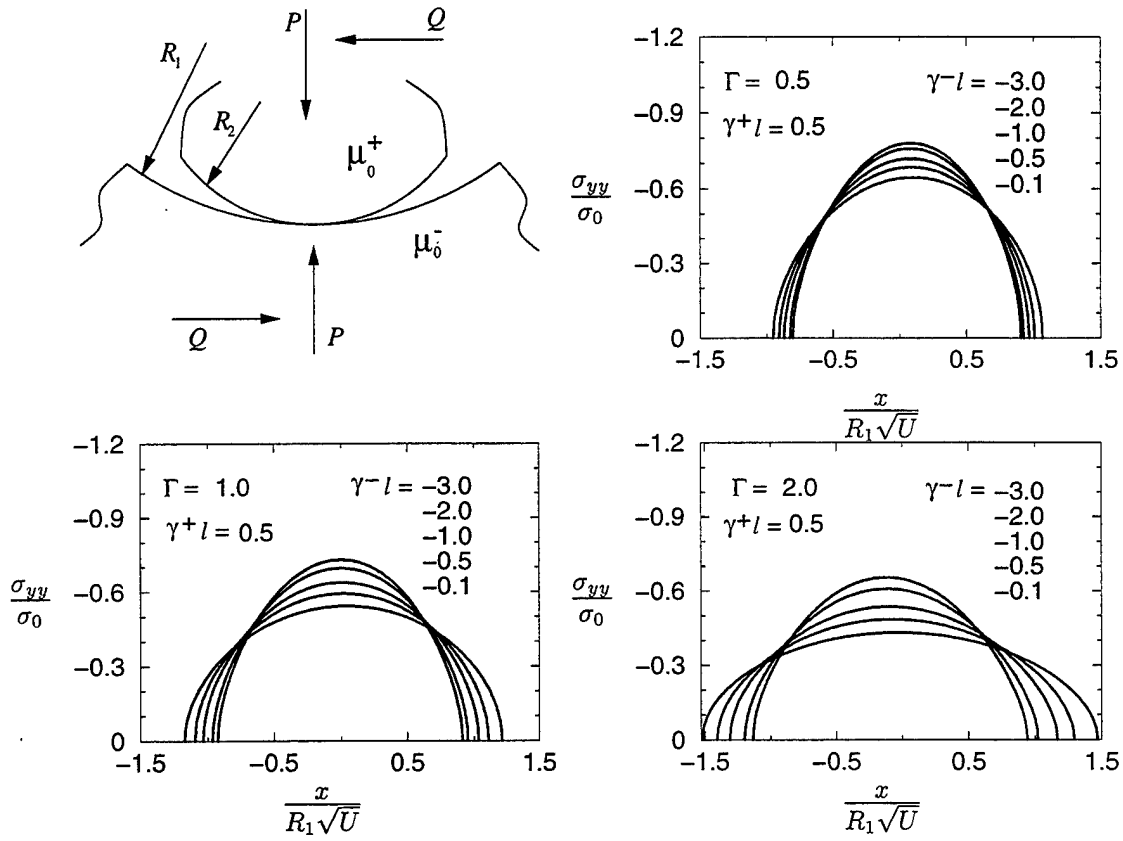

Figure 36: Stress distribution in inhomogeneous cylinders under hertzian contact where $\eta = 0.3$, $\chi = 1.5$, $\sigma_0 = \mu_0^+\sqrt{U}$, $U = \frac{P}{\mu_0^+ R_1}$, $\Gamma = \frac{\mu_0^+}{\mu_0^-}$, $\chi = \frac{R_1}{R_2}$

APPENDIX A

SPALLATION OF FGM COATINGS - A NONLINEAR MODEL

Spallation of FGM Coatings— A Nonlinear Model

T.-C. CHIU and F. ERDOGAN

ABSTRACT

In this study the problem of FGM coating with an interface crack subjected to compressive load parallel to the free surface is considered. First by using a nonlinear continuum theory the problem is reduced to an eigenvalue problem and the instability load is evaluated analytically. Finite element technique is then used for solving the elastic post-buckling problem. The strain energy release rate and stress intensity factors are directly calculated from special crack-tip enriched finite elements. Results obtained for a sample thermal buckling problem are presented and discussed.

INTRODUCTION

Requirements for the protection of hot section components in many high temperature applications such as earth-to-orbit winged planes and advanced turbine systems have led to the application of thermal barrier coatings (TBC) that utilize ceramic coatings over metal substrates. An alternative concept to homogeneous ceramic coatings is the functionally graded materials (FGM) in which the composition of the coating is intentionally graded to improve the bonding strength and to reduce the magnitude of the residual and thermal stresses. Inherent in such layered material systems is a sensitivity to thermally or mechanically induced compressive loading which may result in interface crack growth that eventually leads to spallation. The debonding and spallation problems are also observed in other layered material systems such as surface coatings in electronic devices and fiber reinforced composite laminates.

The technical importance of understanding the delamination and spallation problem has recently received a great deal of attention and many investigations have been performed in composite laminates and TBCs (e.g., [1]-[4]). It is often observed

T.-C. Chiu and F. Erdogan, Department of Mechanical Engineering and Mechanics, Lehigh University, Bethlehem, PA 18015

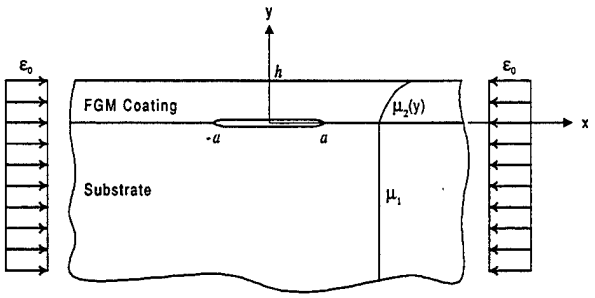

Figure 1 Functionally graded coating bonded to homogeneous substrate with an interface crack subjected to uniform compressive strain.

that spallation occurs as an interface crack reaches a critical size and kinks out of the interface into the coating. The failure of the coating may then be examined either by comparing the calculated strain energy release rate G with the mode mixity-dependent fracture toughness G_c or by using a maximum stress-based rupture theory in the debonded part of the coating. In this paper an FGM coating bonded to a homogeneous substrate containing a through-the-width interface crack is investigated. By using a perturbation technique the nonlinear continuum problem is analyzed and the stability load is obtained analytically. The nonlinear elasticity problem is solved by using finite element technique and the strain energy release rate and stress intensity factors are calculated.

STABILITY ANALYSIS

FORMULATION OF THE PROBLEM

The plane strain problem described in Figure 1 for a layered system subjected to a uniform compressive strain ϵ_0 is considered. The medium consists of an FGM coating of thickness h bonded to a semi-infinite substrate and contains an interface crack of length $2a$. The compressive strain ϵ_0 represents the magnitude of the external load. It is assumed that the substrate is homogeneous with elastic constants μ_1, κ_1, the coating is inhomogeneous with elastic parameters μ_2, κ_2, and μ_2 is approximated by

$$\mu_2(y) = \mu_1 \exp(\gamma y) \tag{1}$$

where μ_i is the shear modulus, $\kappa_i = 3 - 4\nu_i$ for plane strain, ν_i being the Poisson's ratio. The subscripts, $i = 1$ and 2, denote the substrate and coating, respectively. From the mathematical theory of elastic stability [5], the governing equations may be expressed as

$$(\kappa+1)\frac{\partial^2 u_i}{\partial x^2} + (\kappa-1)\frac{\partial^2 u_i}{\partial y^2} + 2\frac{\partial^2 v_i}{\partial x \partial y} + \gamma(\kappa-1)\left(\frac{\partial u_i}{\partial y} + \frac{\partial v_i}{\partial x}\right) - 8\epsilon_0\left(\frac{\kappa-1}{\kappa+1}\right)\frac{\partial^2 u_i}{\partial x^2} = 0, \tag{2a}$$

$$(\kappa-1)\frac{\partial^2 v_i}{\partial x^2}+(\kappa+1)\frac{\partial^2 v_i}{\partial y^2}+2\frac{\partial^2 u_i}{\partial x\partial y}+\gamma(3-\kappa)\frac{\partial u_i}{\partial x}+\gamma(\kappa+1)\frac{\partial v_i}{\partial y} \tag{2b}$$
$$-8\epsilon_0\left(\frac{\kappa-1}{\kappa+1}\right)\frac{\partial^2 v_i}{\partial x^2}=0,$$

where u_i and v_i are the displacement perturbations from the equilibrium state in x- and y-directions, respectively. Equations (2) may be solved by using Fourier transforms with the following boundary and continuity conditions:

$$\sigma_{2yy}(x,h)=0,\ \sigma_{2xy}(x,h)=0,\ -\infty<x<\infty, \tag{3a}$$

$$\sigma_{1yy}(x,-0)=\sigma_{2yy}(x,+0),\ \sigma_{1xy}(x,-0)=\sigma_{2xy}(x,+0),\ -\infty<x<\infty, \tag{3b}$$

$$\sigma_{1yy}(x,-0)=0,\ \sigma_{1xy}(x,-0)=0,\ -a<x<a, \tag{3c}$$

$$u_1(x,-0)=u_2(x,+0),\ v_1(x,-0)=v_2(x,+0),\ |x|>a. \tag{3d}$$

After some analysis the related mixed boundary value problem may be reduced to

$$\frac{1}{\pi}\int_{-a}^{a}\sum_{1}^{2}\left[\frac{\delta_{ij}}{t-x}+g_{ij}(x,t)\right]f_j(t)dt=0,\ i=1,2,\ -a<x<a, \tag{4}$$

$$\int_{-a}^{a}f_i(t)dt=0,\ i=1,2, \tag{5}$$

where

$$f_1(x)=\frac{\partial}{\partial x}[v_2(x,+0)-v_1(x,-0)],\ -\infty<x<\infty, \tag{6a}$$

$$f_2(x)=\frac{\partial}{\partial x}[u_2(x,+0)-u_1(x,-0)],\ -\infty<x<\infty, \tag{6a}$$

and the functions $g_{ij}\,(i,j=1,2)$ are square integrable in $-a\le(x,t)\le a$ and do not contribute to the singular nature of the solution. Since the Cauchy kernels shown in (4) lead to the conventional square-root singularity for f_1 and f_2, it can be shown that the solution of the integral equations (4) satisfying (5) is of the form

$$f_i(x)=\frac{1}{\sqrt{1-\left(\frac{x}{a}\right)^2}}\sum_{1}^{\infty}A_{ij}T_j\left(\frac{x}{a}\right),\ i=1,2, \tag{7}$$

where the orthogonal functions T_0, T_1, ... are Chebysheb polynomials of the first kind and $T_0=1$. By substituting (7) into (4), truncating the series at $j=n$, and using a suitable collocation technique, equations (4) and (5) may be reduced to a system of linear algebraic equations in the unknown coefficients A_{ij} $(i=1,2,$ $j=1,\ ...,\ n)$. Since the right hand side of equations (4) is zero, the resulting linear

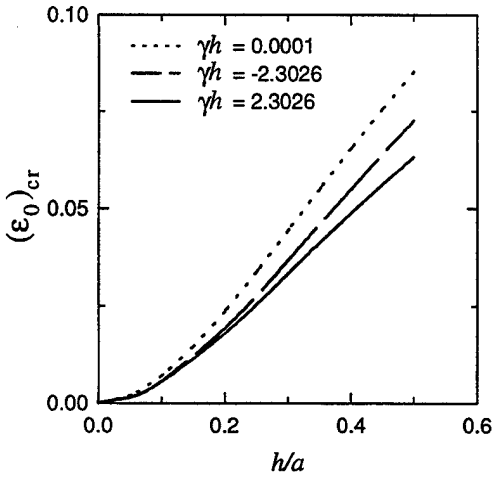

Figure 2 Buckling strain $(\varepsilon_0)_{cr}$ as a function of h/a.

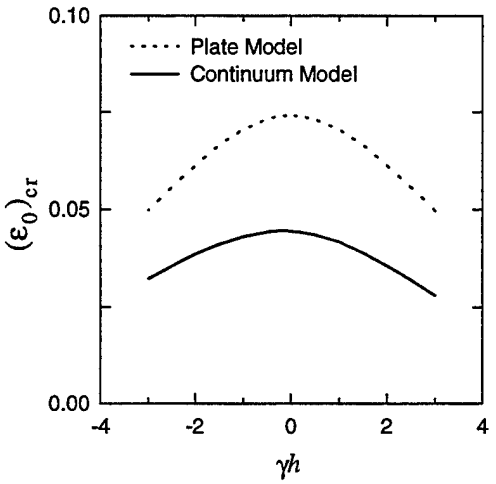

Figure 3 Buckling strain $(\varepsilon_0)_{cr}$ as a function of coating inhomogeneity γh ($h/a = 0.3$).

algebraic equations are homogeneous and have nontrivial solution only for certain values of ϵ_0, which are essentially the eigenvalues of the problem. Physically the smallest eigenvalue corresponds to the instability load.

RESULTS AND DISCUSSION

It was previously shown that in the crack problems for FGMs the effect of the Poisson's ratio is not very significant. Thus, in solving the isothermal nonlinear elasticity problem it is assumed that $\nu_1 = \nu_2 = 0.3$ or $\kappa = 1.8$. Figure 2 shows the calculated critical value of ϵ_0 as a function of the length parameter h/a for some fixed values of γh. Note that γh is the measure of material inhomogeneity and that $\gamma h = 0$ corresponds to a homogeneous medium containing a crack parallel to the surface. The FGM coatings for which $\gamma h = -2.3026$ and $\gamma h = 2.3026$ correspond to $\mu_2(h)/\mu_1 = 0.1$ and $\mu_2(h)/\mu_1 = 10$, respectively. Figure 3 shows the influence of material inhomogeneity on the critical strain for a fixed coating thickness/crack length ratio. Also shown in Figure 3 is the critical strain obtained from the plate theory. It may be seen that the critical strain given by the plate theory is symmetric in γh and becomes maximum for the homogeneous medium. The critical strain obtained from continuum theory shows the same trend except that the maximum is shifted slightly toward negative γh. Note that the relatively large difference observed between the critical strains obtained from the plate and continuum theories may be attributed to the fact that the plate is assumed to have "built-in" ends whereas the continuum theory imposes no such artificial constraints.

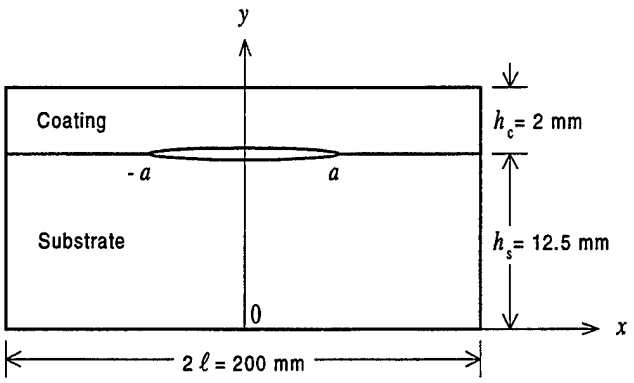

Figure 4 Specimen configuration for the thermal buckling problem

POST-BUCKLING ANALYSIS

The post-buckling continuum problem is analyzed by using a geometrically nonlinear finite element program. Nonlinearity is accounted for by using the Green-Lagrange nonlinear strain-displacement relations. However, in order to extract the information for fracture mechanics analysis, it is assumed that the crack-tip region is locally linear and the crack-tip enriched elements [6] may be used for directly computing the stress intensity factors and strain energy release rate. The equilibrium state is determined by using the principle of stationary potential energy. An incremental-iterative procedure is used for solving the nonlinear equations.

NUMERICAL EXAMPLE

As an example the plane strain problem for a nickel-based Rene-41 substrate coated with zirconia, containing an interface crack and subjected to a uniform temperature drop ΔT is considered. It is assumed that the medium is stress-free before cooling down. The dimensions of the medium are shown in Figure 4 [7]. The relevant thermomechanical properties of the substrate and the coating are

$$E_s = 219.7 \text{ GPa},\ \nu_s = 0.3,\ \alpha_s = 1.67 \times 10^{-5}\,\text{K}^{-1},$$

$$E_c = 151 \text{ GPa},\ \nu_c = 0.3,\ \alpha_c = 1.0 \times 10^{-5}\,\text{K}^{-1}, \tag{8}$$

where E, ν, and α are the Young's modulus, the Poisson's ratio, and the thermal expansion coefficient, respectively. The uniform cool-down problem is also considered for the medium described in Figure 4 in which the homogeneous zirconia coating is replaced by an inhomogeneous FGM coating. A linear variation of the thermomechanical properties in the FGM coating is assumed, i.e.,

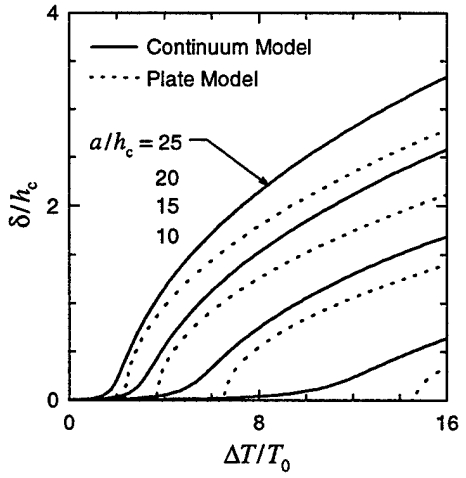

Figure 5 Buckling deflection δ/h_c vs. temperature drop $\Delta T/T_0$ for the homogeneous TBC.

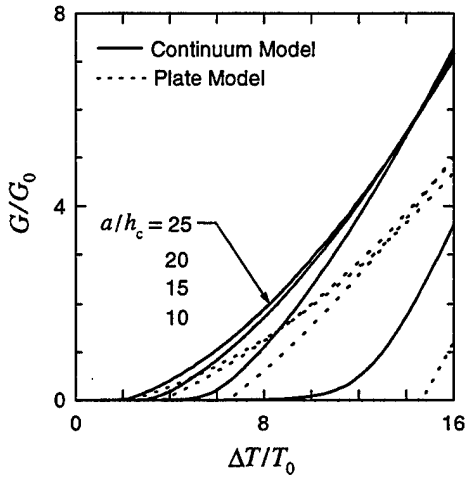

Figure 6 Strain energy release rate G/G_0 vs. temperature drop $\Delta T/T_0$ for the homogeneous TBC.

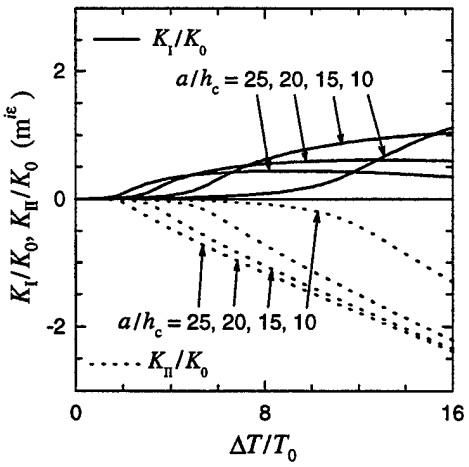

Figure 7 Stress intensity factors vs. temperature drop $\Delta T/T_0$ for the homogeneous TBC.

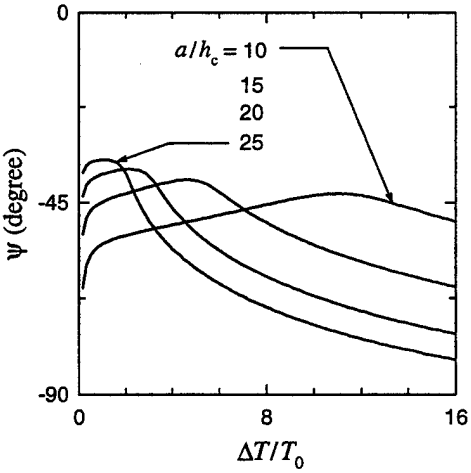

Figure 8 Phase angle ψ vs. temperature drop $\Delta T/T_0$ for the homogeneous TBC.

$$E(y) = \begin{cases} E_s + (E_c - E_s)(\dfrac{y - h_s}{h_c}), & h_s < y < h_s + h_c, \\ E_s, & 0 < y < h_s, \end{cases}$$

$$\alpha(y) = \begin{cases} \alpha_s + (\alpha_c - \alpha_s)(\dfrac{y - h_s}{h_c}), & h_s < y < h_s + h_c, \\ \alpha_s, & 0 < y < h_s. \end{cases} \tag{9}$$

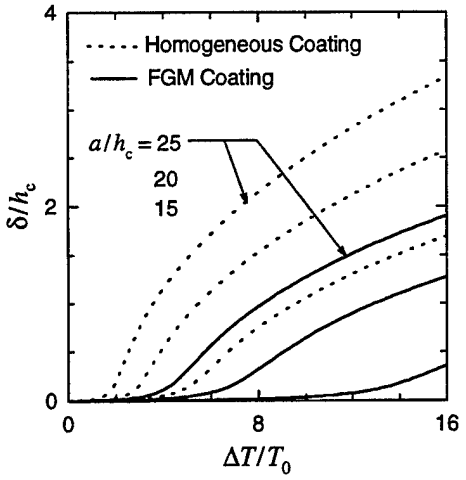

Figure 9 Effect of the application of FGM coating on the thermal buckling deflection δ/h_c.

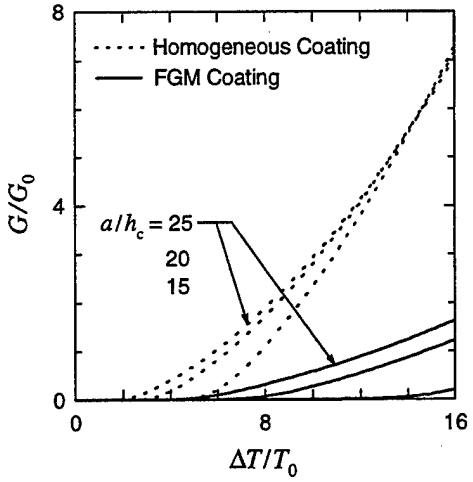

Figure 10 Strain energy release rate G/G_0 vs. temperature drop $\Delta T/T_0$ for FGM and homogeneous coatings.

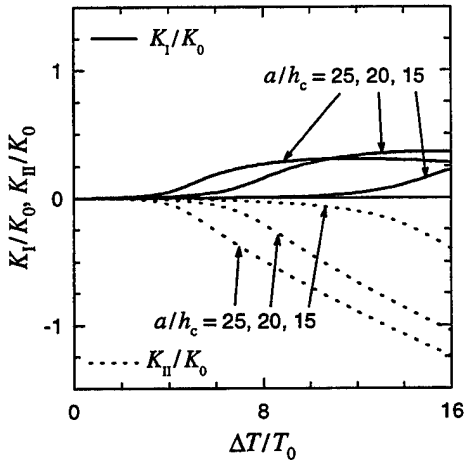

Figure 11 Stress intensity factors K_I/K_0 and K_{II}/K_0 vs. temperature drop $\Delta T/T_0$ for FGM coatings.

Figures 5-8 show the results for the thermal buckling problem in the homogeneous TBCs. The constants used for normalization in these figures are

$$T_0 = 100\ \text{K}, \qquad K_0 = E_s\alpha_s T_0\sqrt{\pi h_c}, \qquad G_0 = (1-\nu_s^2)\frac{K_0^2}{E_s}. \tag{10}$$

Due to the thermal expansion coefficient mismatch between the coating and the substrate, compressive residual stress is developed in the ceramic coating during the cool down process. As a result the coating buckles as the temperature change reaches a critical value. This may be observed in Figure 5 which shows the normalized "crack opening" δ/h_c at $x = 0$ as a function of $\Delta T/T_0$ for some fixed

values of a/h_c. It is also observed in Figures 5 that instead of having an explicit buckling point, the "crack opening" is a smooth function of $\Delta T/T_0$. Figure 6 shows the normalized energy release rate G/G_0 versus temperature drop for various values of a/h_c. Also shown in Figures 5 and 6 are the results obtained by using plate theory with the assumption that the buckled coating has "built-in" ends. By examining Figures 5 and 6 it may be observed that the continuum model gives larger values of buckling deflection and strain energy release rate than the plate model. This may again be attributed to the higher degree of constraint in the plate model resulting from the assumption of "built-in" ends. Furthermore, as in the stability analysis (Figures 2 and 3) the buckling load for the continuum model is lower than that for the plate model. Figures 7 and 8 show, respectively, the normalized stress intensity factors and the phase angle as functions of $\Delta T/T_0$ for various a/h_c. It is important to note that, since the crack is on a bi-material interface, the stress intensity factor is a complex quantity. From Figure 7 it may be seen that K_{II} is the dominant stress intensity factor. This implies the tendency for the crack kinking into the coating and spalling the coating off. However, perhaps a more practical approach to studying the spallation process would be either comparing the calculated strain energy release rate G with the mode mixity-dependent fracture toughness G_c or analyzing the buckled part of the coating by using a maximum stress-based rupture theory.

Figures 9 and 10 show δ/h_c and G/G_0 versus $\Delta T/T_0$, respectively, in the cool down problem for the inhomogeneous FGM coating. For comparison the figures also show the results for the homogeneous TBC. Figure 11 shows the normalized stress intensity factors as a function of $\Delta T/T_0$ for various a/h_c. Basically the results for FGM coating show the same trend as the results for homogeneous coatings. It is, however, observed that for FGM coating the buckling ΔT is much higher and δ/h_c and G/G_0 are much lower compared with the homogeneous coating. This may be attributed to decrease in the magnitude of thermal residual stresses because of the smooth transition of thermomechanical properties in FGM. As a result the FGM coating is expected to be more resistant to cool down induced coating buckling and spallation.

ACKNOWLEDGMENTS

This study was partially supported by AFOSR Grant F49620-98-1-0028.

REFERENCES

1. J. D. Whitcomb, 1989. "Three-Dimensional Analysis of a Postbuckled Embedded Delamination." *Journal of Composite Materials*, 23:862-889.

2. J. W. Hutchinson and Z. Suo, 1992. "Mixed Mode Cracking in Layered Materials," in *Advances in Applied Mechanics*, J. W. Hutchinson and T. Y. Wu, eds. Orlando: Academic Press, pp. 63-191.

3. K.-F. Nilsson, J. C. Thesken, P. Sindelar, A. E. Giannakopoulos, and B. Storåkers, 1993. "A Theoretical and Experimental Investigation of Buckling Induced Delamination Growth." *Journal of Mechanics and Physics of Solids*, 41(4):749-782.

4. W.-X. Wang and Y. Takao, 1995. "Load Buckling of a Layer Bonded to a Half-Space with an Interface Crack." *Journal of Applied Mechanics*, 62:64-70.

5. W. Flügge, 1972. *Tensor Analysis and Continuum Mechanics*. New York: Springer-Verlag, pp. 165-171.

6. A. C. Kaya and H. F. Nied, 1993. "Interface Fracture Analysis of Bonded Ceramic Layers Using Enriched Finite Elements," in *Ceramic Coatings*, K. Kokini, ed. The 1993 ASME Winter Annual Meeting, New Orleans, Louisiana, MD-Vol. 44, pp. 47-71.

7. M. Case and K. Kokini, 1993. "Thermally Induced Initiation of Interface Edge Cracks in Multilayer Ceramic Thermal Barrier Coatings," in *Ceramic Coatings*, K. Kokini, ed. The 1993 ASME Winter Annual Meeting, New Orleans, Louisiana, MD-Vol. 44, pp. 149-162.

APPENDIX B

INTERFACE CRACKING OF FGM COATINGS UNDER UNIFORM THERMAL LOADING

Interface Cracking of FGM Coatings under Uniform Thermal Loading

B. YILDIRIM and F. ERDOGAN

ABSTRACT

In this study the axisymetric crack problem for thermal barrier coatings (TBC) under a uniform temperature change is considered. It is assumed that the disk-shaped specimen consists of a nickel-based super alloy substrate, NiCrAlY bond coat and the TBC. The TBC itself is a two phase metal/ceramic functionally graded material (FGM). The metal phase is NiCrAlY and the ceramic is partially stabilized zirconia (PSZ). The composition of TBC varies from zero percent ceramic on the bond coat/TBC interface to hundred percent on the surface. The crack is a plane edge crack, starts at $r=r_0$ and propagates in a plane perpendicular to the axis of the cylinder, r_0 being the radius of the disk. Modes I and II stress intensity factors and the strain energy release rate are calculated for various sizes and locations of the crack. The main variables in the problem are the inhomogeneity parameter of the FGM coating, the size and the location of the crack and the relative dimensions of the specimen. The finite element method is used to solve the problem. The material property grading is accounted for by developing special inhomogeneous elements and the stress intensity factors are calculated by using enriched crack tip elements.

INTRODUCTION

In many high temperature applications such as advanced turbine systems and earth-to-orbit winged planes, to achieve higher efficiencies, higher velocities and longer lifetime the use of structural ceramics is becoming a necessity for the protection of hot section components. The ceramic thermal barrier coatings used for this purpose, however, seem to have some reliability and durability problems arising largely from high residual and thermal stresses, poor interfacial bonding strength and low coating toughness. Thus, the broader technical issues that need to

B.Yildirim and F. Erdogan, Department of Mechanical Engineering and Mechanics, Lehigh University, Bethlehem, PA 18015.

be addressed in the development of thermal barrier coatings are the improvement of processing techniques from both performance and economic viewpoints, investigation of primary modes of failure, development of testing procedures for mechanical and strength characterization of the coatings and the development of appropriate life prediction methodologies [1], [2].

Because of the susceptibility of conventional homogeneous coatings to cracking and spallation, recently the materials research community has been exploring the possibility of new concepts in coating design. One such concept which may be used to overcome some of these shortcomings would be the introduction of an interfacial zone with graded thermomechanical properties between the coating and bond coat or the replacement of coating by a composite layer with a volume fraction varying between 0% ceramic and 100% metal on the interface and 100% ceramic and 0 % metal near the surface. Such particulate composites with continuously varying volume fractions are called *functionally graded materials* (*FGMs*) (see [3]-[6] for review and recent developments). The application of FGMs as coatings or interfacial zones seems to reduce the magnitude of residual stresses [7] and increase the bonding strength [8]. In FGM coatings, because of the gradual increase of the metal content in thickness direction, the toughness of the medium would also increase, thereby providing the layered material with a natural *R*-curve behavior.

In conventional ceramic coatings, even though one encounters a wide variety of failure modes, it is the interfacial fracture leading to spallation, which ultimately limits their performance. Both conventional and FGM thermal barrier coatings require a bond coat along the interface to shield the substrate against oxidation. In this study, edge cracking of a disk-shaped specimen of finite dimensions and stress-free ends subjected to a uniform temperature change is considered (Fig. 1).

DESCRIPTION OF THE PROBLEM

The axisymmetric problem considered is described(*) in Fig. 1. The medium is free of any mechanical constraints, and a uniform temperature change ΔT is the only nonvanishing external load.

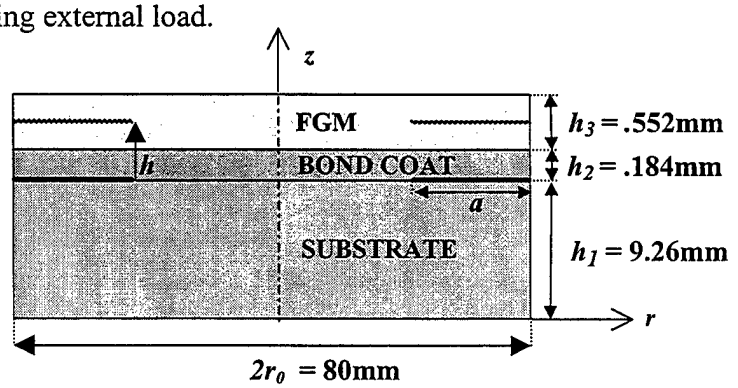

Figure 1. Geometry of the medium.

(*) The dimensions of the specimen used in this study approximately correspond to the dimensions of specimens studied by G. M. Newaz and his colleagues at Wayne State University, Detroit, Michigan.

At reference temperature T_0 the bonded medium is assumed to be stress-free. The volume fraction of ceramic in the FGM coating is varied from 0% on the bond coat/coating interface at $z = h_1+h_2$ to 100% on the surface, at $z = h_1+h_2+h_3$. The following models are used to represent the thickness variation of the thermoelastic parameters in the coating:

$$E(z)=\begin{cases} E_s & , z \le h_1 \\ E_{bc} & , h_1 < z \le h_1+h_2 \\ E_c+(E_{bc}-E_c)\left(\dfrac{h_1+h_2+h_3-z}{h_3}\right)^{p_1} & , h_1+h_2 < z \le h_1+h_2+h_3 \end{cases} \quad (1)$$

$$\alpha(z)=\begin{cases} \alpha_s & , z \le h_1 \\ \alpha_{bc} & , h_1 < z \le h_1+h_2 \\ \alpha_c+(\alpha_{bc}-\alpha_c)\left(\dfrac{h_1+h_2+h_3-z}{h_3}\right)^{p_2} & , h_1+h_2 < z \le h_1+h_2+h_3 \end{cases} \quad (2)$$

$$\nu(z)=\begin{cases} \nu_s & , z \le h_1 \\ \nu_{bc} & , h_1 < z \le h_2+h_1 \\ \nu_c+(\nu_{bc}-\nu_c)\left(\dfrac{h_1+h_2+h_3-z}{h_3}\right)^{p_3} & , h_1+h_2 < z \le h_1+h_2+h_3 \end{cases} \quad (3)$$

where subscripts *s, bc* and *c* stand for substrate, bond coat and ceramic, respectively and p_i (i=1,2,3) is the inhomogeneity constant, $0< p_i<\infty$. From (1)-(3) it may be seen that the limiting cases $p_i=0$ and $p_i=\infty$ correspond to homogeneous TBCs having the properties of bond coat and ceramic, respectively. By adjusting this constant the ceramic-rich ($p_i>1$) and metal rich ($p_i<1$) compositions in the FGM coating may be simulated. Figure 2 shows a sample variation of the Young's modulus for various values of $p_1=p$.

The thermoelastic material properties of ceramic, bond coat and substrate are given in Table 1, where E, ν and α are Young's modulus, Poisson's ratio and thermal expansion coefficient, respectively. The material properties are known at three different temperatures [9]. Consequently, a best fit to the data appears to be a second degree polynomial for E(T) and α (T) and a bilinear function for ν(T) (Figures 3-5).

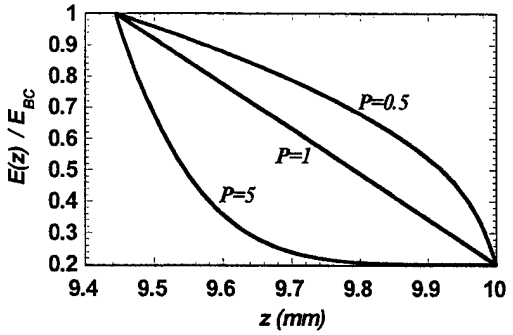

Figure 2. Variation of Young's modulus in the FGM coating.

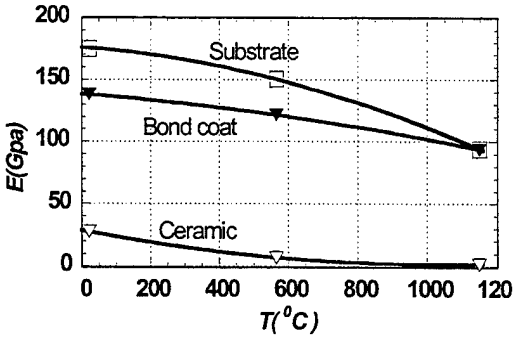

Figure 3. Variation of Young's modulus as a function of temperature.

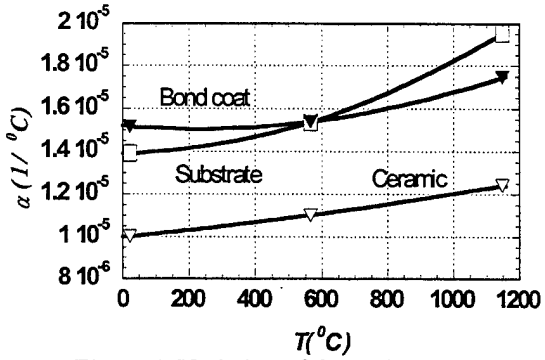

Figure 4. Variation of thermal expansion coefficient as a function of temperature.

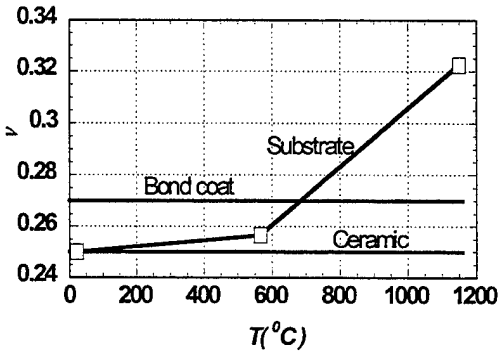

Figure 5. Variation of Poisson's ratio as a function of temperature.

RESULTS AND DISCUSSION

The main results presented in this study are modes I and II stress intensity factors, K_I, K_{II} and the strain energy release rate G which are normalized with respect to (see Fig.1 and Eq.1)

$$K_0 = E_s \alpha_s \Delta T \sqrt{\pi h_3}, \quad G_0 = (1-\nu_s^2)\frac{K_0^2}{E_s} . \tag{4}$$

In the examples shown in Figures 6-8 the stress intensity factors and the strain energy release rate are given as functions of the crack distance h for a fixed crack length $a=h_3$ and for various values of the inhomogenity constant p. Note that at $h=0$ for all p and at $h=h_2$ for $p=\infty$ the crack lies along a bimaterial interface. Consequently, the stress singularity is complex, K_I and K_{II} are discontinuous but, as expected, G is continuous. Similar results are shown in Figures 9-11 for a crack length $a=h_3/2$. On the physical grounds the following observations may be made: In the composite medium under consideration for a uniform change in temperature the stresses are generated by the mismatch in the thermal expansion coefficients and the net ligament stresses in the crack plane are statically self-equilibrating. Therefore, as the crack plane approaches the free surface, that is for $h \to h_2+h_3$ (or noting that, since $h_3=3h_2$, for $h \to 4h_2$), the stress intensity factors and the strain

energy release rate tend to zero, which is seen to be the case in Figures 6-11. The figures also show that for the values of a/h_3 considered, K_I, K_{II} and G are not significantly influenced by the crack length.

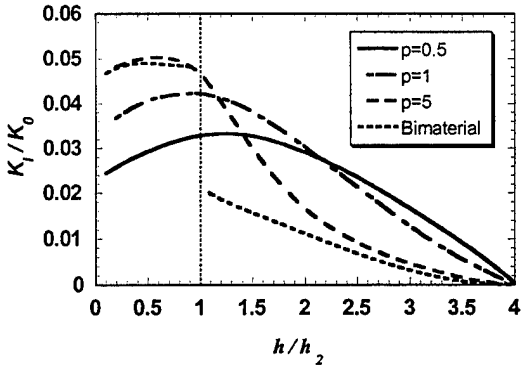

Figure 6. Mode I stress intensity factors vs. crack distance h for different coating types ($a=h_3$).

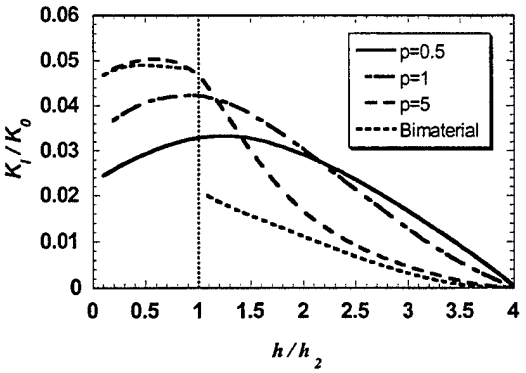

Figure 9. Mode I stress intensity factors vs. crack distance h for different coating types ($a=h_3/2$).

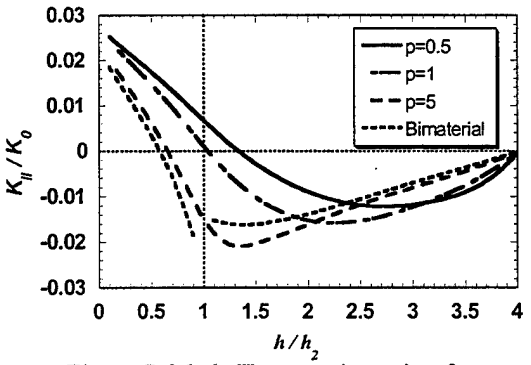

Figure 7. Mode II stress intensity factors vs. crack distance h for different coating types ($a=h_3$).

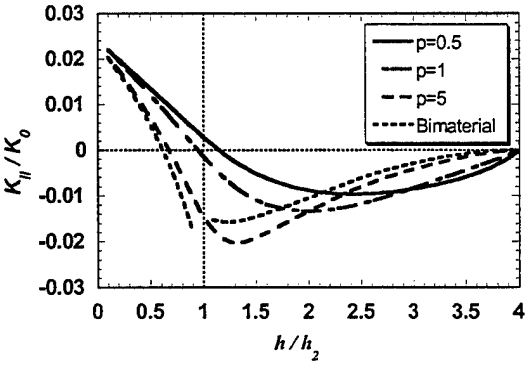

Figure 10. Mode II stress intensity factors vs. crack distance h for different coating types ($a=h_3/2$).

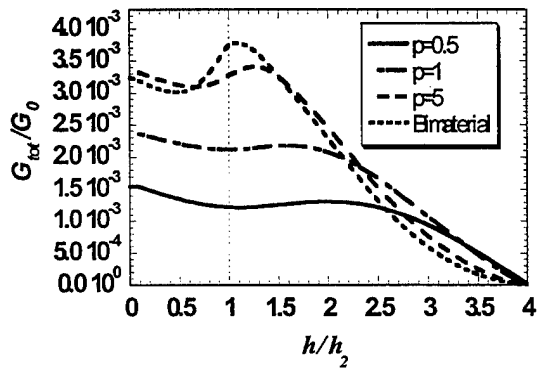

Figure 8. Strain energy release rates vs. crack distance h for different coating types ($a=h_3$).

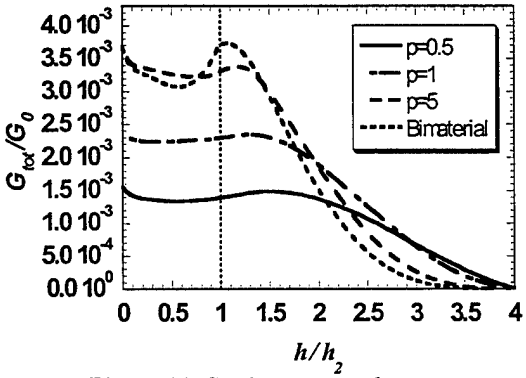

Figure 11. Strain energy release rates vs. crack distance h for different coating types ($a=h_3/2$).

From equation 4 and Figures 6 and 9 it may be seen that $K_I > 0$ for $\Delta T>0$. Also Figures 7 and 10 show that as h increases K_{II} changes sign at a critical value $h=h_{cr}$, $K_{II}>0$ for $0<h<h_{cr}$ and $K_{II} < 0$ for $h_{cr}<h<h_2+h_3$. If K_{II} is nonzero, then the stress state around the crack tip is one of mixed mode and, unles the plane of the crack is a weak cleavage plane, the crack propagation cannot be coplanar. In this case the crack path would deviate at an angle determined by the sign of K_{II} and relative magnitudes of K_I and K_{II}. This is qualitatively shown in Figure 12. The important physical conclusion here is that for a given FGM (or value of p), since the magnitudes of K_I and K_{II} are relatively independent of the crack length, $h=h_{cr}$ plane is a plane of stable crack growth. As physically expected, the figures also

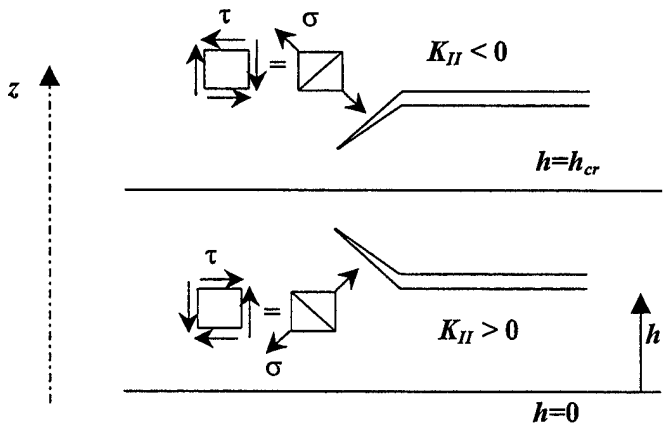

Figure 12. Stable crack growth plane $h=h_c$ and crack propagation direction above and below this plane.

show that the magnitudes of the strain energy release rate decrease as the metal content of the FGM coating increases.

As in any fracture problem, the path of the propagating crack is dependent on the crack dividing force G and the material parameter G_c representing the crack growth resistance, Figures 8 and 11 indicate that for given p, G is approximately maximum around $h=h_2$, that is, along TBC/bond coat interface. If one also considers the fact that usually an oxide scale (normally Al_2O_3) forms along the TBC/bond coat interface as medium is exposed to high temperature over an elongated period of time resulting in a plane of weak fracture resistance, it is reasonable to conclude that the crack propagation in the medium would be confined to a plane at or very near to the TBC/bond coat interface. Thus, in the next set of the results given in Figures 13-18 it is assumed that the crack lies along the

TBC/bond coat interface, $h=h_2$. Again, because of the self equilibrating stress state in the medium, it is physically expected that the stress intensity factors K_I, K_{II} and the strain energy release rate G tend to zero as $a \to 0$ and $a \to r_0$. This is clearly

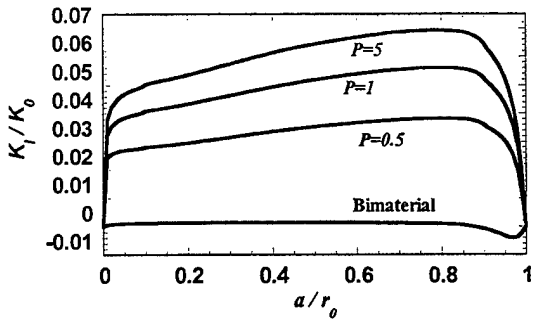

Figure 13. Mode I stress intensity factors vs crack length a for different coating types ($h=h_2$).

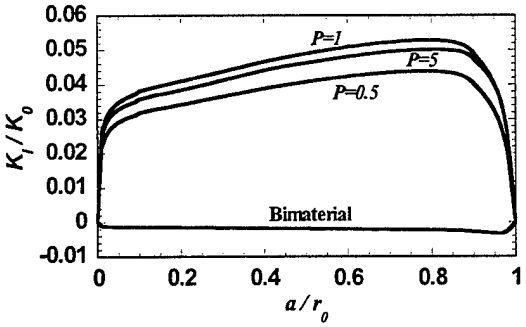

Figure 16. Mode I stress intensity factors vs. crack length a for different coating types ($h=h_2$ and temperature dependent thermoelastic properties used).

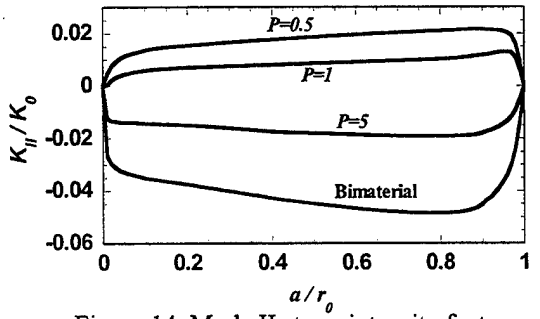

Figure 14. Mode II stress intensity factors Vs. crack length a for different coating types ($h=h_2$).

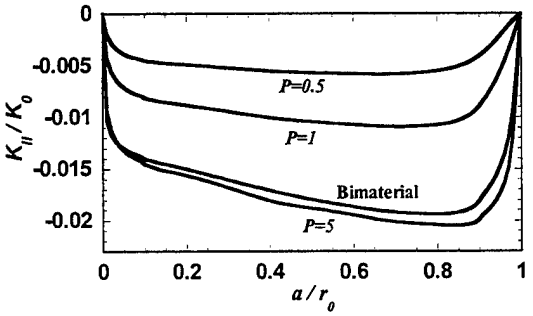

Figure 17. Mode II stress intensity factors vs. crack length a for different coating types ($h=h_2$ and temperature dependent thermoelastic properties used).

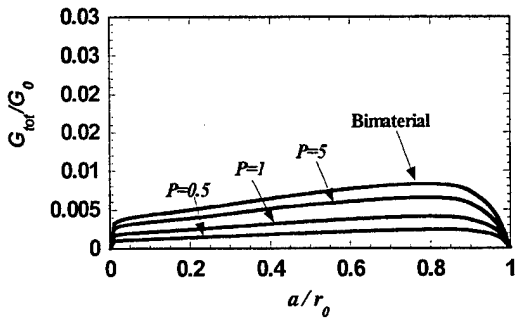

Figure 15. Strain energy release rates vs. crack length a for different coating types ($h=h_2$).

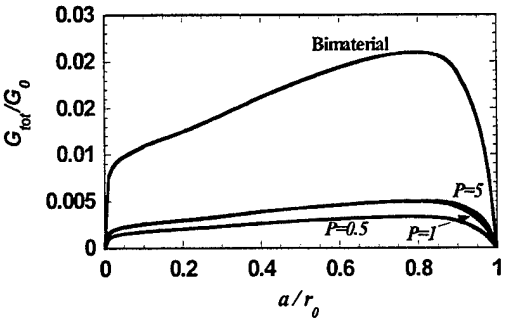

Figure 18. Strain energy release rates vs. crack length a for different coating types ($h=h_2$ and temperature dependent thermoelastic properties used).

seen to be the case in Figures 13-18. The results given in Figures 13-15 are calculated by using temperature-independent material properties corresponding to the reference temperature T_0 (in this case, the room temperature). The influence of the temperature dependence of the material properties (described in Figures 3-5) on K_I, K_{II} and G is shown in Figures 16-18. Figures 13-18 show that the effect of temperature dependence is very significant only in the case of homogenous ceramic TBC (p=∞). The reason for this appears to be excessive softening of ceramic at high temperature (Fig. 3) and the fact that G is inversely proportional to the overall stiffness. For the edge crack considered Figure 19 shows the deformed shape of the specimen and typical finite element mesh used in the study. Finite element formulation for FGM materials and enriched crack tip elements can be found in references [10] and [11].

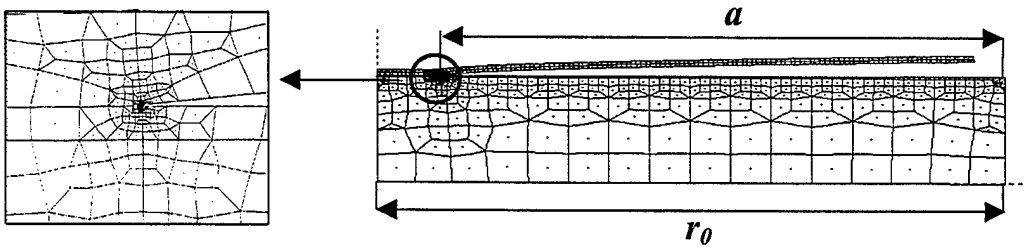

Figure 19. Deformed finite element mesh and a close up view of the crack tip elements.

TABLE I. Material properties at 22, 566 and 1149 °C [9].

Material	E (GPa)	ν	α (°C^{-1})
Substrate	175.8 150.4 94.1	0.2500 0.2566 0.3224	13.91×10^{-6} 15.36×10^{-6} 19.52×10^{-6}
Bond coat	137.9 121.4 93.8	0.27 0.27 0.27	15.16×10^{-6} 15.37×10^{-6} 17.48×10^{-6}
Ceramic	27.6 6.9 1.84	0.25 0.25 0.25	10.01×10^{-6} 11.01×10^{-6} 12.41×10^{-6}

ACKNOWLEDGEMENTS

This study was supported by AFOSR under the Grant F49620-98-10028 and by ARO under the Grant DAAHO4-95-1-0232.

REFERENCES

1. S.M. Meier, D. M. K.D. Nissley, K. D. Sheffler and T. A. Cruse, "Thermal Barrier Coating Life Prediction Model Development, " *Journal of Engineering for Gas Turbine and Power*, Trans. ASME, MD-Vol 44, (1993).
2. K.Kokini, ed. *Ceramic Coatings*, ASME, MD.-Vol 44, (1993).
3. M. Yamanaouchi, M.Koizumi, T. Hirai and I. Shiota (eds.) *FGM-90*, Proceedings of the First International Symposium on Functionally Graded Materials, FGM forum, Tokyo, Japan (1990).
4. J. B. Holt, M. Koizumi, T.Hirai and Z. A. Munir (eds.) Proceedings of the Second International Symposium on Functionally Graded Materials, *Ceramic Transactions*, Vol. 34, American Ceramic Society, Westerville, Ohio (1993).
5. B. Ilschner and N. Cherradi (eds.) Proceedings of the Third International Symposium on Structural and Functional Gradient Materials, Presses Polytechniques et Universitaries Romandes, Lausanne, Switzerland (1995).
6. Functionally Gradient Materials, MRS Bulletin, Vol. 20, No.1 (1995).
7. Y. D. Lee and F. Erdogan, "Residual\Thermal Stresses in FGM and Laminated Thermal Barrier Coating," *International Journal of Fracture*, Vol. 69 (1995) pp. 145-165.
8. K. Kurihara, K. Sasaki and M.Kawarada, "Adhesion Improvement of Diamond Films," in *FGM-90*, Yamanouchi et. Al. (eds.) (1990) pp. 65-69.
9. S. Q. Nusier and G. M. Newaz, "Analysis of Interfacial Cracks in a TBC/Superalloy System Under Thermo-mechanical Loading, " to appear in the Transactions of the ASME (1998).
10. Y. D. Lee and F. Erdogan, "Interface Cracking of Graded Coatings," to appear in *International Journal of Fracture* .
11. A. C. Kaya and H. F. Nied, "Interface Fracture Analysis of Bonded Ceramic Layers Using Enriched Finite Elements," MD-Vol. 44, *Ceramic Coatings* ASME (1993) pp 47-71.

APPENDIX C

CONTACT MECHANICS OF FGM COATINGS

Contact Mechanics of FGM Coatings

M. A. GULER and F. ERDOGAN

ABSTRACT

In this study the contact problem for an FGM coating on a homogeneous substrate in the presence of friction is considered. Different punch profiles such as triangular, semicircular and cylindrical are used to simulate the load transfer in practical applications. The analysis includes the application of Fourier transforms to the governing equations and boundary conditions. The general mixed boundary value problem is reduced to a singular integral equation of the second kind. The asymptotic analysis shows that the stress singularities are of the form $r^{-\alpha}$, $0 < \alpha < 1$, where α depends on the coefficient of friction, η, and the Poisson's ratio on the surface and is independent of non-homogeneity parameter, γh. The calculated results include contact stresses under the punch, the load required for given punch size and stress intensity factors where applicable. The effect of the non-homogeneity parameter and coefficient of friction on the contact stresses is studied for a variety of coating thicknesses in detail.

INTRODUCTION

Many of the present and potential applications of functionally graded materials (FGMs) involve contact problems. These are the basic load transfer problems between two solids, generally in the presence of friction. In the near future FGMs are expected to be used in three groups of practical applications that will require studying the problem from a view point of contact mechanics. The first is tribological applications of FGM coatings in such load transfer components as bearings, gears and cams. In this case the contacting solids are both elastic and one or both may have an FGM coating. The second application of the concept would be in cylinder linings, brake discs and other automotive components for the purpose of improving the wear resistance. In the related contact problem one of the

M. A. Guler and F. Erdogan, Department of Mechanical Engineering and Mechanics, Lehigh University, Bethlehem, PA 18015.

opposing components (e.g., piston rings and brake pads) may have sharp corners. The third area of potential application of FGM coatings involving contact mechanics is in the field of abradable seal design in stationary gas turbines. The concept of abradable seals was developed some years ago to reduce or to eliminate the gas leakage between the tips of the blades and the shroud. With such a design the gain due to increased efficiency seems to outweigh the power loss due to friction. In this case the layered medium consists of the substrate(a superalloy) the FGM(substrate/dense YSZ), and porous ceramic(porous YSZ). The contact is between porous ceramic and the blade. In these applications, the corresponding mechanics problem may be approximated by a quasi-static contact problem for a rigid punch of given profile moving over a graded medium in the presence of friction.

FORMULATION OF THE PROBLEM

The plane strain contact problems under consideration are described by the inserts in Figures 1, 3 and 5. Here the stiff contacting element is represented by a rigid punch and the coating(e.g. the abradable seal) by a graded metal/lowdensity ceramic layer. In the analytical solution, metal substrate is modeled as an elastic half plane. It is assumed that the stamp and the coated medium are in relative motion and the coefficient of friction, η, along the contact region is constant(i.e., $Q = \eta P$). The shear modulus of the FGM coating is approximated by

$$\mu_c(y) = \mu_0 \exp(\gamma y), \tag{1}$$

and $\nu_c = \nu_s = 0.3$, where $\mu_s = \mu_0 \exp(-\gamma h)$ is the shear modulus of the substrate and h is the thickness of the coating. The dimensionless constant γh represents the material inhomogeneity.

Shear stress at the surface of the FGM coating is related to the normal stress by coefficient of friction as follows

$$\sigma_{xy}(x,0) = \eta \sigma_{yy}(x,0) \qquad \text{or} \qquad q(x) = \eta p(x). \tag{2}$$

The related mixed boundary problem may be reduced to the following singular integral equation of the second kind

$$Ap(x) - \frac{1}{\pi}\int_{-a}^{b} \frac{p(t)}{t-x}\,dt + \int_{-a}^{b} k(x,t)dt = f(x), \tag{3}$$

$$A = \eta\frac{\kappa - 1}{\kappa + 1}, \qquad f(x) = \frac{4\mu_0}{\kappa + 1}\frac{\partial}{\partial x}v(x,0), \tag{4}$$

where $v(x,0)$, $-a < x < b$, is a known function giving the profile of the punch.In the singular integral equation (3) the contact pressure $p(x)$ is unknown and $k(x,t)$ is the known Fredholm kernel. But, a and b depend on the shape of the punch profile and are found by applying equilibrium and, if needed, the consistency

conditions. The equilibrium of the punch requires that the total pressure on the contact area should be equal to the total load applied to the punch. This can be expressed as

$$\int_{-a}^{b} p(t)dt = P, \tag{5}$$

where P is the known compressive force per unit depth in z direction.

We can write the singular integral equation in a normalized form by using appropriate change of variables as

$$A\phi(r) - \frac{1}{\pi}\int_{-1}^{1} \frac{\phi(s)}{s-r}\,ds + \int_{-1}^{1} K(r,s)ds = F(r). \tag{6}$$

The fundamental function of the singular integral equation (6) can be expressed as

$$w(r) = (1-r)^{\alpha}(1+r)^{\beta}, \tag{7}$$

$$\alpha = \frac{1}{2\pi i}\log\frac{A+i}{A-i} + N, \quad \beta = -\frac{1}{2\pi i}\log\frac{A+i}{A-i} + M, \tag{8}$$

$$-1 < \Re(\alpha) < 1, \qquad -1 < \Re(\beta) < 1,$$

where N and M are arbitrary(positive, zero, or negative) integers.

The singular integral equation has a Cauchy kernel and a Fredholm kernel. It does not have a closed form solution. The solution is generally obtained either through function-theoretic technique as given by Muskhelishvili [1] or through numerical methods [2], [3]. The plane strain problem for $h = \infty$ was considered in [4]. The corresponding axisymmetric frictionless contact problem was studied in [5] and [6]. In this study the unknown function is represented by an infinite series in Jacobi polynomials associated with the weight function $w(r)$ given by (7). The corresponding singular integral equation may thus be reduced to an infinite system of algebraic equations and solved by using the technique described in [7].

The solution of the normalized singular integral equation can be expresses as

$$\phi(r) = w(r)\sum_{0}^{\infty} C_n P_n^{(\alpha,\beta)}(r), \tag{9}$$

where $P_n^{(\alpha,\beta)}(r)$ are the Jacobi Polynomials associated with the weight function $w(r)$. By substituting (9) into (6) and truncating the series at $n = N$, and using a suitable collocation technique, equation (3) may be reduced to a system of linear algebraic equations in the unknown coefficients $C_0, C_1, \ldots, C_N$. Contact length, then, can be found by using the equilibrium equation (5) and, if needed, the consistency condition.

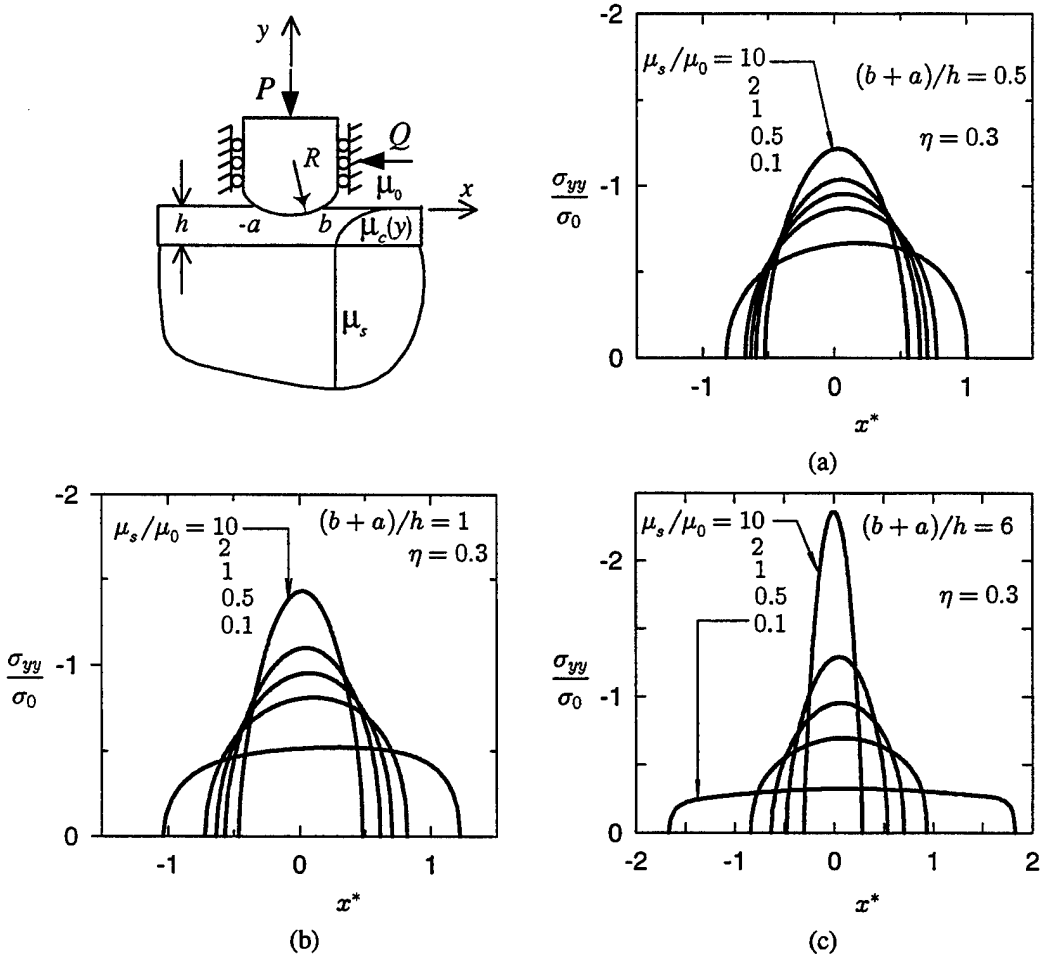

Figure 1 Contact stress distribution under a cylindrical punch for various values of contact zone sizes and the stiffness ratios μ_s/μ_0, in the presence of friction, $\eta = 0.3$. $\sigma_0 = \mu_0\sqrt{U}$, $x^* = x/(R\sqrt{U})$, $U = P/(\mu_0 R)$.

RESULTS AND DISCUSSION

The main results of this study are the contact stresses under the punch, the load required for given punch size, and stress intensity factors as functions of the stiffness ratios μ_s/μ_0 and the basic dimensionless length parameter l/h where l is the contact length for the particular punch profile. The closed form results for the homogeneous half plane is also presented since it can be used to verify the results in limiting cases. As $\gamma h \to 0$, μ_s/μ_0 tends to unity and the results for a homogeneous half plane should be recovered.

In the cylindrical punch problem, described in Figure 1 a rigid half cylinder of radius R is pressed to an FGM coating on an elastic substrate. For small values of b/R and a/R the surface of the cylindrical punch may be approximated by a parabola. Therefore the input function in the singular integral equation (3) becomes,

$$f(x) = \frac{4\mu_0}{\kappa + 1}\frac{x}{R}. \tag{10}$$

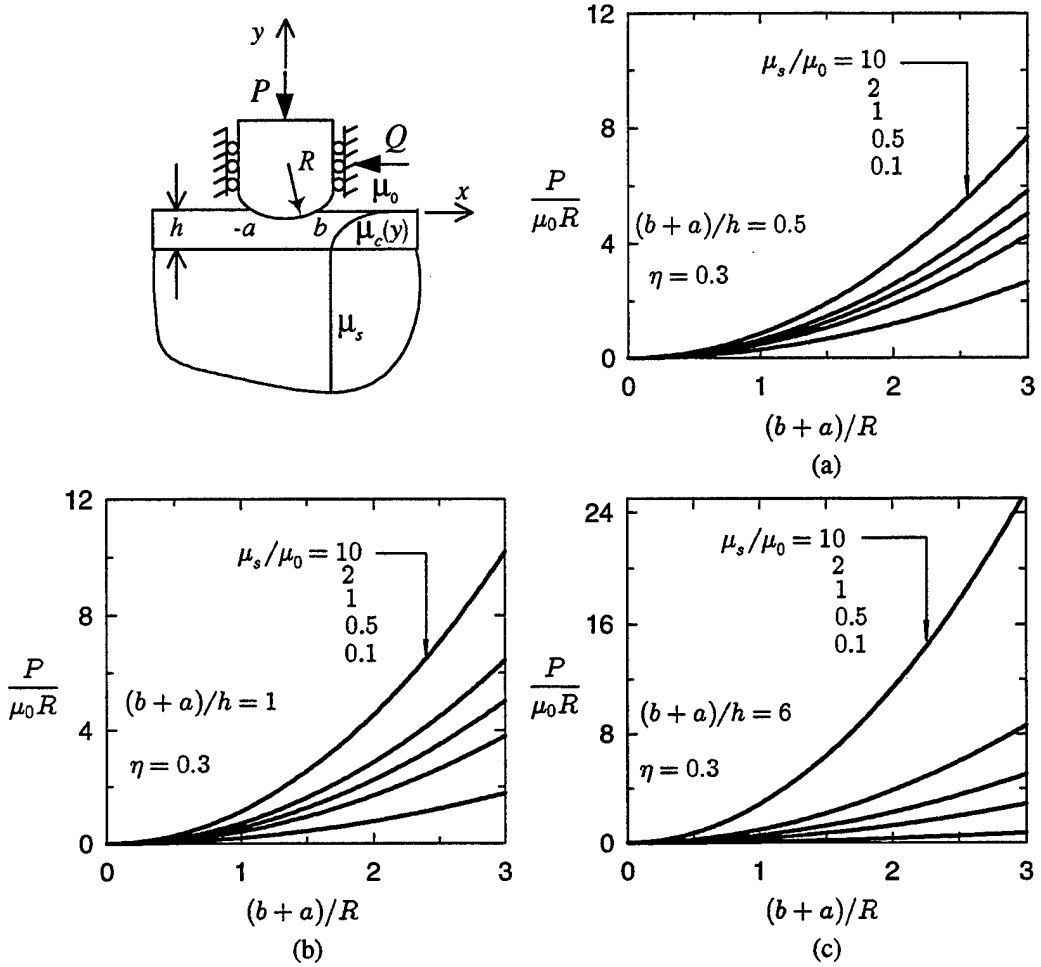

Figure 2 Normalized Applied load versus the normalized contact length for a cylindrical punch for various values of contact zone sizes and the stiffness ratios μ_s/μ_0, in the presence of friction, $\eta = 0.3$.

The location of the end points of the contact region a and b can not be obtained in closed form. The system of equations is nonlinear in $(C_0, ..., C_N, a, b)$, therefore it is necessary to adopt an iterative scheme. The problem is solved by assuming a value for a, and then solve the resulting linear algebraic equations resulting from the integral equation and the consistency condition for $C_0, ..., C_N$ and b. The constant a is then determined from the equilibrium condition (5).

The influence of the stiffness ratios, μ_s/μ_0, on the contact stress distribution under a cylindrical punch is shown in Figure 1. Three cases $(b + a)/h = 0.5$, 1.0, 2.0 have been investigated for the constant coefficient of friction $\eta = 0.3$. In the pressure profiles $\mu_s/\mu_0 > 1$ denotes a compliant surface, such as an abradable seal, and $\mu_s/\mu_0 < 1$ denotes a wear-resistant hardened surface, and $\mu_s = \mu_0$ denotes a homogeneous coating. The exponential model (1) was examined for $\mu_s/\mu_0 = 10$, 2, 1, 0.5, 0.1 which correspond to $\gamma h = -2.3026$, -0.6931, 0.0, 0.6931, 2.3026, respectively. Note that γh is the measure of the gradient in the FGM coating and $\gamma h = 0$ corresponds to a homogeneous medium.

Since there is a smooth contact, contact stress goes to zero at the ends of the

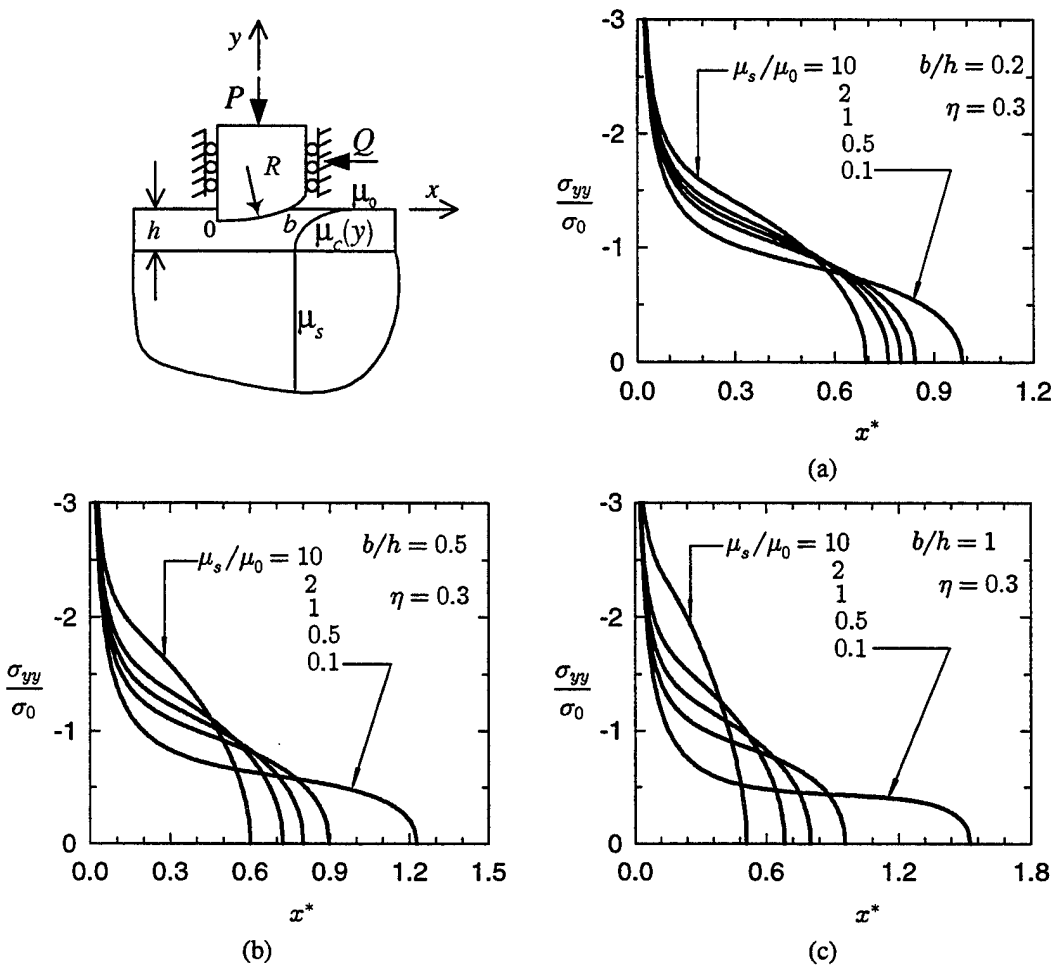

Figure 3 Contact stress distribution under a semicircular punch for various values of the stiffness ratios μ_s/μ_0, in the presence of friction, $\eta = 0.3$. $\sigma_0 = \mu_0\sqrt{U}$, $x^* = x/(R\sqrt{U})$, $U = P/(\mu_0 R)$

contact region. We have a closed form relation for the pressure profile for the homogeneous coating as follows :

$$\frac{p(x)}{\mu_0\sqrt{U}} = \frac{4\sin\pi\alpha}{\kappa+1}(b^* - x^*)^\alpha(x^* + a^*)^\beta \tag{11}$$

where

$$U = \frac{P}{\mu_0 R}, \qquad a^* = \frac{a}{R\sqrt{U}}, \qquad b^* = \frac{b}{R\sqrt{U}}, \qquad x^* = \frac{x}{R\sqrt{U}}. \tag{12}$$

As seen from Figure 1, for $\mu_0 < \mu_s$, the intensity of the contact stress becomes greater. Since there is friction, the pressure profiles are not symmetric and are slanted toward the trailing edge($x = b$) of the contact region. Also, as h decreases the intensity of the contact stress increases for $\mu_0 < \mu_s$ and decreases for $\mu_0 > \mu_s$. As for the contact length, it becomes smaller for stiffening medium and for decreasing h.

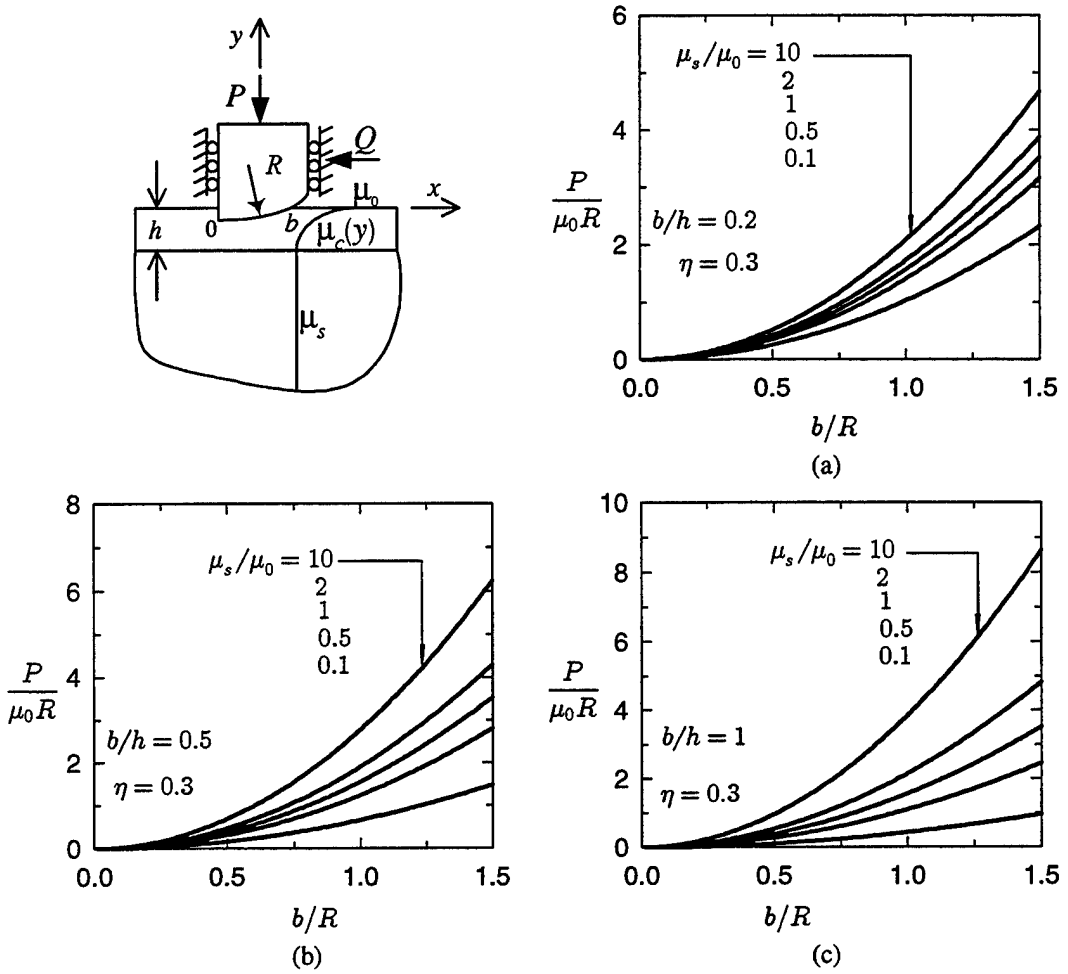

Figure 4 Normalized Applied load vs. the contact length b for a semicircular punch for various values of the stiffness ratios μ_s/μ_0, in the presence of friction, $\eta = 0.3$.

In Figure 2, the normalized load is given as a function of normalized contact length $(b+a)/R$, for $(b+a)/h = 0.5, 1.0, 2.0$ and for various values of the stiffness ratios, μ_s/μ_0. In the case of $\mu_s/\mu_0 > 1$, that is a compliant surface on a stiffer substrate, the normalized load increases as the contact length increases. As the stiffness ratio becomes smaller, $\mu_s/\mu_0 < 1$, load required for the same amount of contact length decreases.

The closed form result for the homogeneous substrate is given by

$$\frac{P}{\mu_0 R} = \frac{2\pi\alpha(1-\alpha)}{\kappa+1}\left(\frac{b+a}{R}\right)^2. \tag{13}$$

Figure 3 gives the contact pressure distribution under a semicircular punch for various values of the stiffness ratios, μ_s/μ_0. Note that for the homogenous coating (i.e. $\mu_s = \mu_0$) there is a closed form relation for the contact stresses in the form

$$\frac{p(x)}{\mu_0\sqrt{U}} = \frac{4\sin\pi\alpha}{\sqrt{(\kappa+1)2\pi\alpha(1+\alpha)}}\left(\alpha+\frac{x}{b}\right)\left(\frac{b-x}{x}\right)^{\alpha}. \tag{14}$$

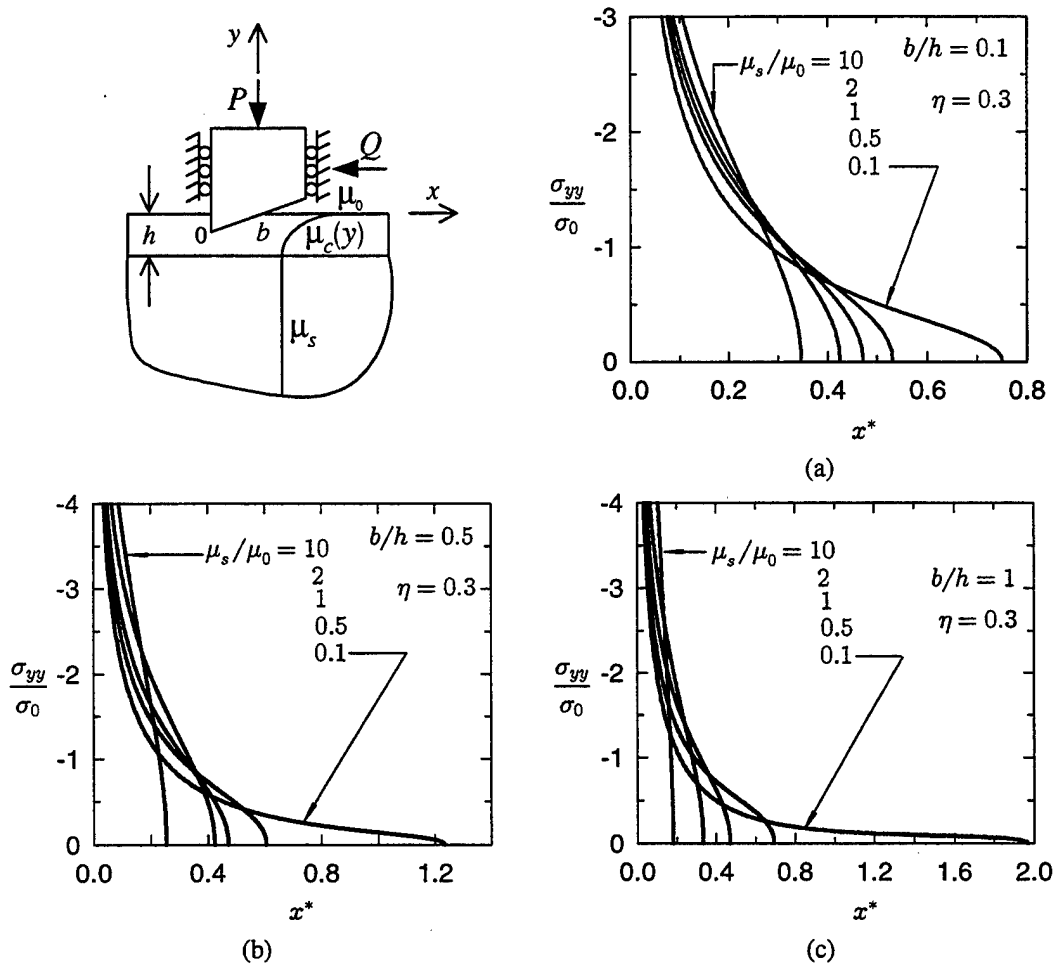

Figure 5 Contact stress distribution under a triangular punch for various values of the contact zone sizes and the stiffness ratios μ_s/μ_0, in the presence of friction, $\eta = 0.3$, $\sigma_0 = \mu_0 m$, $x^* = \mu_0 m x/P$.

Figure 4 gives the normalized load as a function of the normalized contact length b/R, for $b/h = 0.2, 0.5, 1.0$ and for various values of the stiffness ratios, μ_s/μ_0. Also for the same applied load the contact length increases with surface stiffness. The closed form relation for the homogeneous half plane is parabolic and is given by

$$\frac{P}{\mu_0 R} = \frac{2\pi\alpha(1-\alpha)}{\kappa+1}\left(\frac{b}{R}\right)^2. \tag{16}$$

The profile for the triangular punch is shown in Figure 5. For this case, the input function $f(x)$ in equation (3) for this case is

$$f(x) = \frac{4\mu_0}{\kappa+1} m, \tag{17}$$

where m is the slope of the punch profile. The pressure is again zero at $x = b$ due to smooth contact and is unbounded at $x = 0$ due to sharp edge. Note that for $\mu_s/\mu_0 = 1$ the medium is homogeneous and contact stress $p(x)$ and the resultant force P are known in closed form and are given by

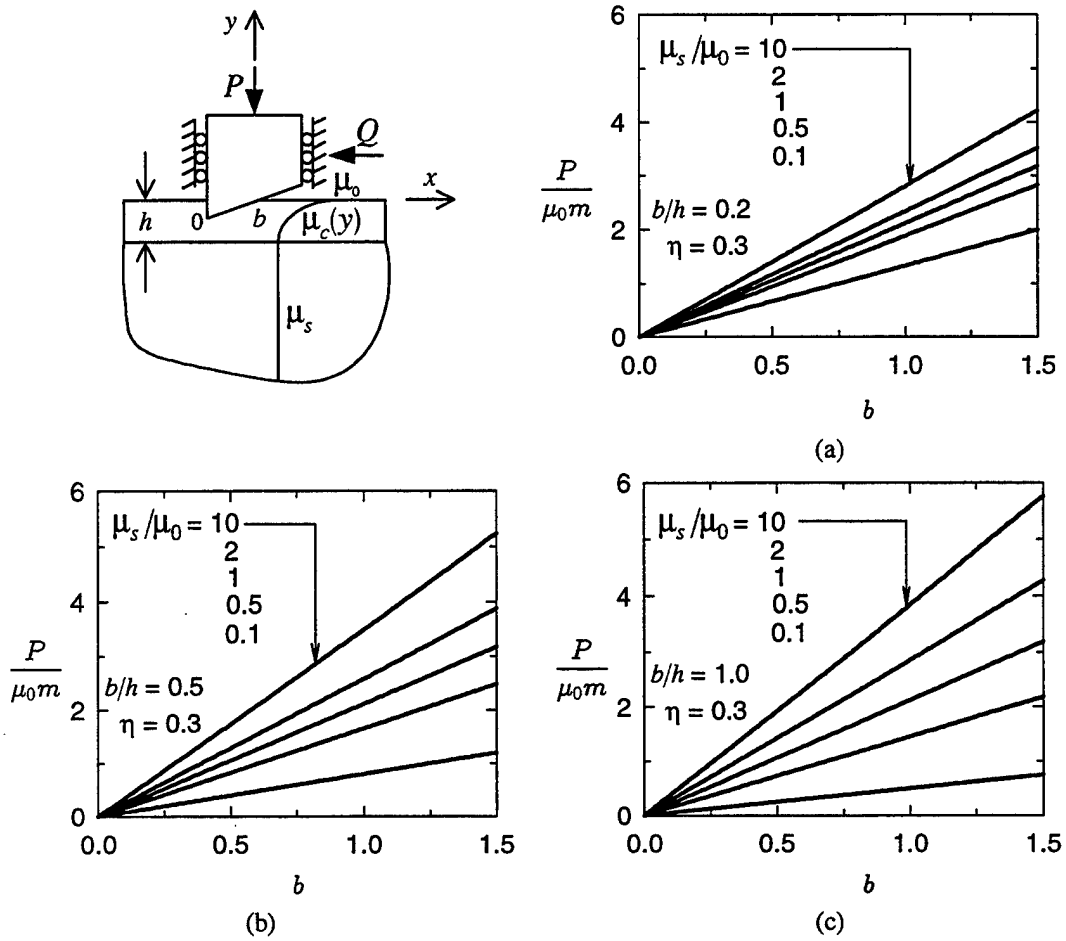

Figure 6 Applied load versus the contact length b for a triangular punch for various values of the stiffness ratios μ_s/μ_0, in the presence of friction, $\eta = 0.3$.

$$\frac{p(x)}{\mu_0 m} = \frac{4\sin\pi\alpha}{\kappa+1}\left(\frac{b-x}{x}\right)^{\alpha}, \qquad \frac{P}{\mu_0 m} = \frac{4\pi\alpha}{\kappa+1}b. \tag{18}$$

Figure 5 gives the contact pressure distribution and Figure 6 gives the normalized load as a function of the contact length b under a triangular punch for various values of the stiffness ratios, μ_s/μ_0.

Mode I Stress intensity factors(SIF) for the semicircular and triangular punch at the sharp end($x = 0$) may be defined as

$$k_1(0) = \lim_{x\to 0} x^{\alpha} p(x). \tag{19}$$

Stress intensity factors for both profiles are normalized with respect to the SIF in corresponding homogeneous case. For the semicircular and triangular stamps the SIFs for the homogeneous cases ($\mu_s/\mu_0 = 1$) respectively are

$$k_{1h}^{s}(0) = \frac{2\sin\pi\alpha}{\pi(1+\alpha)}\frac{P}{b^{1-\alpha}}, \qquad k_{1h}^{t}(0) = \frac{\sin\pi\alpha}{\pi\alpha}\frac{P}{b^{1-\alpha}}. \tag{20}$$

Table 1 gives an idea about the influence of the variation of μ_s/μ_0 on the normalized stress intensity factors for various values of coating thicknesses.

TABLE 1 STRESS INTENSITY FACTORS

	Semicircular punch $k_1(0)/k_{1h}^s(0)$					Triangular punch $k_1(0)/k_{1h}^t(0)$				
μ_s/μ_0 b/h	10.0	2.0	1.0	0.5	0.1	10.0	2.0	1.0	0.5	0.1
0.2	0.868	0.959	1.000	1.042	1.149	0.845	0.947	1.000	1.062	1.254
0.5	0.634	0.899	1.000	1.112	1.435	0.690	0.884	1.000	1.145	1.663
1.0	0.464	0.813	1.000	1.212	1.854	0.525	0.809	1.000	1.250	2.184

ACKNOWLEDGEMENT

This study was partially supported by AFOSR under the Grant F49620-98-1-0028.

REFERENCES

1. N. L. Muskhelishvili, 1953. *Singular Integral Equations*, P. Noordhoff, Groningen, The Netherlands.

2. F. Erdogan, and G. D. Gupta, 1972. "On the Numerical Solution of Singular Integral Equations", *Quarterly of Applied Mathematics*, Vol. 29, pp. 525-534.

3. A. C. Kaya, F. Erdogan, 1987. "On the Solution of Integral Equation with a Generalized Cauchy Kernel", *Quarterly of Applied Mathematics*, Vol. xiv, pp. 455-469.

4. M. A. Guler, 1996. *The problem of a rigid punch with friction on a graded elastic medium*, M. S. Thesis, Lehigh University.

5. A. Giannakopoulos and S. Suresh, 1997. "Indentation of solids with gradients in elastic properties: Part II. Axisymmetric indentors", *Int. J. Solids & Structures*, Vol. 34, No 19, pp. 2393-2428.

6. S. Suresh, A. E. Giannakopoulos and J. Alcala, 1997. "Spherical indentation of compositionally graded materials: theory and experiments." , *Acta Mater*, Vol. 45, No 4, pp. 1307-1321.

7. F. Erdogan, G. D. Gupta and T. S. Cook, 1973. "Numerical Solution of Singular Integral Equations", *Method of Analysis and Solution of Crack Problems*, G. C. Sih (ed.), Noordhoff Int. Publ., Leyden, pp. 368-425.

APPENDIX D

AXISYMMETRIC CRACK PROBLEM IN A FUNCTIONALLY GRADED SEMI-INFINITE MEDIUM

Axisymmetric Crack Problem in a Functionally Graded Semi-Infinite Medium

A. SAHIN and F. ERDOGAN

ABSTRACT

In this study the axisymmetric crack problem in a functionally graded semi-infinite medium is considered. It is assumed that the penny-shaped crack is located parallel to the free surface and the mechanical properties of the medium vary in depth direction only. By using a superposition technique the problem is reduced to a perturbation problem in which crack surface tractions are the only external forces. The corresponding mixed boundary value problem is then reduced to an integral equation with a generalized Cauchy kernel and solved numerically to obtain stress intensity factors and crack opening displacements. Results obtained for different nonhomogeneity and length parameters are presented and discussed. The problem has applications to the investigation of the general question of spallation fracture.

INTRODUCTION

In recent years the requirements for high temperature applications of structural materials have become increasingly more stringent. Since very often the conventional materials were not adequate for modern technologies, various forms of composites and bonded materials have been used in such technological applications as power generation, transportation, aerospace and microelectronics. In high temperature applications, metals and metal alloys appear to be very susceptible to oxidation, creep and generally to loss of structural integrity [1]. Similarly, low strength and low toughness have always been the disadvantages of ceramics. Thus, as an alternative to conventional homogeneous thermal barrier ceramic coatings, the concept of functionally graded materials (FGM) was proposed. FGMs are essentially two-phase particulate composites synthesized in a such way that the volume fractions of the constituents vary continuously in the thickness direction to give a predetermined composition profile.

A. Sahin and F. Erdogan, Division of Applied Mathematics, Lehigh University, Bethlehem, PA 18015

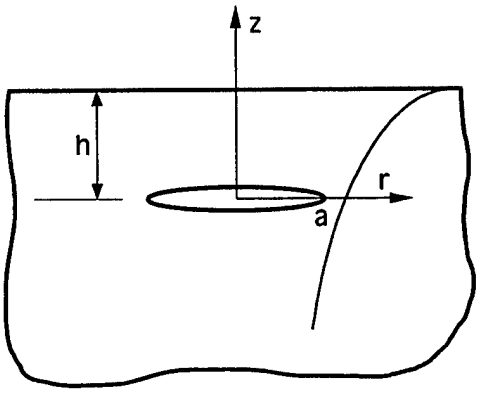

Figure 1 Crack geometry and notations

In this study it is assumed that the functionally graded medium contains an initial dominant flaw which can be approximated by a penny-shaped crack parallel to the surface (Figure 1). With the applications to fatigue and fracture in mind, the primary objective of the study has been the calculation of the stress intensity factors and the crack opening displacements. The previous studies have shown that in linear elastic crack problems for FGMs the fracture mechanics parameters are not very sensitive to the Poisson's ratio, ν, [2],[3]. Thus, in this study, too, it is assumed that ν is constant throughout the medium. It is also assumed that the Young's modulus may be represented by an exponential function of the depth coordinate z (Figure 1). Under these assumptions the problem becomes analytically tractable and may be reduced to a system of singular integral equations by using the Hankel transforms [4].

FORMULATION OF THE PROBLEM

Consider the axisymmetric crack problem in a nonhomogeneous semi-infinite medium described in Figure 1 with the crack radius a and the distance h. Let the Lame 's constants be approximated by

$$\mu(z) = \mu_0 \exp(\alpha z), \qquad \lambda(z) = \lambda_0 \exp(\alpha z). \tag{1}$$

For the perturbation problem under consideration the only nonvanishing external loads are assumed to be

$$\sigma_{1zz}(r, 0^+) = \sigma_{2zz}(r, 0^-) = p_1(r), \qquad 0 \le r < a, \tag{2a}$$

$$\sigma_{1rz}(r, 0^+) = \sigma_{2rz}(r, 0^-) = p_2(r), \qquad 0 \le r < a, \tag{2b}$$

Using the kinematic relation and the Hooke's law in the absence of body forces, the equilibrium equations can be expressed as follows :

$$(\kappa+1)\left(\frac{\partial^2 u}{\partial r^2}+\frac{1}{r}\frac{\partial u}{\partial r}-\frac{u}{r^2}+\frac{\partial^2 w}{\partial r\partial z}\right)+(\kappa-1)\alpha\left(\frac{\partial u}{\partial z}+\frac{\partial w}{\partial r}\right)$$

$$+(\kappa-1)\left(\frac{\partial^2 u}{\partial z^2}-\frac{\partial^2 w}{\partial r\partial z}\right)=0, \tag{3a}$$

$$(\kappa+1)\left(\frac{\partial^2 u}{\partial r\partial z}+\frac{1}{r}\frac{\partial u}{\partial z}+\frac{\partial^2 w}{\partial z^2}\right)-(3-\kappa)\alpha\left(\frac{\partial u}{\partial r}+\frac{u}{r}\right)$$

$$+(\kappa+1)\alpha\frac{\partial w}{\partial z}-(\kappa-1)\left(\frac{\partial^2 u}{\partial r\partial z}-\frac{\partial^2 w}{\partial r^2}\right)-\frac{(\kappa-1)}{r}\left(\frac{\partial u}{\partial z}-\frac{\partial w}{\partial r}\right)=0, \tag{3b}$$

where $\kappa=3-4\nu$, $\lambda/\mu=2\nu/(1-2\nu)$, ν being the Poisson's ratio. The function $u(r,z)$ and $w(r,z)$ are the r and z components of the displacement vector. Equation (3) may be solved by using Hankel transforms with the following boundary and continuity conditions:

$$\sigma_{1zz}(r,h)=0, \qquad \sigma_{1rz}(r,h)=0, \qquad 0<r<\infty, \tag{4a}$$

$$\sigma_{1zz}(r,0)=\sigma_{2zz}(r,0), \quad \sigma_{1rz}(r,0)=\sigma_{2rz}(r,0), \quad 0<r<\infty, \tag{4b}$$

$$w_1(r,0^+)-w_2(r,0^-)=0, \qquad a<r<\infty, \tag{4c}$$

$$u_1(r,0^+)-u_2(r,0^-)=0, \qquad a<r<\infty, \tag{4d}$$

where subscripts 1 and 2 refer to the domains $0<z<h$ and $z<0$, respectively. After some lengthy analysis the mixed boundary conditions (2a,b) and (4c,d) may be reduced to the following system of integral equations

$$\frac{1}{\pi}\int_{-a}^{a}\frac{\phi_1(s)}{s-r}\,ds+\frac{1}{\pi}\int_0^a\sum_{j=1}^{2}k_{1j}(s,r)\phi_j(s)\,ds=\frac{(\kappa+1)}{2\mu_0}p_1(r), \qquad 0\le r<a \tag{5a}$$

$$\frac{1}{\pi}\int_{-a}^{a}\frac{\phi_2(s)}{s-r}\,ds+\frac{1}{\pi}\int_0^a\sum_{j=1}^{2}k_{2j}(s,r)\phi_j(s)\,ds=-\frac{(\kappa+1)}{2\mu_0}p_2(r), \quad 0\le r<a \tag{5b}$$

$$\int_{-a}^{a}\phi_1(s)\,ds=0, \tag{5c}$$

$$\int_{-a}^{a} s\,\phi_2(s)\,ds = 0, \tag{5d}$$

where

$$\phi_1(r) = \frac{\partial}{\partial r}(w(r,0^+) - w(r,0^-)), \qquad 0 \le r < \infty, \tag{6a}$$

$$\phi_2(r) = \frac{1}{r}\frac{\partial}{\partial r}(ru(r,0^+) - ru(r,0^-)), \qquad 0 \le r < \infty, \tag{6b}$$

ϕ_1 and ϕ_2 are unknown functions and the Fredholm kernels $k_{ij}(s,r)$, $(i,j = 1,2)$, are square integrable in the domain $0 \le (r,s) \le a$. Although in practice these kernels are generally bounded and continuous in the interval $(0,a)$, in axisymmetric problems $k_{ij}(s,r)$ invariably contains a logarithmic singularity at $r = s$ [5]. Since there is no "closed form" solution for (5), an effective numerical solution may be developed by using a quadrature formula of the Gaussian type to evaluate the integral with Fredholm kernels for appropriately selected values of r_i, $(i = 1,..,n)$, and reducing the problem to a system of linear algebraic equations in the unknowns $\phi(s_j)$, $(j = 1,..,n)$. It can also be shown that the solution of the integral equations (5) may be expressed in terms of the following infinite series :

$$\phi_1(s) = \frac{1}{\sqrt{1-\left(\frac{s}{a}\right)^2}} \sum_{n=0}^{\infty} A_n T_n\left(\frac{s}{a}\right), \tag{7a}$$

$$\phi_2(s) = \frac{1}{\sqrt{1-\left(\frac{s}{a}\right)^2}} \sum_{n=0}^{\infty} B_n T_n\left(\frac{s}{a}\right), \tag{7b}$$

where the orthogonal functions T_n are Chebyshev polynomials of the first kind and $T_0 = 1$. A_n and B_n are the new unknowns which may be determined from the linear algebraic system obtained by substituting (7) into (5) and by using a method of reduction.

RESULTS AND DISCUSSION

The main results of this study are the stress intensity factors calculated for various loading conditions as functions of the dimensionless nonhomogeneity constant αa defined by (1) and the basic dimensionless length parameter h/a. For a homogeneous infinite medium modes I and II crack problems are uncoupled and the stress intensity factors are given by

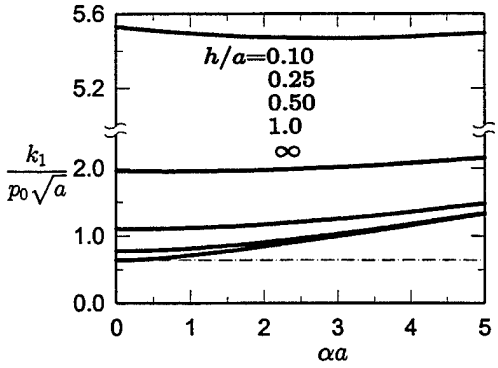

Figure 2 Normalized SIF for various h/a, $\sigma_{zz}(r,0) = -p_0,\ \sigma_{rz}(r,0) = 0$

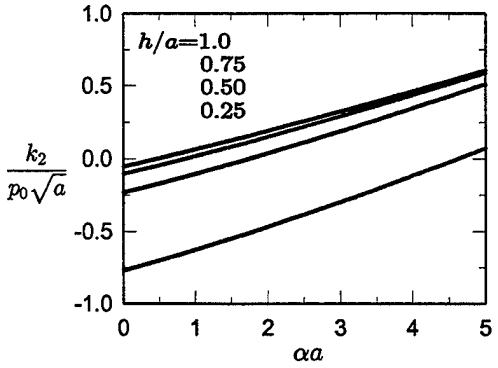

Figure 3 Normalized SIF for various h/a, $\sigma_{zz}(r,0) = -p_0,\ \sigma_{rz}(r,0) = 0$

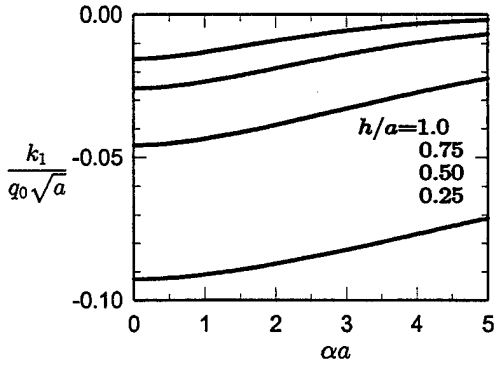

Figure 4 Normalized SIF for various h/a, $\sigma_{zz}(r,0) = 0,\ \sigma_{rz}(r,0) = -q_0$

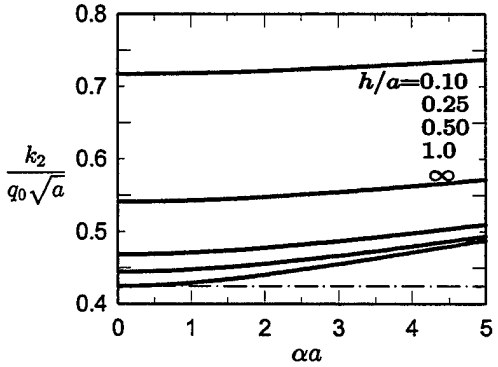

Figure 5 Normalized SIF for various h/a, $\sigma_{zz}(r,0) = 0,\ \sigma_{rz}(r,0) = -q_0$

$$k_1 = -\frac{2}{\pi\sqrt{a}}\int_0^a \frac{rp_1(r)}{\sqrt{a^2-r^2}}dr, \qquad k_2 = -\frac{2}{\pi\sqrt{a^3}}\int_0^a \frac{r^2p_2(r)}{\sqrt{a^2-r^2}}dr. \tag{8}$$

In Figures 2-17, the stress intensity factors and the crack opening displacements are shown for two different loading conditions, namely $p_1(r) = -p_0$, $p_2(r) = 0$ and $p_2(r) = -q_0(r/a)$, $p_1(r) = 0$. For the problem under consideration the normalized stress intensity factors and the crack opening displacements are calculated for a constant Poisson's ratio ($\nu = 0.3$) by varying h/a and αa. Note that the problem is formulated and can be solved for arbitrary crack surface tractions. Figure 2-9 show the normalized mode I and mode II stress intensity factors k_1 and k_2 for two primary loading conditions with the dimensionless constants αa and h/a as the variables. For large h/a values, the calculated stress intensity factors agree with the results given in [3].

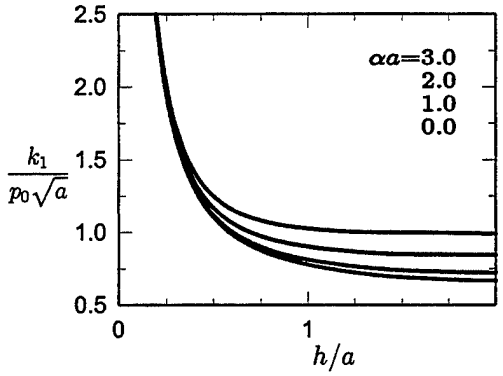

Figure 6 Normalized SIF for various αa, $\sigma_{zz}(r,0) = -p_0,\ \sigma_{rz}(r,0) = 0$

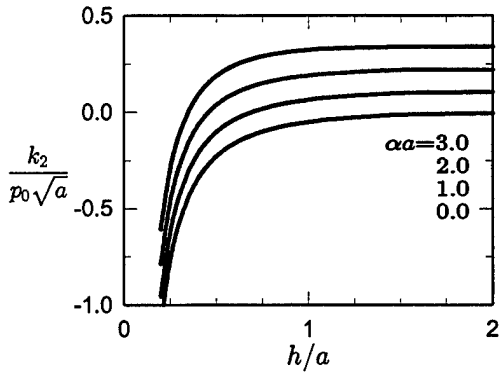

Figure 7 Normalized SIF for various αa, $\sigma_{zz}(r,0) = -p_0,\ \sigma_{rz}(r,0) = 0$

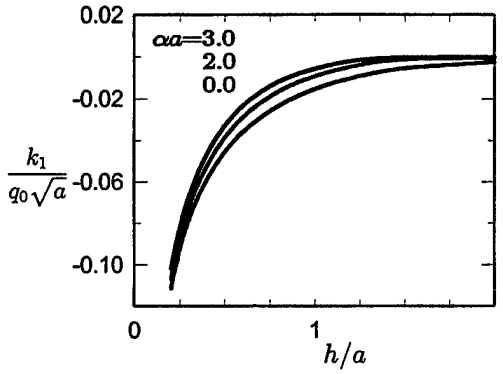

Figure 8 Normalized SIF for various αa, $\sigma_{zz}(r,0) = 0,\ \sigma_{rz}(r,0) = -q_0$

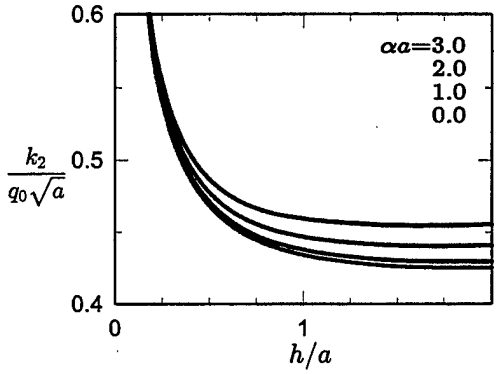

Figure 9 Normalized SIF for various αa, $\sigma_{zz}(r,0) = 0,\ \sigma_{rz}(r,0) = -q_0$

When there was only normal loading ($\sigma_{zz}(r,0) = -p_0,\ \sigma_{rz}(r,0) = 0$), it was observed that for large values of h/a, normalized stress intensity factor k_1 increases slowly as the nonhomogeneity parameter αa increases. However, for small values of h/a, (such as $h/a = 0.10$), the normalized stress intensity factor k_1 first decreases and then slowly increases with increasing αa (Figure 2). Under the same loading k_2 increases with increasing αa for all values of h/a. On the other hand for shear loading ($\sigma_{zz}(r,0) = 0,\ \sigma_{rz}(r,0) = -q_0$), stress intensity factor k_1 increases for all values of h/a with increasing αa, however, the values of k_1 are small. Similarly, k_2 increases for all values of h/a with increasing αa, but the values of k_2 are small compared to k_1 under the normal loading.

From Figures 10 and 11 it may also be observed that values of k_1 under normal loading and k_2 under shear loading were almost symmetric with respect to αa ($-5 < \alpha a < 5$) for large values of h/a. Since the stress intensity factors do not depend on the magnitude of the shear modulus μ_0 for a crack in an infinite medium, this result is expected.

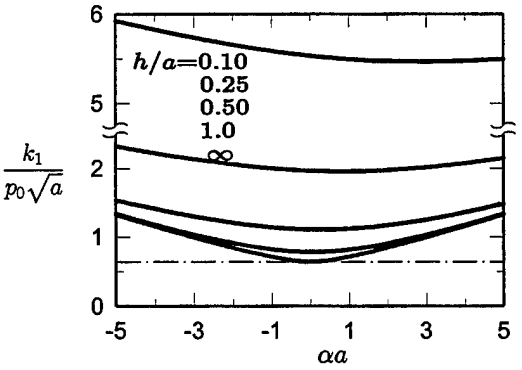

Figure 10 Normalized SIF for various h/a, $\sigma_{zz}(r,0) = -p_0,\ \sigma_{rz}(r,0) = 0$

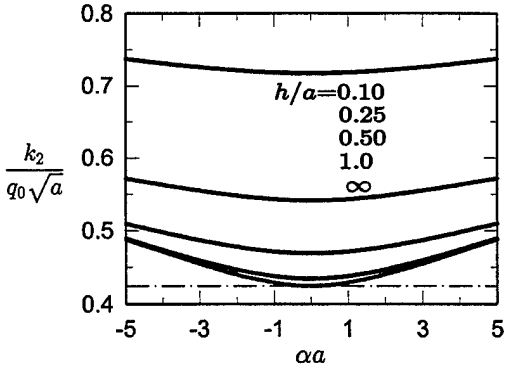

Figure 11 Normalized SIF for various h/a, $\sigma_{zz}(r,0) = 0,\ \sigma_{rz}(r,0) = -q_0$

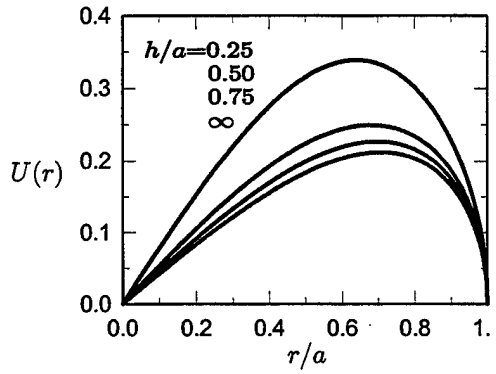

Figure 12 Normalized COD for $\alpha a = 0$, $\sigma_{zz}(r,0) = 0,\ \sigma_{rz}(r,0) = -q_0$

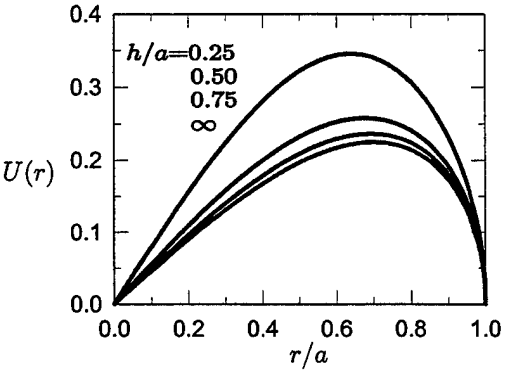

Figure 13 Normalized COD for $\alpha a = 2$, $\sigma_{zz}(r,0) = 0,\ \sigma_{rz}(r,0) = -q_0$

It was also observed that stress intensity factors k_1 and k_2 under respectively normal and shear loading tend to certain limiting values as h/a increases. On the other hand as expected, same stress intensity factors tend to infinity when h/a goes to zero. For large values of h/a the results agree with [3]. Also, for fixed values of αa the stress intensity factors $k_1$and k_2 under shear and normal loading, respectively, tend to certain limiting values which are, however, negligibly small.

Figures 12-17, show some sample results for the normalized crack opening displacements $U(r)$ and $W(r)$, which are respectively the r and z components of the relative crack opening defined by (Figure 1)

$$U(r) = \frac{u(r,0^+) - u(r,0^-)}{\frac{aq_0(\kappa+1)}{2\mu}}, \qquad W(r) = \frac{w(r,0^+) - w(r,0^-)}{\frac{ap_0(\kappa+1)}{2\mu}} \tag{9}$$

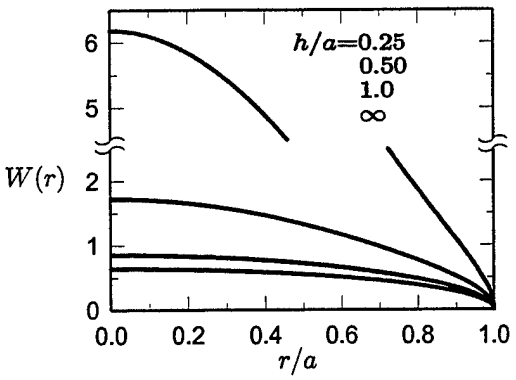

Figure 14 Normalized COD for $\alpha a = 0$, $\sigma_{zz}(r,0) = -p_0,\ \sigma_{rz}(r,0) = 0$

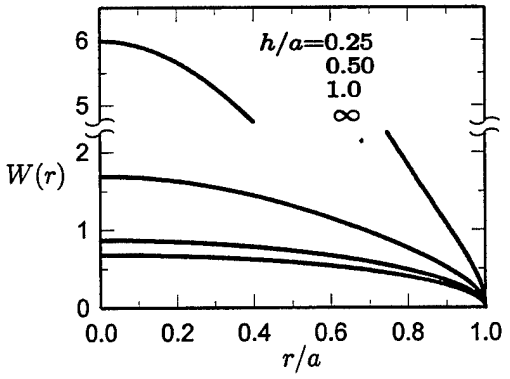

Figure 15 Normalized COD for $\alpha a = 0.5$, $\sigma_{zz}(r,0) = -p_0,\ \sigma_{rz}(r,0) = 0$

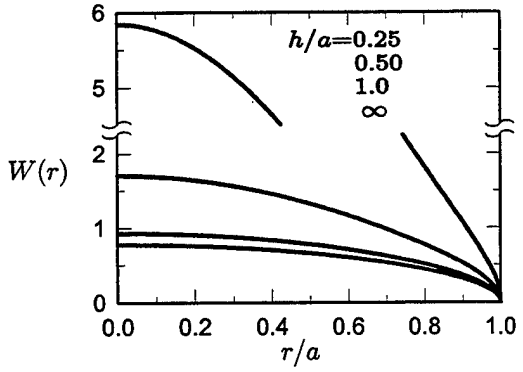

Figure 16 Normalized COD for $\alpha a = 1$, $\sigma_{zz}(r,0) = -p_0,\ \sigma_{rz}(r,0) = 0$

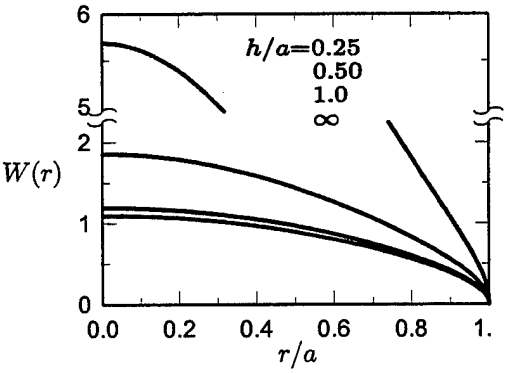

Figure 17 Normalized COD for $\alpha a = 2$, $\sigma_{zz}(r,0) = -p_0,\ \sigma_{rz}(r,0) = 0$

The figures show that the influence of the nonhomogeneity constant αa on the crack opening displacements is not very significant. On the other hand $U(r)$ and $W(r)$ are seen to be rather heavily dependent on h/a (particularly for small values of h/a). Again, for large values of h/a the results agree with that given in [3]. The problem was solved under the assumption that the Poisson's ratio ν is constant. Theoretically this is not possible. The assumption can only be justified if the fracture mechanics parameters of interest, in this case the stress intensity factors, prove to be relatively insensitive to variations in the Poisson's ratio. In the problem considered, it was observed that stress intensity factors are relatively insensitive to variations in the Poisson's ratio for small values of nonhomogeneity parameter αa and for all values of h/a. But for large αa and small h/a the effect of Poisson's ratio may not be negligible. Some results are presented in Tables 1-4 to give an idea about the influence of the variation in ν on the stress intensity factors. It may be seen that, generally, the influence of ν on the stress intensity factors is not very significant.

TABLE 1 THE VARIATION OF SIF WITH ν FOR $h/a = 2.0$ AND $\sigma_{zz}(r,0) = -p_0,\ \sigma_{rz}(r,0) = 0$.

ν	$\alpha a = 0.1$		$\alpha a = 1.0$		$\alpha a = 2.0$		$\alpha a = 4.0$	
	$\frac{k_1}{p_0\sqrt{a}}$	$\frac{k_2}{p_0\sqrt{a}}$	$\frac{k_1}{p_0\sqrt{a}}$	$\frac{k_2}{p_0\sqrt{a}}$	$\frac{k_1}{p_0\sqrt{a}}$	$\frac{k_2}{p_0\sqrt{a}}$	$\frac{k_1}{p_0\sqrt{a}}$	$\frac{k_2}{p_0\sqrt{a}}$
0.00	.6676	.0037	.7041	.1021	.7962	.2162	1.0598	.4636
0.10	.6677	.0037	.7094	.1024	.8101	.2170	1.0870	.4657
0.20	.6678	.0037	.7157	.1028	.8266	.2179	1.1186	.4682
0.30	.6679	.0037	.7236	.1033	.8465	.2189	1.1562	.4711
0.40	.6681	.0037	.7337	.1038	.8710	.2201	1.2021	.4747
0.45	.6681	.0037	.7398	.1041	.8857	.2208	1.2292	.4768

TABLE 2 THE VARIATION OF SIF WITH ν FOR $h/a = 2.0$ AND $\sigma_{zz}(r,0) = 0,\ \sigma_{rz}(r,0) = -q_0$.

ν	$\alpha a = 0.1$		$\alpha a = 0.5$		$\alpha a = 1.0$		$\alpha a = 1.5$	
	$\frac{k_1}{q_0\sqrt{a}}$	$\frac{k_2}{q_0\sqrt{a}}$	$\frac{k_1}{q_0\sqrt{a}}$	$\frac{k_2}{q_0\sqrt{a}}$	$\frac{k_1}{q_0\sqrt{a}}$	$\frac{k_2}{q_0\sqrt{a}}$	$\frac{k_1}{q_0\sqrt{a}}$	$\frac{k_2}{q_0\sqrt{a}}$
0.00	−.0025	.4253	−.0018	.4285	−.0008	.4370	−.0001	.4638
0.10	−.0025	.4254	−.0017	.4288	−.0007	.4380	−.0001	.4659
0.20	−.0025	.4254	−.0016	.4292	−.0006	.4391	.0000	.4683
0.30	−.0025	.4254	−.0015	.4296	−.0005	.4406	.0000	.4712
0.40	−.0025	.4254	−.0013	.4303	−.0004	.4423	.0000	.4747
0.45	−.0025	.4254	−.0012	.4307	−.0003	.4434	.0000	.4768

TABLE 3 THE VARIATION OF SIF WITH ν FOR $h/a = 0.25$ AND $\sigma_{zz}(r,0) = -p_0,\ \sigma_{rz}(r,0) = 0$.

ν	$\alpha a = 0.1$		$\alpha a = 1.0$		$\alpha a = 2.0$		$\alpha a = 4.0$	
	$\frac{k_1}{p_0\sqrt{a}}$	$\frac{k_2}{p_0\sqrt{a}}$	$\frac{k_1}{p_0\sqrt{a}}$	$\frac{k_2}{p_0\sqrt{a}}$	$\frac{k_1}{p_0\sqrt{a}}$	$\frac{k_2}{p_0\sqrt{a}}$	$\frac{k_1}{p_0\sqrt{a}}$	$\frac{k_2}{p_0\sqrt{a}}$
0.00	1.9598	−.7568	1.9490	−.6297	1.9564	−.4780	2.0285	−.1435
0.10	1.9598	−.7568	1.9502	−.6289	1.9606	−.4753	2.0407	−.1362
0.20	1.9598	−.7568	1.9517	−.6280	1.9657	−.4720	2.0552	−.1276
0.30	1.9599	−.7568	1.9536	−.6267	1.9720	−.4679	2.0729	−.1173
0.40	1.9599	−.7567	1.9560	−.6251	1.9802	−.4627	2.0952	−.1045
0.45	1.9599	−.7567	1.9576	−.6241	1.9852	−.4596	2.1088	−.0969

TABLE 4 THE VARIATION OF SIF WITH ν FOR $h/a = 0.25$ AND $\sigma_{zz}(r,0) = 0,\ \sigma_{rz}(r,0) = -q_0$.

ν	$\alpha a = 0.1$		$\alpha a = 1.0$		$\alpha a = 2.0$		$\alpha a = 4.0$	
	$\frac{k_1}{q_0\sqrt{a}}$	$\frac{k_2}{q_0\sqrt{a}}$	$\frac{k_1}{q_0\sqrt{a}}$	$\frac{k_2}{q_0\sqrt{a}}$	$\frac{k_1}{q_0\sqrt{a}}$	$\frac{k_2}{q_0\sqrt{a}}$	$\frac{k_1}{q_0\sqrt{a}}$	$\frac{k_2}{q_0\sqrt{a}}$
0.00	−.0925	.5412	−.0915	.5425	−.0887	.5463	−.0799	.5591
0.10	−.0925	.5412	−.0914	.5426	−.0883	.5467	−.0790	.5601
0.20	−.0925	.5412	−.0912	.5428	−.0878	.5472	−.0780	.5612
0.30	−.0925	.5412	−.0910	.5430	−.0872	.5478	−.0768	.5626
0.40	−.0925	.5412	−.0907	.5432	−.0865	.5486	−.0754	.5642
0.45	−.0925	.5412	−.0906	.5434	−.0860	.5490	−.0745	.5652

ACKNOWLEDGEMENT

This study was partially supported by AFOSR under the Grant F49620-98-1-0028 and by ARO under the Grant DAAH04-95-1-0232.

REFERENCES

1. W.Y. Lee, Y.W. Bae, C.C. Berndt, F. Erdogan, Y.D. Lee and Z. Mutasim, 1996. "The Concept of FGMs for Advanced Thermal Barrier Coating Applications." *Journal of American Ceramic Society*, 79 [12] : 3003-3012.

2. F. Delale and F. Erdogan, 1988. "Interface Crack In Nonhomogeneous Medium." *Int. Journal of Engineering Science*, Vol. 26, pp. 559-568.

3. M. Ozturk and F. Erdogan, 1993. "Axisymmetric Crack Problem in a Nonhomogeneous Medium." *ASME Journal of Applied Mechanics*, Vol. 60, pp. 406-414.

4. F. Erdogan, G.D. Gupta and T.S. Cook, 1973. "Numerical Solution of Singular Integral Equations." in *Method of Analysis and Solution of Crack Problems,* G.C. Sih, eds. Leyden: Noordhoff Int. Publ., pp: 368-425.

5. F. Erdogan, 1965. "Simultaneous Dual Integral Equations with Trigonometric and Bessel Kernels." *Zeitschrift Fur Angewandte Mathematik und Mechanik,* Vol.48 n4 pp:217-225

APPENDIX E

WAVE PROPAGATION IN A FUNCTIONALLY GRADED ELASTIC MEDIUM

Wave Propagation in a Functionally Graded Elastic Medium

T.-C. CHIU and F. ERDOGAN

ABSTRACT

In this study the one-dimensional wave propagation in a functionally graded elastic slab is considered. It is assumed that the stiffness and density of the medium vary continuously in thickness direction and it is initially at rest and stress-free. The slab is subjected to a pressure pulse on one surface and vanishing stress or displacement condition on the other. The solution is obtained in wave summation form. Propagation of a rectangular pressure pulse in a graded medium that consists of either nickel/zirconia or aluminum /silicon carbide is studied as examples. It is shown that there is considerable wave distortion in time and the distortion is much more pronounced in slabs with fixed/free boundary conditions. A simple approximate expression giving the peak stress is developed. Also it is demonstrated that the energy balance principle may be used as a convergence criterion in the calculation of stresses.

INTRODUCTION

In layered materials involving functionally graded coatings and interlayers, generally the dominant modes of failure appear to be cracking and spallation. Aside from the appropriate fracture mechanics, dealing with these failure problems requires a detailed stress analysis for identifying the likely sites of failure initiation and for determining the peak values of stresses. In some cases the loading of these inhomogeneous components may be dynamic in nature. Thus, an important area of interest in considering the applications of functionally graded materials(FGMs) would be to study the dynamic response of the component to, for example, impact or blast loading. In elastodynamics of materials with continuously varying properties, usually the pulse shape is distorted in time, the wave propagation speed is not constant, and there are no sharp interfaces that would cause wave reflections.

T.-C. Chiu and F. Erdogan, Department of Mechanical Engineering and Mechanics, Lehigh University, Bethlehem, PA 18015

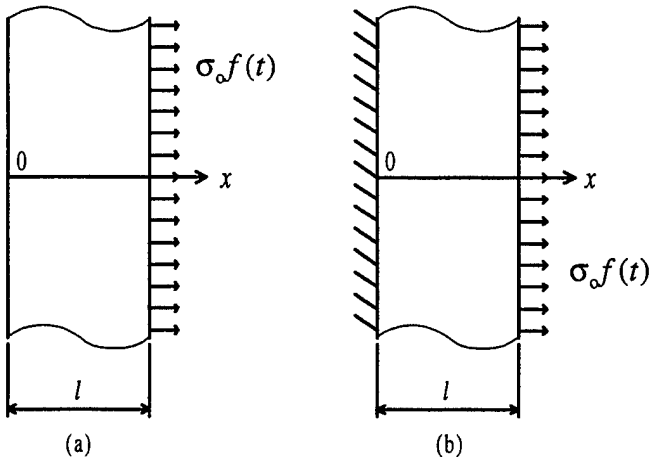

Figure 1 Boundary conditions and loading for an FGM slab; (a) free/free, (b) fixed/free boundaries, $\sigma_{xx}(l,t) = \sigma_0 f(t)$ stress pulse.

Consequently, even in the simple case of one-dimensional wave propagation the locations and magnitudes of peak stresses cannot be determined by inspection.

Because of its relevance in geophysics and soil mechanics, in the past there has been quite considerable interest in the elastodynamics of inhomogeneous media (e.g., [1]-[5]). In the present paper we consider the one-dimensional problem in elastodynamics for an FGM plate in which material properties vary only in thickness direction. The boundary conditions are assumed to be either free/free or fixed/free. Laplace transform technique is used to solve the problem. Even-though the technique could accommodate arbitrary inputs, the problem is solved under zero initial conditions with a rectangular pressure pulse as the external load.

ON THE FORMULATION OF THE PROBLEM

The one-dimensional elastodynamic problem under consideration is described in Figure 1. It is assumed that the slab is isotropic and inhomogeneous with the following properties:

$$E'(x) = E'_0(a\frac{x}{l}+1)^m, \qquad \rho(x) = \rho_0(a\frac{x}{l}+1)^n, \tag{1}$$

where ρ is the mass density, l is the thickness, a, m, and n are arbitrary real constants with $a > -1$, E'_0 and ρ_0 are the elastic constant and density at $x = 0$, and the elastic constant E' is determined under the assumption that $\sigma_{yy} = \sigma_{zz}$ and the slab is fully constrained at infinity. It can, thus, be shown that

$$E' = \frac{E(1-\nu)}{(1+\nu)(1-2\nu)}, \tag{2}$$

$E(x)$ and $\nu(x)$ being the Young's modulus and the Poisson's ratio of the inhomogeneous material. It is assumed that initially the slab is at rest. By introducing the normalized quantities

$$X = x/l,\ T = c_0 t/l,\ U = u/l,\ c_0 = \sqrt{E_0'/\rho_0}, \tag{3}$$

and using Laplace transform, the solution of the wave equation for the inhomogeneous medium may be obtained as follows [6]:

$$\frac{u(x,t)}{l} = U(X,T) = \frac{1}{2\pi \mathrm{i}} \int_{\gamma-\mathrm{i}\infty}^{\gamma+\mathrm{i}\infty} \widehat{U}(X,p) \mathrm{e}^{pT} dp, \tag{4a}$$

$$\sigma_{xx}(x,t) = \frac{E'}{2\pi \mathrm{i}} \int_{\gamma-\mathrm{i}\infty}^{\gamma+\mathrm{i}\infty} \frac{d\widehat{U}}{dX} \mathrm{e}^{pT} dp, \tag{4b}$$

where

$$\widehat{U}(X,p) = \begin{cases} (aX+1)^{\frac{1-m}{2}} \left[C_1 \mathrm{I}_\alpha \left(\left| \frac{p}{\beta a} \right| (aX+1)^\beta \right) \right. \\ \qquad \left. + C_2 \mathrm{K}_\alpha \left(\left| \frac{p}{\beta a} \right| (aX+1)^\beta \right) \right], \qquad m \neq n+2, \\ \\ C_3 (aX+1)^{s_3} + C_4 (aX+1)^{s_4}, \qquad m = n+2, \end{cases} \tag{5}$$

$\mathrm{I}_\beta(z)$ and $\mathrm{K}_\beta(z)$ are the modified Bessel functions of the first and second kind, respectively, α and β are functions of m and n, and s_3 and s_4 are known functions of p. The pairs of unknown functions $(C_1(p), C_2(p))$ or $(C_3(p), C_4(p))$ are to be determined from the boundary conditions at $x = 0$ and $x = l$. At $x = 0$ the condition is

$$\sigma_{xx}(0,t) = 0,\ t > 0,\ (\text{"free" boundary}) \tag{6a}$$

or

$$u(0,t) = 0,\ t > 0,\ (\text{"fixed" boundary}). \tag{6b}$$

At $x = l$ the slab is subjected to a stress pulse given by

$$\sigma_{xx}(l,t) = \sigma_0 f(T),\ T = c_0 t/l,\ t > 0 \tag{7}$$

where the constant σ_0 is the magnitude of the pulse, the function f describes its time profile, and without any loss in generality, it is assumed that $|f| \leq 1$.

From a viewpoint of failure mechanics there is a greater interest in the evaluation of stresses than the displacements. The inversion of transforms such as (4) may be accomplished by a technique of either residue summation or wave summation. The residue summation is best suited to study the long time response, whereas the wave summation technique is more appropriate for short time analysis and is more descriptive in displaying the wave character of the response. In this study the main interest is in the transient response of the medium and, hence, only the wave solution is developed. Referring to the Abel-Tauber theorems regarding the asymptotic results, it is observed that for a given transform pair $g(T)$ and $\widehat{g}(p)$ the asymptotic behavior of $\widehat{g}(p)$ for large values of p corresponds to the behavior of $g(T)$ for small values of T. Thus, through the asymptotic analysis (4b) may be expressed in a form

TABLE I – PROPERTIES OF MATERIALS USED IN THE EXAMPLES

	E (GPa)	ν	ρ (kg/m^3)
ZrO_2	151	0.33	5331
Ni	207	0.31	8900
SiC	210	0.17	3100
Al	71	0.33	2710

TABLE II – MATERIAL CONSTANTS OF FGMS USED IN THE EXAMPLES AND DEFINED BY EQUATIONS (1) AND (2)

	Ni/ZrO_2	ZrO_2/Ni	SiC/Al	Al/SiC
E_0' (GPa)	286.922	223.728	225.719	105.197
ρ_0 (kg/m^3)	8900	5331	3100	2710
a	0.14096	-0.12354	-0.53395	1.14568
m	-1.8866	-1.8866	1.0000	1.0000
n	-3.8866	-3.8866	0.17611	0.17611

suitable for evaluating the small time response [6]. In the asymptotic expression if only the first terms in the expansions are kept, the following approximations for the stress component σ_{xx} are obtained that are valid for small values of T only:

$$\frac{\sigma_{xx}(X,T)}{\sigma_0} \cong \left(\frac{aX+1}{a+1}\right)^{\frac{m+n}{4}} \sum_{k=0}^{\infty} \Big[f(T-\xi_{1k})\mathrm{H}(T-\xi_{1k}) - f(T-\xi_{2k})\mathrm{H}(T-\xi_{2k}) \Big] \tag{8a}$$

for the free/free boundary conditions (Figure 1a), and

$$\frac{\sigma_{xx}(X,T)}{\sigma_0} \cong \left(\frac{aX+1}{a+1}\right)^{\frac{m+n}{4}} \sum_{k=0}^{\infty} (-1)^k \Big[f(T-\eta_{1k})\mathrm{H}(T-\eta_{1k}) + f(T-\eta_{2k})\mathrm{H}(T-\eta_{2k}) \Big] \tag{8b}$$

for the fixed/free boundary conditions (Figure 1b), where $\mathrm{H}(t)$ is the Heaviside function and ξ_{ik} and η_{ik}, $i = 1, 2$, are functions of X [6].

RESULTS AND DISCUSSION

As a first example we consider an FGM slab that consists of nickel and zirconia. We assume that the thickness of the plate is $l = 5$ mm, on one surface the medium is pure nickel, on the other surface pure zirconia, and the material properties $E'(x)$ and $\rho(x)$ vary smoothly in thickness direction. A pressure pulse defined by

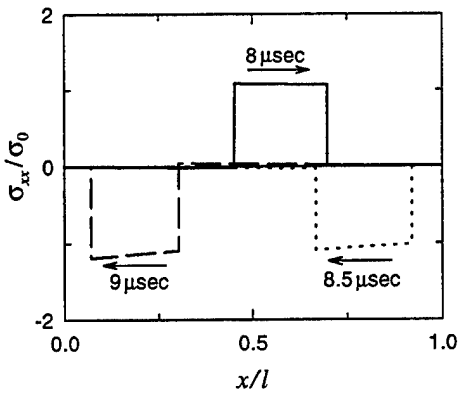

Figure 2 σ_{xx}/σ_0 vs. x at three different t for a Ni/ZrO_2 FGM slab under free/free boundary conditions, the arrows indicate the direction of pulse propagation.

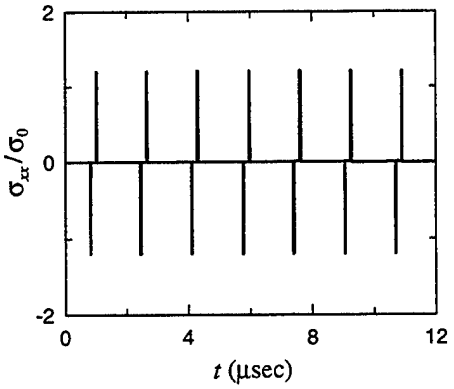

Figure 3 The variation of σ_{xx}/σ_0 with t at $x = l/50$ in a Ni/ZrO_2 FGM slab under free/free boundary conditions.

$$\sigma_{xx}(l,t) = -\sigma_0\Big[\mathrm{H}(t) - \mathrm{H}(t-t_0)\Big] \tag{9}$$

is applied to the surface $x = l$ and the boundary $x = 0$ is either "free" or "fixed" (Figure 1). The pulse duration is assumed to be $t_0 = 0.2$ μsec. The properties of the constituent materials used in the examples are given in Table I. The material parameters defined by (1) and (2) for the FGMs used in the examples are given in Table II. Six-term asymptotic approximations are used in the examples for calculating the stresses. The results for the case of Ni/ZrO_2 slab with free/free boundaries are shown in Figures 2-4. Figure 2 shows the stress as a function of location x for three different values of time. Figures 3 and 4 show the time dependence of the stress at $x = l/50$ and $x = l/2$, respectively. Note that at $x = 0$ the stress is zero and $x = l/50$ was selected to have some idea about the spallation stress near the boundary. Figures 5 and 6 show the time-dependence of the stress at the fixed boundary (Figure 1b) $x = 0$ for Ni/ZrO_2 and ZrO_2/Ni FGM slab, respectively. By examining the results given in Figures 2-4 where the boundaries of the slab is stress-free and the pulse is applied on the less stiff side, it may be observed that the duration of the pulse remains constant (at $\Delta t = t_0 = 0.2$ μsec), the pulse shape is distorted as time increases, at a given location the jump $\Delta\sigma$ in stress corresponding to leading and trailing edges of the pulse remains constant but its value is dependent on the location x, at $x = l$ $\Delta\sigma = \sigma_0$, for $0 < x < l$ $\Delta\sigma > \sigma_0$, and as x decreases, $\Delta\sigma$ increases slightly but monotonically. After the pulse passes through the stress does not drop to zero and this overshoot seems to increase with time. These deviations from the homogeneous materials are much more pronounced in the case of fixed/free boundaries than in free/free boundaries. This can be clearly seen from Figures 5 and 6. Figures 5 and 6 also show the standard doubling of the amplitude of the pulse reflected from the fixed boundary at $x = 0$. However, if the fixed boundary $x = 0$ is the stiffer side of FGM, then the jump $2\Delta\sigma$ in the reflected pulse is greater than $2\sigma_0$ (Figure 5) and if $x = 0$ is the less stiff side, then $2\Delta\sigma < 2\sigma_0$

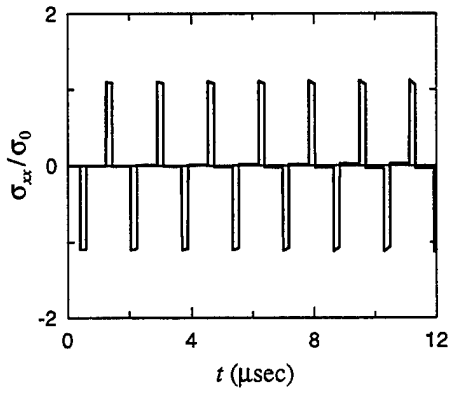

Figure 4 The variation of σ_{xx}/σ_0 with t at $x = l/2$ in a Ni/ZrO_2 FGM slab under free/free boundary conditions.

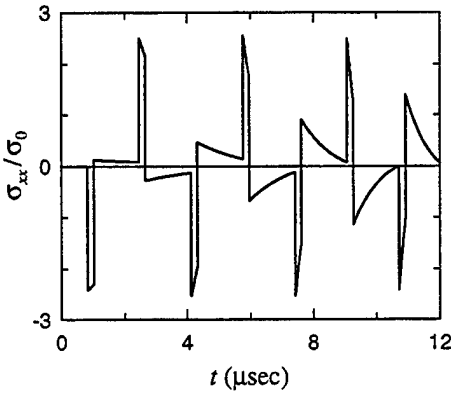

Figure 5 The variation of σ_{xx}/σ_0 with t at $x = 0$ in a Ni/ZrO_2 FGM slab under fixed/free boundary conditions.

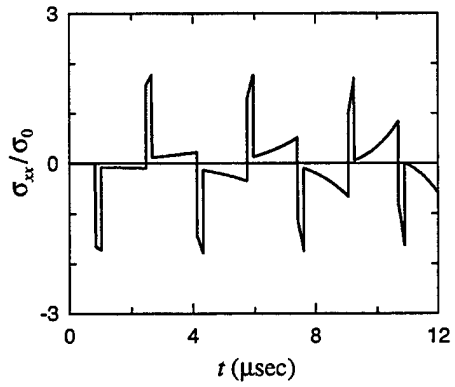

Figure 6 The variation of σ_{xx}/σ_0 with t at $x = 0$ in a ZrO_2/Ni FGM slab under fixed/free boundary conditions.

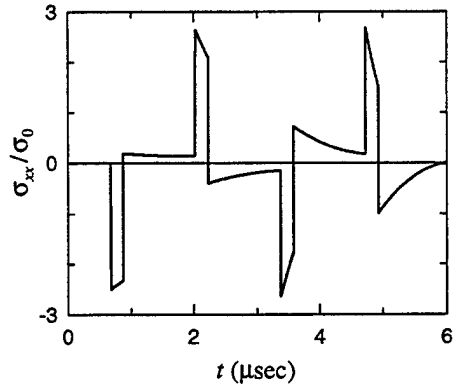

Figure 7 The variation of σ_{xx}/σ_0 with t at $x = 0$ in a SiC/Al FGM slab under fixed/free boundary conditions.

(Figure 6). One may also observe that in the case of fixed/free boundaries, the magnitude of the overshoot is no longer small compared to σ_0. Since at a given location $\Delta\sigma$ is constant, this could be an additional source of stress amplification.

Most of the observations made in this section may be verified by examining the one term approximations (8). The fact that the pulse duration $\Delta t = t_0$ is constant may be seen from (9) and one term asymptotic expressions (8). The wave summation aspects of the solutions representing the interactions of waves with boundaries are similar to those in homogeneous media, except that due to material inhomogeneity the wave speeds are variable. The asymptotic results show that the magnitude of the jump discontinuity in stress may be expressed as

$$\frac{\Delta\sigma}{\sigma_0} = \psi_0(x) = \left[\frac{a(x/l)+1}{a+1}\right]^{\frac{m+n}{4}} = \left[\frac{E'(x)\rho(x)}{E'(l)\rho(l)}\right]^{\frac{1}{4}}. \tag{10}$$

Thus, from (10) it is seen that $\psi_0(l) = 1$, $\psi_0(x) > 1$ for the case of pulse acting on the pure zirconia side and $\psi_0(x) < 1$ for the case of pulse acting on the pure nickel

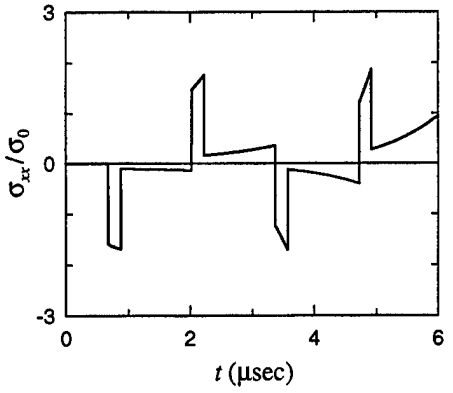

Figure 8 The variation of σ_{xx}/σ_0 with t at $x = 0$ in an Al/SiC FGM slab under fixed/free boundary conditions.

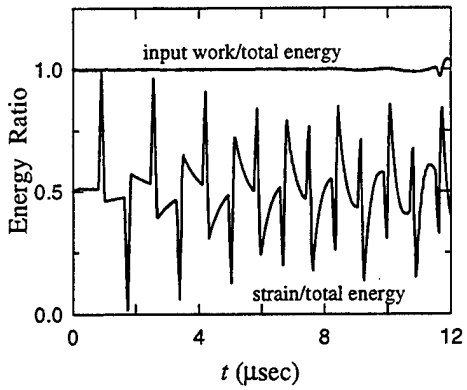

Figure 9 The energy balance in a Ni/ZrO_2 FGM slab under fixed/free boundary conditions subjected to the pulse defined by (9).

side. Needless to say, the actual values of $(\sigma_{xx})_{\max}$ will be the sum of $\Delta\sigma$ and the overshoot. The results described by the figures indicate that the overshoot is dependent on the boundary conditions and the material composition, and there is no simple way of estimating its magnitude. In many cases, however, the overshoot may be negligible and at a given location x the maximum stress may be approximated by

$$\left(\sigma_{xx}(x,t)\right)_{\max} \cong K\psi_0(x)\,\sigma_0 \tag{11}$$

where $K = 1$ for free/free and $K = 2$ for fixed/fixed boundaries. If we further assume that the density and the Poisson's ratio are constant, then (10) becomes $\psi_0(x) = \left[E(x)/E(l)\right]^{1/4}$. This is the result found by Steele [3] from the leading term of an asymptotic solution based on geometric optics.

As a second example we consider the pulse propagation in an FGM slab that consists of aluminum and silicon carbide. Referring to (1) and Table II, it is seen that $m \neq n+2$ and consequently the solution is somewhat more complicated. Again the thickness of the slab is $l = 5$ mm, pulse duration is $t_0 = 0.2$ μsec, and the pulse is applied at $x = l$. For SiC/Al and Al/SiC FGMs, the time-dependent stress at $x = 0$ is given by Figures 7 and 8, respectively. The results of the two examples considered show that if the pulse is applied on the stiffer side of the graded medium, the amplitude ratio $\Delta\sigma/\sigma_0$ decreases in thickness direction. Since in FGM coatings the surface subjected to the impact loading is usually stiffer, this general result indicate one of the advantages of graded coatings.

In the absence of an exact solution, one may use the energy balance to examine the accuracy of the asymptotic solutions. Initially the medium is stress-free and is at rest, meaning that for $t \leq 0$ the elastic energy U_V and the kinetic energy U_T are zero. For $t > 0$, since the medium is nondissipative, the energy balance principle requires that the sum of elastic and kinetic energies be equal to the work W of external loads, that is

$$W(t) = U_V(t) + U_T(t),\ t > 0. \tag{12}$$

In the FGM plate shown in Figure 1, for a unit surface area the external work, the total strain energy, and the total kinetic energy may be written as

$$W(t) = \int_0^t \sigma_{xx}(l,s)du(l,s),$$

$$U_V(t) = \int_0^l \frac{\sigma_{xx}^2(x,t)}{2E'(x)}dx, \qquad U_T(t) = \int_0^l \frac{\rho(x)}{2}\Big[\frac{\partial}{\partial t}u(x,t)\Big]^2 dx, \tag{13}$$

respectively. For the Ni/ZrO_2 FGM plate with fixed/free boundary conditions (Figure 1b), the energy balance is shown in Figure 9. Here the terminology "total energy" and "input work" are used for $U_V(t)+U_T(t)$ and $W(t)$, respectively. The figure show $U_V/(U_V+U_T)$ and $W/(U_V+U_T)$ as functions of time. Theoretically one should have $W(t)/[U_V(t)+U_T(t)] = 1$. Figure 9 shows that the agreement between theoretical and calculated total energies is nearly perfect up to 11 microseconds. For $t > 11$ μsec there are signs of greater discrepancy between the two results, indicating that for longer values of time one needs to retain more than six terms in the asymptotic series giving the stress and the displacement.

ACKNOWLEDGMENTS

This study was supported by AFOSR under the Grant F49620-98-1-0028 and by ARO under the grant DAAH04-95-1-0232.

REFERENCES

1. F. C. Karal and J. B. Keller, 1959. "Elastic Wave Propagation in Homogeneous and Inhomogeneous Media." *The Journal of the Acoustical Society of America*, 31:694-705.

2. U. S. Lindholm and K. D. Doshi, 1965. "Wave Propagation in an Elastic Nonhomogeneous Bar of Finite Length." *Journal of Applied Mechanics*, 32:135-142.

3. C. R. Steele, 1969. "Asymptotic Analysis of Stress Waves in Inhomogeneous Elastic Solids." *AIAA Journal*, 7:896-902.

4. M. J. Yedlin, B. R. Seymour, and B. C. Zelt, 1987. "Truncated Asymptotic Representation of Waves in a One-Dimensional Elastic Medium." *Geophysics*, 52:755-764.

5. A. Karlsson, H. Otterheim, and R. Stewart, 1993. "Transient Wave Propagation in Composite Media: Green's Function Approach." *Journal of the Optical Society of America A, Optics and Image Science*, 10:886-895.

6. T.-C. Chiu, 1995. "One Dimensional Wave Propagation in a Functionally Graded Elastic Medium," Master's Thesis, Department of Mechanical Engineering and Mechanics, Lehigh University, Bethlehem, PA.

APPPENDIX F

THE MIXED MODE CRACK PROBLEM IN AN ORTHOTROPIC GRADED MEDIUM

The Mixed-Mode Crack Problem in an Orthotropic Graded Medium*

Fazil Erdogan and Murat Ozturk

Lehigh University, Bethlehem, PA 18015

Abstract

The mixed-mode crack problem in plane elasticity for a graded and oriented material is considered. The material property grading is intentional, whereas the property orientation or orthotropy is usually the consequence of material processing. It is assumed that the crack is located in a plane perpendicular to the direction of property grading and the principal axes of orthotropy are parallel and perpendicular to the crack. The corresponding mixed boundary value problem is reduced to a system of integral equations which is solved for various loading conditions and material parameters. The results presented consist of the strain energy release rate, the stress intensity factors and the crack opening displacements. It is found that generally the stress intensity factors increase with increasing material inhomogeneity parameter and shear parameter and with decreasing stiffness ratio.

1. Introduction

Within the past decade there has been a great deal of interest in the concept of material property grading as a tool for new material design in certain advanced technology applications, primarily in high temperature components, microelectronics and machine tools. Most of the work in this area is concerned with metal/ceramic particulate composites with continuously varying volume fractions. The main objective has been to combine such desirable properties as strength, toughness and temperature, wear and corrosion resistance in a single material system. Two important potential applications of the concept appear to be coatings and interfacial zones. It has been shown that in these components grading the material composition reduces the magnitude of processing related and thermally or mechanically induced stresses (Choules and Kokini, 1993, Lee and

* This study was supported by ARO under the Grant DAAH04-95-1-0232

Erdogan, 1995) and significantly increases the bonding strength (Kurihara et al., 1990). A comprehensive review and discussion of the issues relating to the processing, design and mechanics of the graded materials may be found in Yamanouchi et al. (1990), Holt et al. (1993) and Ilschner and Cherradi (1995).

Generally, in coatings the subcritical crack growth and spallation-related failures involve two types of cracking, namely a surface crack propagating perpendicular to the boundary and an interface crack. This is partly due to the fact that because of the techniques used in processing, the graded medium is seldom isotropic and the two crack planes mentioned correspond to the principal planes of material orthotropy and consequently, to relatively weak fracture planes. For example, the materials processed by using a plasma spray technique have generally a lamellar structure. Flattened splats and relatively weak splat boundaries provide an oriented material with higher stiffness and weak cleavage planes parallel to the boundary (Sampath et al., 1995). On the other hand, graded materials processed by an electron beam physical vapor deposition technique would invariably have a columnar structure, resulting in a higher stiffness in thickness direction and weak fracture planes perpendicular to the boundary (Kaysser and Ilschner, 1995). Clearly, in studying the mechanics of these materials assuming the medium to be isotropic would not be very realistic and as a first approximation one could assume that the graded material is orthotropic with principal directions parallel and perpendicular to the boundary.

Since the material property grading is usually in thickness direction, and the residual and thermal stresses are generally parallel to the boundary, in the first crack problem of interest, namely in surface crack problem the plane of the crack is a plane of symmetry in material properties and loading. Consequently, the problem is a mode I crack problem for an orthotropic inhomogeneous medium. In the second problem of interest relating to spallation fracture, the crack is located in a plane perpendicular to the direction of material property variation. Therefore, the problem is inherently a mixed mode crack problem. In this study we consider the basic mixed mode problem in plane elasticity for an orthotropic inhomogeneous medium described in Fig. 1. The main interest in this study is in the influence of material orthotropy and inhomogeneity on the stress intensity factors and crack opening displacements.

2. Formulation and Solution of the Crack Problem

Consider the crack problem for an orthotropic inhomogeneous medium described by Fig. 1. In the usual notation let u_i and σ_{ij}, $(i,j=1,2,3)$ be the displacement and stress components and E_{ii}, G_{ij} and ν_{ij}, $(i,j=1,2,3)$ be the engineering elastic constants $((\nu_{ij}/E_{ii}) = (\nu_{ji}/E_{jj}))$. To simplify the equations of

the plane elasticity we introduce the following averaged constants (Krenk, 1979, Cinar and Erdogan, 1973) :

$$E = \sqrt{E_{11}E_{22}}, \quad \nu = \sqrt{\nu_{12}\nu_{21}}, \quad \delta^4 = \frac{E_{11}}{E_{22}} = \frac{\nu_{12}}{\nu_{21}}, \qquad \kappa_0 = \frac{E}{2G_{12}} - \nu, \quad (1)$$

for generalized plane stress and

$$E = \sqrt{\frac{E_{11}E_{22}}{(1-\nu_{13}\nu_{31})(1-\nu_{23}\nu_{32})}}, \quad \nu = \sqrt{\frac{(\nu_{12}+\nu_{13}\,\nu_{32})(\nu_{21}+\nu_{23}\,\nu_{31})}{(1-\nu_{13}\,\nu_{31})(1-\nu_{23}\,\nu_{32})}},$$

$$\delta^4 = \frac{E_{11}}{E_{22}}\frac{(1-\nu_{23}\nu_{32})}{(1-\nu_{13}\nu_{31})}, \qquad \kappa_0 = \frac{E}{2G_{12}} - \nu, \qquad (2)$$

for plane strain. We also use the stiffness ratio δ to scale the independent and dependent variables as

$$x = x_1/\sqrt{\delta},\ y = x_2\sqrt{\delta},\ u(x,y) = \sqrt{\delta}\,u_1(x_1,x_2),\ v(x,y) = u_2(x_1,x_2)/\sqrt{\delta},$$

$$\sigma_{xx}(x,y) = \sigma_{11}(x_1,x_2)/\delta,\ \sigma_{yy}(x,y) = \delta\sigma_{22}(x_1,x_2),\ \sigma_{xy}(x,y) = \sigma_{12}(x_1,x_2). \qquad (3)$$

In terms of the new variables the stress-displacement relations become

$$\sigma_{xx}(x,y) = \frac{E^*(x,y)}{1-\nu^2}\left(\frac{\partial}{\partial x}u(x,y) + \nu\frac{\partial}{\partial y}v(x,y)\right),$$

$$\sigma_{yy}(x,y) = \frac{E^*(x,y)}{1-\nu^2}\left(\frac{\partial}{\partial y}v(x,y) + \nu\frac{\partial}{\partial x}u(x,y)\right),$$

$$\sigma_{xy}(x,y) = \frac{E^*(x,y)}{2(\kappa_0+\nu)}\left(\frac{\partial}{\partial y}u(x,y) + \frac{\partial}{\partial x}v(x,y)\right), \qquad (4)$$

where

$$E^*(x,y) = E(x_1,x_2). \qquad (5)$$

The general problem with elastic parameters as arbitrary functions of x and y appears to be analytically intractable. To simplify the problem we make two assumptions regarding the distribution of the elastic parameters. First the material inhomogeneity is assumed to be such that the variations in the stiffnesses E_{11}, E_{22} and G_{12} are proportional. The second assumption is concerned with the Poisson's ratio ν. The previous results indicate that the solution of the crack problem in inhomogeneous materials are not very sensitive to ν. Consequently, in the problem under consideration it may be assumed that ν is a constant throughout the medium. These two assumptions imply that the parameters κ_0 and δ as well as ν are independent of x_1 and x_2 and the inhomogeneity in the medium is represented by

$E(x_1, x_2)$. If we further assume that the material properties vary only in x_2 direction and within that part of the medium perturbed by the crack the function E may be approximated by

$$E(x_1, x_2) = E(x_2) = E_0\, e^{\alpha x_2} = E^*(x, y) = E_0 e^{\gamma y}, \quad \gamma = \alpha/\sqrt{\delta}, \tag{6}$$

substituting (4) into the equilibrium equations it may be seen that

$$\frac{\partial^2 u}{\partial y^2} + \beta_1 \frac{\partial^2 u}{\partial x^2} + \beta_2 \frac{\partial^2 v}{\partial x \partial y} + \gamma \left(\frac{\partial u}{\partial y} + \frac{\partial v}{\partial x} \right) = 0,$$

$$\frac{\partial^2 v}{\partial x^2} + \beta_1 \frac{\partial^2 v}{\partial y^2} + \beta_2 \frac{\partial^2 u}{\partial x \partial y} + \gamma \beta_1 \left(\frac{\partial v}{\partial y} + \nu \frac{\partial u}{\partial x} \right) = 0, \tag{7}$$

where $\beta_1 = 2(\kappa_0 + \nu)/(1 - \nu^2)$ and $\beta_2 = 1 + \nu\beta_1$. Equations (7) are solved under the following boundary and continuity conditions :

$$\sigma_{22}(x_1, +0) = \sigma_{22}(x_1, -0), \ \sigma_{12}(x_1, +0) = \sigma_{12}(x_1, -0), \ -\infty < x < \infty, \tag{8}$$

$$\sigma_{22}(x_1, +0) = \sigma_0(x_1), \quad \sigma_{12}(x_1, +0) = \tau_0(x_1), \quad -a < x_1 < a, \tag{9}$$

$$u_2(x_1, +0) = u_2(x_1, -0), \quad u_1(x_1, +0) = u_1(x_1, -0), \quad a < |x_1| < \infty. \tag{10}$$

By using Fourier transforms and defining

$$\varphi_1(x_1) = \frac{\partial}{\partial x_1}(u_1^+ - u_1^-), \ \varphi_2(x_1) = \frac{\partial}{\partial x_1}(u_2^+ - u_2^-), \tag{11}$$

the problem may be reduced to a system of singular integral equations of the form (see Ozturk and Erdogan, 1996)

$$\frac{1}{\pi} \int_{-a}^{a} \left[\frac{\varphi_1(s_1)}{s_1 - x_1} + N_{11}(x_1, s_1)\varphi_1(s_1) + N_{12}(x_1, s_1)\varphi_2(s_1) \right] ds_1 = \frac{\tau_0(x_1)}{E_0\, c_0 \delta},$$

$$\frac{1}{\pi} \int_{-a}^{a} \left[\frac{\varphi_2(s_1)}{s_1 - x_1} + N_{21}(x_1, s_1)\varphi_1(s_1) + N_{22}(x_1, s_1)\varphi_2(s_1) \right] ds_1 = \frac{\delta \sigma_0(x_1)}{E_0\, c_0},$$

$$-a < x_1 < a, \tag{12}$$

where $N_{ij}, (i, j = 1, 2)$, are known functions (see Ozturk and Erdogan, 1996) and

$$c_0 = \frac{1}{2(r_1 + \bar{r}_1)}, \qquad r_1 = \sqrt{\kappa_0 + i\kappa_1}, \qquad \kappa_1 = \sqrt{1 - \kappa_0^2}\,. \tag{13}$$

Expressing now the unknown functions in the form

$$E_i f_i(t) = \frac{1}{\sqrt{1 - t^2}} \sum_{n=0}^{\infty} A_{in} T_n(t), \quad f_i(t) = \varphi_i(s_1), \quad (i = 1, 2), \quad t = s_1/a,$$

$$E_1 = E_0 c_0 \delta, \quad E_2 = E_0 c_0/\delta, \quad -1 < t < 1, \tag{14}$$

(12) may be reduced to a system of linear algebraic equations in A_{in}. In (14) $T_n(t)$ are the Chebyshev polynomials of the first kind.

From the single-valuedness conditions it may be shown that $A_{10} = A_{20} = 0$. After obtaining the coefficients A_{in}, the stress intensity factors may be defined by and evaluated from

$$k_1(a) = \lim_{x \to a+0} \sqrt{2(x_1 - a)}\, \sigma_{22}(x_1, +0) = -\sqrt{a} \sum_1^\infty A_{2n},$$

$$k_2(a) = \lim_{x \to a+0} \lim \sqrt{2(x_1 - a)}\, \sigma_{12}(x_1, +0) = -\sqrt{a} \sum_1^\infty A_{1n}. \tag{15}$$

Similarly, from (11) and (14) the crack opening displacements may be expressed as

$$u_1(x_1, +0) - u_1(x_1, -0) = -\frac{1}{E_1} \sqrt{a^2 - x_1^2} \sum_1^\infty \frac{1}{n} A_{1n} U_{n-1}(x_1/a),$$

$$u_2(x_1, +0) - u_2(x_1, -0) = -\frac{1}{E_2} \sqrt{a^2 - x_1^2} \sum_1^\infty \frac{1}{n} A_{2n} U_{n-1}(x_1/a), \tag{16}$$

where $U_n(t)$ are the Chebyshev polynomials of the second kind. Also, by expressing the asymptotic values of the stresses and the crack opening displacements in terms of the stress intensity factors and by using the conventional crack closure energy concept, the strain energy release rate may be evaluated at, for example, the crack tip $x_1 = a$ as

$$\mathcal{G} = \frac{\pi}{4E_0 c_0} \left(\delta k_1^2(a) + \frac{1}{\delta} k_2^2(a) \right). \tag{17}$$

In the corresponding isotropic material $\delta = 1$, $\kappa = 1$, $c_0 = 1/4$, and $\mathcal{G}$ becomes

$$\mathcal{G} = \frac{\pi}{E_0} \left(k_1^2(a) + k_2^2(a) \right), \tag{18}$$

where $E_0 = E(0)$ for plane stress and $E_0 = E(0)/(1 - \nu^2)$ for plane strain, $E(x_2)$ and ν being the elastic parameters of the inhomogeneous medium.

4. Results and Discussion

Referring to Fig. 1, since the material properties vary in x_2 direction only and x_1 and x_2 are the principal axes of orthotropy, $x_1 = 0$ is a plane of symmetry with regard to the geometry of the medium and material properties. Therefore, by decomposing the external loads $\sigma_0(x_1)$ and $\tau_0(x_1)$ in (9) into even and odd components, it may be shown that the stresses and displacements are either even or

odd functions in x_1. Consequently, it is sufficient to evaluate the stress intensity factors at one crack tip only ($x_1 = a$).

In the examples given it will be assumed that the crack surface tractions are described by

$$\sigma_0(x_1) = -p_0 - p_1\left(\frac{x_1}{a}\right) - p_2\left(\frac{x_1}{a}\right)^2, \tau_0(x_1) = -q_0 - q_1\left(\frac{x_1}{a}\right) - q_2\left(\frac{x_1}{a}\right)^2. \tag{19}$$

In (6) α has a dimension of 1/length. Thus expressing the exponent by $\alpha x_2 = (\alpha a)(x_2/a)$, it is seen that the inhomogeneity parameter α enters the analysis only through the dimensionless constant αa.

Some sample results for the strain energy release rate calculated from (17) in an orthotropic inhomogeneous medium under uniform tension $\sigma_{22}(x_1, \mp\infty) = p_0$ or $\sigma_0(x_1) = -p_0$, $\tau_0(x_1) = 0$ are given in Figures 2 and 3. The normalizing strain energy release rate $\mathcal{G}_0 = \pi p_0^2 a/E_0$ corresponds to a homogeneous isotropic medium. Figure 2 gives the result for a fixed shear parameter κ_0 and varying αa and δ. Note that in an isotropic homogeneous medium $\alpha a = 0$, $\kappa_0 = 1$, $\delta = 1$ giving $\mathcal{G}/\mathcal{G}_0 = 1$. Also the figure shows that quantitatively $\mathcal{G}/\mathcal{G}_0$ may deviate from unity quite considerably, meaning that the influence of κ_0, αa and δ on $\mathcal{G}$ can be very significant. Figure 3 shows the variation of $\mathcal{G}$ with αa and κ_0.

Some calculated results for the stress intensity factors are shown in Figures 4-6. The external loads in these results are the uniform tractions p_0 and q_0 defined by (19). These figures show that, regardless of the values of orthotropy constants κ_0, δ (and ν), as αa tends to zero the stress intensity factors approach their respective values for the corresponding homogeneous medium, that is, $p_0\sqrt{a}$ and $q_0\sqrt{a}$. This, of course, is the well-known result. The figures also show that the effect of the material inhomogeneity parameter on the mode I stress intensity factor is more pronounced than on the mode II stress intensity factor.

Typical results showing the crack opening displacements obtained from (16) for $\nu = 0.3$, $\kappa_0 = 0.5$ and $\delta^4 = 10$ are given in Figures 7 and 8. It may again be seen that the results are highly dependent on the inhomogeneity parameter αa. More detailed results for stress intensity factors covering broad range of parameters αa, κ_0, δ and ν may be found in the report by Ozturk and Erdogan (1996).

References

Cinar, A. and Erdogan, F., 1983, *Int. J of Fracture*, **19**, 83-102.

Choules, B.D. and Kokini, K., 1993, *Ceramic Coatings*, K. Kokini, ed., ASME MD-Vol 44, 73-86.

Holt, J.B., Koizumi, M., Hirai, T. and Munir, Z.A., (eds.) 1993, *Proceedings of the Second International Symposium on Functionally Graded Materials*,

Ceramic Transactions, Vol. 34, American Ceramic Society, Westerville, Ohio.

Ilschner, B. and Cherradi, N. (eds.), 1995, *Proceedings of the Third International Symposium on Structural and Functional Gradient Materials*, Presses Polytechniques et Universitaires Romands, Lausanne, Switzerland.

Kaysser, W.A. and Ilschner, B., 1995, "FGM Research Activities in Europe," *M.R.S. Bulletin*, Vol.XX, No. 1, 22-26.

Krenk, S., 1979, *Journal of Composite Materials*, **13**, 108-116.

Kurihara, K., Sasaki, K. and Kawarada, M., 1990, *FGM-90*, Yamanouchi et al. (eds.), 65-69.

Lee, Y.D. and Erdogan, F., 1995, *Int. J. of Fracture*, **69**, 145-165.

Ozturk, M. and Erdogan, F., 1996, "The Mixed-Mode Crack Problem in an inhomogeneous Orthotropic Medium," Project Report, U.S. Army Research Office, Grant DAAH04-95-1-0232.

Sampath, S., Herman, H., Shimoda, N. and Saito, T., 1995, "Thermal Spray Processing of FGMs," *M.R.S. Bulletin*, Vol. XX, No. 1, 27-31.

Yamanouchi, M., Koizumi, M., Hirai, T. and Shiota, I. (eds.), 1990, *FGM-90, Proceedings of the First International Symposium on Functionally Graded Materials*, FGM Forum, Tokyo, Japan.

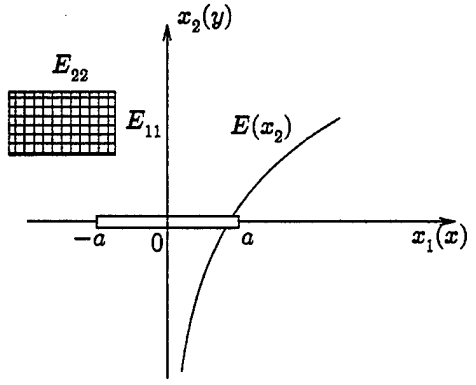

Fig.1 Geometry and notation for mixed mode crack problem in an orthotropic inhomogeneous medium

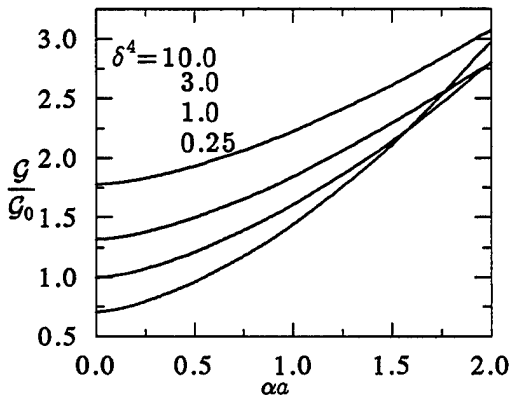

Fig.2 Variation of the normalized strain energy release rate with αa and δ in a graded orthotropic medium under uniform tension, $\kappa_0 = 1$, $\nu = 0.3$, $\sigma_{22}(x_1, \pm\infty) = p_0$, $\mathcal{G}_0 = \pi p_0^2 a/E_0$.

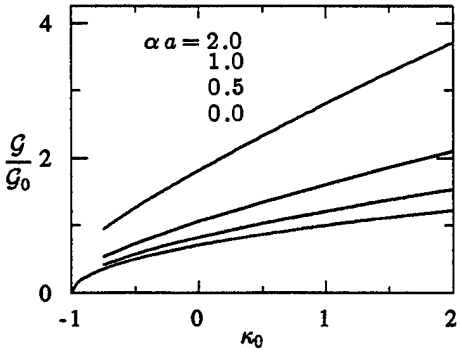

Fig. 3 Variation of the normalized strain energy release rate with κ_0 and αa in a graded orthotropic medium under uniform tension $\sigma_{22}(x_1, \pm\infty) = p_0$, $\delta = 1, \nu = 0.3, \mathcal{G}_0 = \pi p_0^2 a/E_0$.

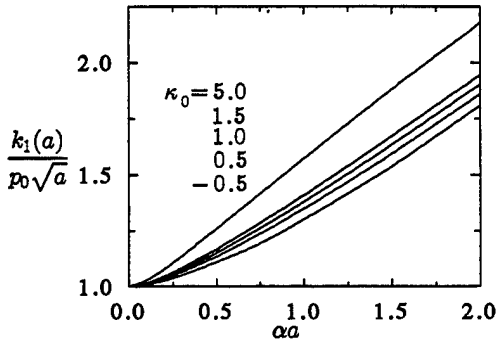

Fig. 4 Variation of the normalized stress intensity factor for an inhomogeneous orthotropic medium containing a crack under uniform pressure loading $\sigma_0(x_1) = -p_0, \tau_0(x_1) = 0, \delta^4 = 0.25, \nu = 0.3$.

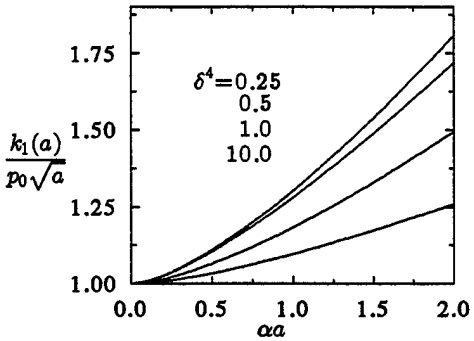

Fig. 5 Variation of the normalized stress intensity for an inhomogeneous orthotropic medium containing a crack under uniform pressure loading $\sigma_0(x_1) = -p_0, \tau_0(x_1) = 0$, $\kappa_0 = -0.5$, $\nu = 0.3$.

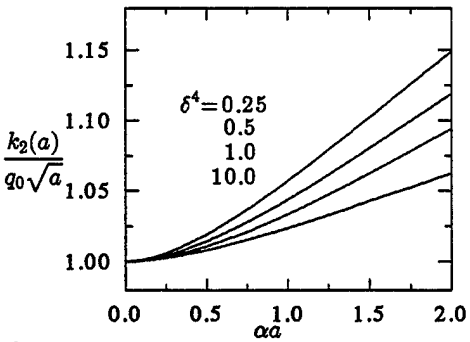

Fig.6 Variation of the normalized stress intensity factor for an inhomogeneous orthotropic medium containing a crack under uniform shear loading $\sigma_0(x_1) = 0$, $\tau_0(x_1) = -q_0, \kappa_0 = -0.5, \nu = 0.3$.

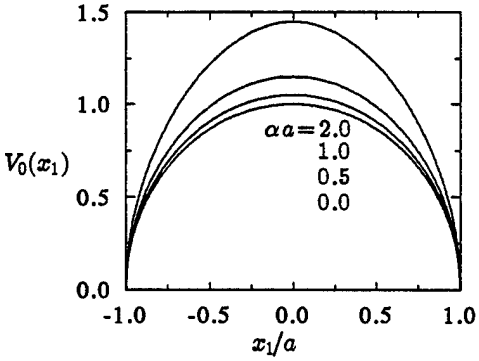

Fig. 7 The influence of αa on the crack opening displacement V_0 for an inhomogeneous orthotropic medium under uniform pressure loadings, $\tau_0(x_1) = 0$, $\sigma_0(x_1) = -p_0$, $\delta^4 = 10.0, \nu = 0.3, \kappa_0 = 0.5$, $V_0 = (u_2(x_1, +0) - u_2(x_1, -0))/v_0$, $v_0 = ap_0/E_2$

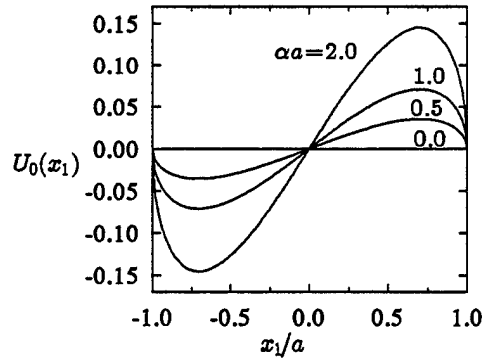

Fig. 8 The influence of αa on the crack opening displacement U_0 for an inhomogeneous orthotropic medium under uniform pressure loadings, $\tau_0(x_1) = 0, \sigma_0(x_1) = -p_0$, $\delta^4 = 10.0, \nu = 0.3$, $\kappa_0 = 0.5$, $U_0 = (u_1(x_1, +0) - u_1(x_1, -0))/u_0$, $u_0 = ap_0/E_1$